Published in final edited form as:
Am Mineral. 2021 March ; 106(3): 325–350. doi:10.2138/am-2020-7564.

An evolutionary system of mineralogy. Part III: Primary chondrule mineralogy (4566 to 4561 Ma)

Robert M. Hazen[1,*], **Shaunna M. Morrison**[1], **Anirudh Prabhu**[2]

[1]Earth and Planets Laboratory, Carnegie Institution for Science, 5251 Broad Branch Road NW, Washington, D.C. 20015, U.S.A.

[2]Tetherless World Constellation, Department of Earth and Environmental Sciences, Rensselaer Polytechnic Institute, Troy, New York 12180, U.S.A.

Abstract

Information-rich attributes of minerals reveal their physical, chemical, and biological modes of origin in the context of planetary evolution, and thus they provide the basis for an evolutionary system of mineralogy. Part III of this system considers the formation of 43 different primary crystalline and amorphous phases in chondrules, which are diverse igneous droplets that formed in environments with high dust/gas ratios during an interval of planetesimal accretion and differentiation between 4566 and 4561 Ma. Chondrule mineralogy is complex, with several generations of initial droplet formation via various proposed heating mechanisms, followed in many instances by multiple episodes of reheating and partial melting. Primary chondrule mineralogy thus reflects a dynamic stage of mineral evolution, when the diversity and distribution of natural condensed solids expanded significantly.

Keywords

Classification; mineral evolution; natural kinds; chondrules; chondrite meteorites; planetesimals

Introduction

The “evolutionary system” of mineralogy focuses on the inexorable emergence of mineral diversity and distribution through billions of years of cosmic evolution. This data-driven approach emphasizes the numerous information-rich aspects of minerals—attributes that point to various physical, chemical, and ultimately biological mineral-forming processes (Hazen et al. 2008; Hazen and Ferry 2010; Hazen 2019). The first three parts of this evolutionary system focus on relatively unaltered components of chondrite meteorites: presolar “stardust” grains (see Part I; Hazen and Morrison 2020); refractory inclusions [i.e., calcium-aluminum-rich inclusions (CAIs), amoeboid olivine aggregates (AOAs), and ultra-refractory inclusions (URIs), as described in Part II; Morrison and Hazen 2020]; and primary chondrule phases (Part III, this study), all of which preserve episodes of mineral evolution prior to their incorporation into planetesimals (the subject of Part IV of this series) and

* rhazen@carnegiescience.edu.

extensive alteration by planetesimal processing, as recorded, for example, in both highly altered chondrite and achondrite meteorites (to be reviewed in Part V).

This system builds on classification protocols of the International Mineralogical Association (IMA), as codified by the Commission on New Minerals, Nomenclature and Classification (e.g., Burke 2006; Mills et al. 2009; Schertl et al. 2018). We attempt to amplify and modify the IMA approach, which distinguishes each mineral "species" based on unique combinations of end-member composition and idealized crystal structure, leading to >5500 approved mineral species (rruff.info/ima; accessed 7 April 2020).

The power and simplicity of the IMA classification system lie in its recognition of mineral species based on the minimum information (measured in bits; e.g., Krivovichev 2012, 2013) necessary to distinguish among species. By design, IMA protocols do not consider such revelatory aspects of minerals as trace and minor elements, fractionated isotopes, structural defects, varied electromagnetic properties, textures and morphologies, compositional zoning, or inclusions. Neither does the IMA take into account mineral ages or petrologic contexts when classifying mineral species. However, these and many other characteristics of minerals and their assemblages collectively provide powerful testimony regarding each mineral's origins, as well as its subsequent deep-time interactions with changing chemical and physical environments. The evolutionary system, by distinguishing minerals formed in different paragenetic contexts from stars to nebulae to dynamic planetary surfaces and interiors, thus provides a framework for classifying minerals in their spatial and temporal context.

The evolutionary system employs IMA nomenclature for most natural condensed solids, but it deviates from those protocols in three important ways. In some instances, we split IMA species into two or more "natural kinds," based on diagnostic combinations of attributes that arise from distinct paragenetic modes. Thus, isotopically anomalous hibonite condensed in the expanding, cooling atmospheres of AGB stars (labeled "*AGB hibonite*") is measurably distinct from hibonite condensed from the solar nebula to form a primary phase in a calcium-aluminum-rich inclusion ("*CAI hibonite*"). Many of the most common rock-forming minerals display multiple paragenetic contexts, each of which tells a different story about stages of planetary evolution; these species are thus split into two or more "natural kinds" in our system (Hazen 2019). Note that we employ a binomial nomenclature, with the first name designating the paragenetic mode and the second name the mineral species, which in the great majority of cases is the same as the approved IMA species name.

In several cases, we lump two or more approved IMA species into one natural kind when those multiple species satisfy two criteria: (1) the species are part of a continuous phase region that may be bounded by several different idealized end-members, and (2) all examples form by the same paragenetic mode. For example, CAIs hold a variety of micrometer-scale refractory metal "nuggets" that occur as alloys of Mo, Ir, Os, Ru, Rh, Re, Pt, and W (Weber and Bischoff 1997; Berg et al. 2009; MacPherson 2014). These alloys, which are among the earliest high-temperature condensates in the solar nebula, occur in a range of elemental proportions, with Os, Ru, Re, or Mo as the dominant element in some individual sub-micrometer-scale grains. IMA protocols thus would name coexisting nuggets

as “osmium,” “ruthenium,” “rhenium,” or “molybdenum” (though the latter two native elements have not been approved as species by the IMA). By contrast, we lump all of these metal alloys together into platinum group element alloys (“*CAI PGE alloy*”). Similar lumping occurs in several oxide and silicate minerals in chondrules, including members of the oxide spinel, olivine, and clinopyroxene groups.

A third deviation from IMA protocols relates to non-crystalline condensed phases, notably a variety of low-temperature interstellar condensates (e.g., amorphous H_2O), impact phases (e.g., maskelynite), and rapidly quenched silicate glasses that are especially important in the context of chondrules. These materials, though not generally incorporated in the current IMA scheme (e.g., Hazen et al. 2013, Table 3; Hazen 2019), are important in discussions of planetary evolution (e.g., Bradley 1994a, 1994b; Abreu and Brearley 2011), and they represent distinct condensed solid phases that should be included in any comprehensive catalog of planetary materials.

Each of these considerations—splitting, lumping, and amorphous phases—comes into play when considering primary chondrule minerals, which provide the focus of Part III of this series.

Chondrules and chondrites

Chondrite meteorites, the oldest sedimentary rocks in the solar system, hold vivid clues to the origins and evolution of stars and planets. Here we review the nature and origin of chondrules, the classification of chondrite meteorites in which they are found, and a chronology of the earliest stages of mineral evolution. Chondrule types, properties, origins, and implications have been the subject of several comprehensive reviews (King 1983; Kerridge and Matthews 1988; Hewins et al. 1996; Brearley and Jones 1998; Hutchison 2004; Connolly and Desch 2004; Krot et al. 2014; Scott and Krot 2014; Rubin and Ma 2017, 2021; Russell et al. 2018). What follows, therefore, is a brief summary in the context of chondrule mineralogy.

Classification of chondrules

Chondrules are igneous particles that were once partially to completely melted. Most chondrules range in size from tens of micrometers to ~10 mm in diameter, though extreme examples vary from submicrometer (Rubin et al. 1982) to several centimeters (Prinz et al. 1988) in diameter. Chondrules often occur as near-spherical solidified droplets (e.g., Weyrauch and Bischoff 2012; Charles et al. 2018), though other chondrules and their fragments are preserved in irregular shapes as a consequence of incomplete melting of precursor dust and grains, adhesion and sintering of conjoined objects, or sculpting by dynamic nebular processes (e.g., Rubin 2006). Most chondrules are dominated by silicates, commonly olivine, pyroxene, and feldspar, but many other phases, including metal alloys, sulfides, nitrides, phosphides, and several varieties of glass, occur in varying proportions that point to a formation in diverse physical and chemical environments. Indeed, chondrules span the range from nearly pure silica to nearly pure metal, with textures from holocrystalline to glass. Given that chondrites account for as many as 80% of observed meteorite falls, and that chondrules are the most abundant components of most chondrites, a significant fraction of

the material that now comprises terrestrial planets and moons may have once been stored in the form of these small igneous droplets.

Chondrule classification is based on a combination of mineralogical, textural, and compositional attributes. From a petrographic perspective, most common chondrules (more than 80% in ordinary chondrites) display porphyritic textures, including types designated porphyritic olivine (PO), porphyritic olivine + pyroxene (POP), and porphyritic pyroxene (PP)—conventions introduced by Gooding and Keil (1981). Other textural types include barred olivine (BO) with skeletal olivine plate-like crystals that were evidently quenched from a peak temperature close to the liquidus of the chondrule; granular olivine pyroxene (GOP) with small uniform grains; radial pyroxene (RP) with needlelike pyroxene crystals radiating from a point on the chondrule periphery; cryptocrystalline chondrules with crystallites <2 μm in diameter; and rare glassy chondrules. An important component of most chondrules is fine-grained or glassy mesostasis—solidified residual melt that surrounds phenocrysts (Connolly et al. 1998; Hewins et al. 2005).

Chondrules are also classified by their chemical characteristics (e.g., McSween 1977a). Type I chondrules, featuring Mg-rich olivine and pyroxene, are relatively reduced with most iron in the form of Fe metal rather than silicates. They are further divided into types IA (Si poorer; olivine dominant), IB (Si richer; pyroxene dominant), and IAB (intermediate, with both olivine and pyroxene) chondrules. Type II chondrules are more oxidized, typically with >10 mol% of the Fe end-member in Mg silicates (Grossman and Brearley 2005). The A, B, and AB designations for olivine- and pyroxene-bearing chondrules apply to type II chondrules, as well.

In addition, a suite of aluminum-rich chondrules displays a range of compositions, between Ca-Al and Na-Al members, and Na-Al-Cr chondrules (Bischoff and Keil 1983, 1984), as well as plagioclase-olivine inclusions or “POIs” (Sheng et al. 1991a). These objects have mineralogical and compositional attributes intermediate between CAIs and chondrules. Unlike other chondrules, POIs contain a suite of relatively refractory primary minerals (e.g., spinel, fassaite, and perovskite), as well as several minerals not reported as primary phases from other types of chondrules (e.g., armalcolite, rutile, sapphirine, and zirconolite). Additional chondrule-like objects range from silicarich, with >90 wt% SiO_2, to sulfide-metal nodules, with <10 wt% silicates and oxides (e.g., Brearley and Jones 1998; Zhang and Hsu 2009; Scott and Krot 2014; Wang et al. 2016).

At the smallest extreme, microchondrules no more than 40 μm in diameter have been recorded as decorating the rims of larger chondrules in the least altered ordinary chondrite meteorites (Mueller 1962; Rubin et al. 1982; Rubin 1989; Krot and Rubin 1996; Krot et al. 1997a). These tiny objects, which display a range of textures analogous to their larger counterparts, may form during rapid reheating events that melt the exterior portions of parent chondrules (Bigolski et al. 2016) or by splattering following random collisions (Dobriça and Brearley 2016).

Classification of chondrite meteorites

Chondrules occur in chondritic meteorites, which contain the most refractory rock-forming elements in ratios close to those observed in the solar photosphere. They accreted initially as accumulations of nebular particles with four principal components (Brearley and Jones 1998, Table 3): (1) chondrules, typically the most abundant constituent, composing up to 80 vol% in many meteorites, though sometimes completely lacking; (2) refractory inclusions, including CAIs, URIs, and AOAs, representing from 0 to ~10 vol%; (3) opaque assemblages of metallic Fe-Ni alloys and sulfides, which usually constitute <5 vol% but exceed 90 vol% in some examples; and (4) fine-grained (10 nm to 5 μm in diameter) matrix with some combination of oxide, silicate, sulfide, metal, and organic phases, often with a small fraction of presolar grains. While chondrules are often the dominant constituent of chondrites, the ratios of these four components vary widely. Note that in this contribution we consider primary chondrule mineralogy, whose formation (along with the refractory inclusions) is assumed to predate the incorporation of chondrules into chondritic meteorites. These primary phases are best identified and described from the most pristine chondrites, which have experienced relatively little alteration by thermal, aqueous, and/or impact processes on their parent asteroidal bodies. Note, however, that many chondrules experienced some degree of alteration prior to chondrite formation through reactions with nebular gas, secondary heating events, and/or high-velocity collisions with other particles (e.g., Ruzicka 2012; Ebel et al. 2018). Therefore, the distinction between primary and secondary processes is sometimes difficult to discern.

Chondrite meteorites have been classified under various systems based on the ratios of constituents, bulk composition, primary mineralogy, mineralogical textures, and isotopic characteristics. Additional chondrite subdivisions are based on degrees of aqueous, thermal, and/or shock alteration within their parent body (Van Schmus and Wood 1967; Stöffler et al. 1991; Weisberg et al. 2006; Krot et al. 2014), as well as through weathering at or near Earth’s surface (Wlotzka 1993).

Traditional classification of tens of thousands of chondrite meteorite finds and falls divides more than 99.5% of specimens into 14 groups, each represented by multiple examples (e.g., Scott and Krot 2014). Six of these groups, including those in the classes of ordinary, enstatite, and R chondrites, collectively are termed non-carbonaceous chondrites (NC). The most abundant meteorites, comprising as many as 80% of falls, and more than 90% of chondrites (i.e., excluding achondrite, iron, and stonyiron meteorites), are ordinary chondrites (OC), which occur in three broad groups—H, L, and LL. These three groups are generally similar in their high percentage of chondrules (typically ~0.3 to 0.6 mm in diameter, comprising 60 to 80 vol%; Friedrich et al. 2015), with 10 to 15 vol% matrix and few CAIs. However, they vary significantly in metal composition, as well as in the mineralogy of Fe-bearing metal and silicate phases. H stands for high total Fe, L for low total Fe, and LL for even lower total Fe and low metal.

Enstatite chondrites (EC), including EH and EL groups (for higher and lower total Fe-Ni metal alloy, respectively; Sears et al. 1982), are relatively rare, comprising fewer than 2% of falls (Weisberg and Kimura 2012). They are distinguished by an extremely reduced suite of minerals (Brearley and Jones 1998; Jacquet et al. 2018; Weyrauch et al. 2018; Rubin and Ma

2021), with almost all of their iron in the form of metal or sulfide, in association with near end-member enstatite ($MgSiO_3$) and forsterite (Mg_2SiO_4). These oxygen- and water-poor rocks feature such rare minerals as oldhamite (CaS), niningerite (MgS), alabandite (MnS), daubréelite ($FeCr_2S_4$), caswellsilverite ($NaCrS_2$), and perryite [$(Ni,Fe)_8(Si,P)_3$]. EH and EL groups differ in the average size of chondrules and in the composition of Fe metal alloys, but for the most part they have similar mineralogy.

Eight chondrite groups, abbreviated CI, CM, CO, CV, CR, CH, CB, and CK, form the carbonaceous chondrite class (CC), which accounts for ~4% of falls. They share several compositional and isotopic characteristics, most notably: (1) suites of organic molecules; (2) relatively high volatile content; (3) enrichment relative to solar average in refractory lithophile elements such as Ca, Al, and Ti; and (4) relatively low $^{17}O/^{16}O$ compared to Earth —all characteristics that may be consistent with formation farther from the Sun than other chondrite groups. However, the several carbonaceous chondrite groups differ significantly from each other in their relative percentages of chondrules, refractory inclusions, metal, and matrix, as well as chondrule size, degree of oxidation, and extent of aqueous alteration and thermal metamorphism. Note that all known CI, CK, and CM carbonaceous chondrites display significant thermal and/or aqueous alteration (e.g., Brearley and Jones 1998; Scott and Krot 2014); consequently, their mineralogy will be considered in Part V of this series.

Chondrite classification is further complicated by additional rare grouped meteorites, as well as more than a dozen ungrouped chondrites that do not fit neatly into the above scheme. A few of these unusual meteorites are carbonaceous chondrites (e.g., Ivanova et al. 2008; Wang and Hsu 2009; Kimura et al. 2014); others are distinguished by unusual combinations of chemical, isotopic, and/or matrix characteristics (e.g., Pratesi et al. 2019). For example, K chondrites (named for the Kakangari meteorite) combine aspects of both CC and NC groups, while R chondrites (for Rumuruti) are related to ordinary chondrites, though they are highly oxidized, unusually rich in matrix, and have an anomalously high $^{17}O/^{16}O$ compared to other NC meteorites. It should be noted that chondrite classification is likely incomplete, as thousands of finds have yet to be fully characterized and hundreds of new specimens are recovered every year.

An important consideration when cataloging “primary” chondrule minerals is the degree of alteration experienced in the chondrite meteorite’s parent body. A non-intuitive numbering system, first introduced by Van Schmus and Wood (1967) and now in general use, defines the least altered and therefore unequilibrated chondrites as “3.0.” Increasing numbers from 3 to 7 (with higher resolution between 3.0 and 3.9 for CO, L, LL, and H chondrites) designate increasing degrees of thermal alteration, whereas decreasing numbers below 3.0 relate to increased degrees of aqueous alteration. Additional refinements by Grossman and Brearley (2005) subdivide OC and CO 3.0 to 3.2 chondrites into an even higher resolution scale from 3.00 to 3.15.

Many primary chondrule minerals have been modified by progressive degrees of thermal metamorphism and metasomatism within their parent bodies. Common changes include gradual equilibration of silicate compositions through diffusion, as well as silicate glass devitrification, most commonly characterized by the nucleation of feldspar and possibly Ca-

rich clinopyroxene (Sears and Hasan 1987; Scott et al. 1994). By the time a chondrule reaches type 3.9, corresponding to metamorphism close to 600 °C, olivine compositions have equilibrated among a meteorite's diverse chondrules, whereas pyroxene remains unequilibrated. Feldspar may occur in a high-temperature Al-Si disordered state (Sears et al. 1995) and display alteration effects, including Ca-Na zoning and textural changes (Lewis and Jones 2016, 2019). In this treatment, we focus on minerals found in the least equilibrated chondrites (optimally those designated 3.0, though in some instances we consider minerals in more-altered chondrites, as some meteorite groups always display some degree of metamorphism).

Formation mechanisms of chondrules

The diversity of chondrule types points to a variety of precursor materials and formation events at different heliocentric distances and with a range of paragenetic conditions (Krot et al. 2005; Rubin 2000, 2010; Desch et al. 2012; Scott and Krot 2014; Ebel et al. 2018; Hubbard and Ebel 2018). Most chondrules are thought to have formed from presolar and protoplanetary disk dust aggregates, as well as from a combination of earlier generations of chondrules, chondrule fragments, refractory amoeboid olivine aggregates (AOAs) that formed as nebular condensates, and possibly debris from differentiated planetesimals (Weinbruch et al. 2000; Libourel et al. 2006; Sanders and Scott 2012; Weyrauch and Bischoff 2012; Ebert and Bischoff 2016; Krot et al. 2018; Marrocchi et al. 2019).

The dominant chondrule formation hypothesis for the past several decades has been rapid heating (perhaps at rates $>10^6$ °C/h; Tachibana and Huss 2005) and melting of dust aggregates. Note that even to partially melt these droplets required energy comparable to the gravitational potential energy of the nebular disk itself (King and Pringle 2010). Melting is thought to have occurred by any one of several processes (Boss 1996; Desch et al. 2012; Connolly and Jones 2016): FU Orionis-type flares (Bertout 1989; Bell et al. 2000; Hubbard and Ebel 2014); direct illumination in proximity to the protosun (Shu et al. 1996; Morlok et al. 2012); solar shock waves induced by the in-fall of gas (Iida et al. 2001; Morris and Boley 2018); planetary embryo-produced bow shocks (Desch and Connolly 2002; Hood and Weidenschilling 2012; Morris and Boley 2018), as well as associated magnetic effects (Mann et al. 2016; Mai et al. 2018); shocks produced by density waves (Wood 1996a; Boss and Durisen 2005); current sheet heating in partly ionized disk regions (McNally et al. 2014; Hubbard and Ebel 2015; Zhdankin et al. 2017); and nebular lightning (Sorrell 1995; Desch and Cuzzi 2000). Given the range and frequency of these rapid heating events in the solar nebula, many chondrules may have experienced multiple secondary melting events (Baecker et al. 2017).

Isotope systematics from chondrules and matrix also support the dust origins hypothesis by pointing to chondrule formation through localized melting events of dust aggregates in the protoplanetary disk. Kleine et al. (2018) find that ages of CV and CR chondrites are tightly constrained at 4565.1 ± 0.8 and 4563.7 ± 0.6 Ma, respectively. These dates suggest that the formation interval for each chondrite type is significantly less than 1 million years, and that chondrule formation and chondrite accretion were temporally linked.

Other researchers favor additional chondrule formation scenarios related to planetesimal impacts (e.g., Krot et al. 1993; Asphaug et al. 2011; Sanders and Scott 2012). Johnson et al. (2012, 2014, 2018) argue for the role of impact jetting, by which high-velocity impacts on growing planetesimals generate jets of partially molten materials. Chondrules form from cooling droplets, which are rapidly accreted to planetesimal surfaces. Sanders and Scott (2012, 2018) posit a similar scenario for chondrule origins through impact splashing (as opposed to the higher velocity jetting), with chondrules contaminated by mineral dust and larger grains, thus generating a variety of relict grains and a range of chemical and isotopic compositions (however, see Baecker et al. 2017).

Finally, a small population of CB and CH group chondrules appears to have formed by direct condensation from a superheated silicate gas within an impact plume (Krot et al. 2001b; Campbell et al. 2002, 2005a, 2005b; Rubin et al. 2003; Campbell and Humayun 2004; Gounelle et al. 2007; Fedkin et al. 2015). Evidence for a different origin of these chondrules includes a complete lack of relict grains, fine-grained textures, and condensation calculations suggesting formation in a high-density impact plume environment.

Temperature, pressure, and cooling histories of chondrules

Numerous attributes of chondrules, including mineralogy, crystal growth textures, disequilibrium partition coefficients among phases, diffusion-controlled zoning, exsolution, the presence of glassy or cryptocrystalline phases, and olivine defect density, point to their complex and varied thermal histories (e.g., Jones et al. 2018). All chondrules experienced one or more episodes of rapid heating close to or above their liquidus (~1500 to 2100 K), followed by initial cooling to solidus temperatures (~1300 to 1500 K) at rates from 100 °C/h to thousands of °C/h, with slower rates (10 °C/h to hundreds of °C/h) below the solidus (e.g., Miyamoto et al. 2009; Chaumard et al. 2018; Cuvillier et al. 2018; Ebel et al. 2018). Variations in mineralogy, texture, and other chondrule attributes point to significant variability in formation conditions, in some cases suggesting different modes of chondrule origin.

Adding to their complex thermal histories, many chondrules display evidence for rapid heating events after their initial crystallization (Krot et al. 1997a, 2004a, 2018; Rubin 2010; Ruzicka 2012; Baecker et al. 2017). At least four lines of evidence point to multiple subsequent heating events for many, if not most, chondrules: (1) many chondrule phenocrysts nucleate on earlier generations of olivine or pyroxene relict grains with different chemical properties (Marrocchi et al. 2019); (2) some chondrules appear to envelop others (Wasson et al. 1995; Hobart et al. 2015); (3) many chondrules display thin igneous rims of re-melted material (Rubin 1984a); and (4) normal-sized chondrules are sometimes surrounded by “microchondrules” (Krot and Rubin 1996; Krot et al. 1997a).

A significant unresolved question regards the pressures at which chondrules formed (Wood 1996b; Hewins and Zanda 2012; Connolly and Jones 2016; Ebel et al. 2018). The presumed average pressure of the protoplanetary disk was $<10^{-3}$ atm. At such a low pressure and the maximum temperatures of chondrule formation (1700 to 2000 K), even with cooling rates as great as 1000 °C/h one would expect characteristic Rayleigh fractionation of volatile elements and their isotopes (Hashimoto 1983; Davis et al. 1990; Richter et al. 2011; see Ebel

et al. 2018, and references therein). However, such fractionation is not generally observed in volatile elements such as S, Zn, Cd, or Cu (Luck et al. 2005; Tachibana and Huss 2005; Wombacher et al. 2008; Moynier et al. 2009). In addition, careful analyses of olivine phenocrysts indicate that Na was not completely lost, suggesting an ambient vapor pressure significantly greater than 10^{-3} atm (Alexander et al. 2008; Fedkin and Grossman 2013). One possible explanation was offered by Galy et al. (2000), who proposed that the partial pressure of hydrogen (H_2) gas in chondrule-forming regions was ~1 bar—conditions that would inhibit volatile element loss and promote the stability of silicate melts (Ebel 2006). However, astrophysical models of the protoplanetary nebula do not support such a high hydrogen gas concentration. Indeed, a maximum pressure of ~10^{-3} atm is suggested by models of disk processes (D'Alessio et al. 2005).

An alternative explanation for the lack of volatile element fractionation relates to "high solid densities" during chondrule formation, where solid density refers to the ratio of nebular dust to gas relative to the solar average. Several investigators (Wood and Hashimoto 1993; Ebel and Grossman 2000; Alexander et al. 2008; Alexander and Ebel 2012; Bischoff et al. 2017; Ebel et al. 2018) propose that chondrule-forming regions had a chondruleto-gas ratio sufficiently high—perhaps 10^3 to 10^4 times that of the Sun—so that stable chondrule melts achieved equilibrium with the surrounding hot gas. High volatile partial pressures from evaporated dust thus reduced the evaporative loss of volatiles from large melt droplets in spite of the relatively low ambient gas pressure (Alexander et al. 2008), while leading to the observed significant fraction of compound chondrules (Wasson et al. 2003; Cuzzi and Alexander 2006). Note that clear evidence exists for significant chondrule-gas exchange, for example through the reaction of forsterite plus SiO gas to form enstatite rims (Krot et al. 2004b; Libourel et al. 2006; Friend et al. 2016; Hezel et al. 2018; though see Rubin 2018).

A chronology of nebular mineralization

The evolutionary system of mineralogy considers the diversity and distribution of minerals through deep time, as novel physical, chemical, and ultimately biological processes led to new mineral-forming environments. Developing a chronology of the earliest mineral-forming events in the evolving protoplanetary disk is thus important for setting the stage as planets and moons emerge from nebular dust and gas. Efforts to determine the ages of the most ancient minerals preserved in chondrites, both through direct radiometric or other measurements and by contextual inferences, have led to an emerging (though as yet incomplete and at times contentious) chronology of the first few million years of nebular history (Table 1). At least three complementary aspects of chondrite meteorites: (1) radiometric geochronology; (2) textural relationships; and (3) the distribution of their components among two major groups of meteorites—reveal aspects of the earliest evolution of the protoplanetary disk.

Presolar grains.—The oldest solid objects from our solar system are refractory inclusions with radiometric ages close to 4567 Ma (Connelly et al. 2012; Krot 2019). Presolar grains, by definition, predate those first nebular condensates and are the most ancient known solid objects. Heck et al. (2020) employed cosmic ray exposure ages of presolar moissanite (SiC) grains to identify individual mineral grains as old as 7 billion years, though the majority of

stardust preserved in chondrite meteorites is <5 billion years old and the youngest observed stellar SiC grain formed only 3.9 ± 1.6 million years before CAIs (i.e., ~4571 million years ago). Estimates of when the first condensed solid phase formed in the universe must remain somewhat speculative. However, astrophysical calculations of stellar nucleosynthesis processes (e.g., Burbidge et al. 1957; Cameron 1957; Schatz 2010; Bertulani 2013), coupled with increasingly high-resolution imaging of the first generations of stars in galaxies at distances >13 billion light years (Abel et al. 2002; Bond et al. 2013; Howes et al. 2015; Robertson et al. 2015; Bowman et al. 2018), suggest that large carbon-forming stars occurred early in cosmic history. We conclude that carbon-rich phases, including diamond, graphite, and moissanite, formed within the first billion years of the Big Bang, perhaps >13 Ga.

Refractory inclusions.—The formation of calcium-aluminumrich inclusions at 4567.3 ± 0.16 Ma (Connelly et al. 2012; see also, Amelin et al. 2002, 2010; Connelly et al. 2008; Bouvier and Wadhwa 2010; Krot 2019) provides the benchmark date for nebular mineralogy. Radiometric dating of CAI components, including ^{207}Pb-^{206}Pb (Amelin et al. 2010; Connelly et al. 2012), ^{182}Hf-^{182}W (Holst et al. 2013; Budde et al. 2015), and ^{26}Al-^{26}Mg (Kita et al. 2013; Nagashima et al. 2018) systematics, establish that CAIs were the first solids to condense in the solar nebula (Krot 2019). CAIs evidently were produced during an interval of <300 000 yrs (Kita et al. 2013; Krot et al. 2018), with the great majority of CAIs forming within the first 200 000 yrs after ~4567.3 Ma (MacPherson et al. 2010, 2012; Kita et al. 2013).

That early interval of nebular evolution must have been a dynamic time. Recent studies of significant diversity in the size, mineralogy, textures, contexts, and chemical and isotopic fractionation of CAIs, URIs, and AOAs point to multiple generations of these refractory objects, perhaps arising from distinct nebular reservoirs and a range of processes, including episodic melting, evaporation, condensation, and aggregation (Krot et al. 2008; Kööp et al. 2016a, 2016b, 2018; see Krot 2019, and references therein).

Ultra-refractory inclusions, usually lumped with CAIs, display extreme enrichments by factors up to 1000 in Sc, Zr, Y, Ti, and other high field strength elements (El Goresy et al. 2002; Rubin and Ma 2017). These unusual compositions result in distinctive URI mineralogy, including a variety of rare, micrometer-scale oxide and silicate phases such as tistarite (Ti_2O_3), kaitianite ($\left(Ti_2^{3+}Ti^{4+}O_5\right)$), anosovite [$(Ti^{4},Ti^{3+},Mg,Sc,Al)_3O_5$], lakargiite ($CaZrO_3$), kangite [$(Sc,Ti,Al,Zr,Mg,Ca)_{1.8}O_3$], tazheranite [$(Zr,Sc,Ca,Y,Ti)O_{1.75}$], allendeite ($Sc_4Zr_3O_{12}$), eringaite [$Ca_3(Sc,Y,Ti)_2Si_3O_{12}$], davisite [$Ca(Sc,Ti^{3+},Ti^{4+},Mg,Zr)AlSiO_6$], warkite [$Ca_2(Sc,Ti,Al,Mg,Zr)_6Al_6O_{20}$], and thortveitite ($Sc_2Si_2O_7$) (Rubin and Ma 2017, 2021; Morrison and Hazen 2020). Such extreme elemental fractionation points to an early period of condensation of the most refractory elements in the protoplanetary disk.

Amoeboid olivine aggregates display isotopic and trace element compositions that indicate formation in a low-pressure, high-temperature environment with high gas-to-dust ratio—conditions that prevailed within the first 300 000 yrs of the protoplanetary nebula (Krot et al. 2004a). However, the forsterite-dominated mineralogy of AOAs indicates slightly lower

condensation temperatures compared to CAIs (Ebel 2006; Ebel et al. 2012). Wasserburg et al. (2012) suggested that AOAs are younger than the first CAIs by up to 25 000 yrs, a model supported by the observation that many AOAs incorporate small spinel-pyroxene-anorthite CAIs (Krot et al. 2004a). Note, however, that at least one group of CAIs (forsterite-bearing type B CAIs) evidently formed by melting AOAs, and thus are younger (Krot et al. 2001a; Bullock et al. 2012). In any event, AOAs, like CAIs, formed during the earliest period of the protoplanetary disk, prior to 4567.0 Ma.

Formation of planetesimals and proto-Jupiter.—Recent models of the origin and early evolution of the solar system underscore the important links between nebular dynamics and mineral condensation (Warren 2011; Budde et al. 2016; Kruijer et al. 2017; Desch et al. 2018; Burkhardt et al. 2019). Nebular gas and dust within 2 AU of the protosun were exposed at an early stage (within 100 000 yrs of the protosun's formation) to temperatures high enough to vaporize almost all constituents (Pollack et al. 1996; Warren 2011; Davis and Richter 2014; Kruijer et al. 2017), though a significant fraction of presolar grains, gas, and organic matter more remote from the Sun was not heated above a few hundred degrees Kelvin (Mendybaev et al. 2002; Cody et al. 2011).

Important constraints on the nature and timing of refractory inclusion formation are provided by a striking dichotomy in the isotopic characteristics of carbonaceous chondrites (CC) vs. non-carbonaceous chondrites (NC) meteorites, notably isotopes of O, Cr, Ti, Ni, and Mo, which reveal two distinct genetic lineages (Trinquier et al. 2007, 2009; Burkhardt et al. 2011; Warren 2011; Kruijer et al. 2017). The bimodal compositional characteristics of CC vs. NC meteorites is underscored by the distribution of CAIs, which occur much more frequently in CC meteorites. This concentration of CAIs beyond Jupiter's orbit contrasts with their rarity in NC meteorites, including ordinary chondrites and enstatite chondrites.

One model posits that CC parent bodies accreted beyond Jupiter's orbit—far from where CAIs are thought to have originated. NC parent bodies, by contrast, consolidated inside Jupiter's orbit (Warren 2011; Budde et al. 2016). According to this model, these two groups of planet-forming materials remained physically separated, most plausibly by the formation of embryonic Jupiter within the first 500 000 yrs of the protoplanetary disk (Lambrechts et al. 2014; Morbidelli et al. 2016; Desch et al. 2018; Kruijer et al. 2017). Jupiter's gravitational field created a barrier for exchange between NC meteorites of the inner solar system and CC meteorites beyond the ~3 AU orbit of Jupiter.

An early formation of embryonic Jupiter is consistent with other evidence for rapid planetesimal formation. Isotopic studies of iron meteorites suggest that their parent bodies must have reached diameters of 10 km to hundreds of kilometers and differentiated within the first 300 000 yrs (Kruijer et al. 2014), with Mars-sized objects forming significantly earlier than 1 million years, and perhaps as early as 100 000 yrs after the oldest CAIs (Chambers 2004; Chiang and Youdin 2010; Johansen et al. 2014). Note that the occurrence of protoplanets at this early stage of solar system evolution has important implications for the possible origins of some chondrule groups through impact-generated jetting or splashing (Johnson et al. 2018; Sanders and Scott 2018; however, for an opposing view see Baecker et al. 2017).

In spite of the isotopic differences between two chondrite populations, both NC (with a greater percentage of chondrules) and CC meteorites (with the majority of CAIs and AOAs) hold populations of highly refractory minerals that are thought to have formed within 2 AU of the protosun. One model posits that CAIs represent the earliest condensates (by ~4567.2 Ma), most of which were transported within the solar nebula's first 100 000 yrs by strong disk winds to beyond what would become Jupiter's orbit (Shu et al. 1996; though see Desch et al. 2010). This postulated dispersal and sequestration of CAIs resulted in the distinctive chemical and isotopic fractionation of solar system material, with carbonaceous meteorites predominating beyond the orbit of Jupiter (e.g., Kruijer et al. 2017). Many chondrules, which represent a second generation of condensates perhaps 1 to 5 million years after CAIs, formed primarily near the protosun, and the majority of these objects did not migrate from the inner solar system (Warren 2011; Kruijer et al. 2017; Desch et al. 2018), though other chondrules, notably those in carbonaceous chondrites, may have formed beyond the orbit of Jupiter (Rubin 2010, 2011).

Chondrules.—Most researchers conclude that chondrules formed significantly after CAIs, AOAs, and URIs, probably commencing ~4566 million years ago. Important evidence comes from composite chondrule-CAI objects and bulk chondrule compositions, which suggest that refractory inclusions were already present when chondrules formed (Rubin and Wasson 1988; Kita and Ushikubo 2012; MacPherson et al. 2012; Kawasaki et al. 2015; Krot et al. 2017).

Pb-Pb, Hf-W, and Al-Mg radiometric dating indicate that chondrules formed over an interval of ~4 to 5 million years (Bizzarro et al. 2017; Johnson et al. 2018; Kleine et al. 2018; Connelly and Bizzarro 2018). This extended chronology of chondrule formation is complicated by multiple paragenetic modes—i.e., different mechanisms for rapid heating—spanning several million years. According to the canonical view (however, see Krot 2019), the oldest chondrules appear to have formed ~1.5 million years after CAIs (e.g., Nagashima et al. 2018), as revealed by ^{26}Al-^{26}Mg isotope systematics. The rapid decay of short-lived ^{26}Al to ^{26}Mg (half-life ~0.71 million years) results in measurable excess ^{26}Mg in the most ancient Al-rich, Mg-poor minerals formed in the protoplanetary disk, with a systematic decrease in initial ^{26}Al/^{27}Al through the first few million years of solar system history.

Different groups of unequilibrated chondrules appear to have formed over relatively narrow time windows (Table 1). For example, CO and CV chondrules have both been dated as originating at 4565.1 ± 0.8 Ma (Kurahashi et al. 2008; Budde et al. 2015; Kleine et al. 2018), whereas CR chondrules formed more than a million years later at 4563.7 ± 0.6 Ma (Schrader et al. 2017; Kleine et al. 2018).

The formation of CB chondrules, the youngest group identified thus far and likely representing late-stage droplets of impact melts, is even more tightly constrained at 4562.5 ± 0.2 Ma (Krot et al. 2005; Gilmour et al. 2009; Bollard et al. 2015), suggesting a single origin event near the end of the era of chondrule formation.

The ages of chondrules in enstatite chondrites are poorly constrained, but they may have formed closer to the end of the interval of chondrule formation. Whitby et al. (2002)

employed iodine-xenon dating to estimate ages of EH chondrules to between 4564 and 4561 Ma, whereas Trieloff et al. (2013) dated individual presumably primary sphalerite grains to 4562.7 ± 0.5 Ma. Thus, chondrules in enstatite chondrites may be among the younger known groups.

In spite of the widespread agreement regarding a significant temporal gap of more than a million years between the end of CAI formation and the beginning of chondrule formation, an alternative hypothesis has recently emerged. Contrary to Al-Mg and Hf-W results, recent Pb-Pb ages suggest that the earliest chondrules formed contemporaneously with CAIs at ~4567.3 Ma (Connelly et al. 2012; Bollard et al. 2017; Connelly and Bizzarro 2018; Krot 2019). If heterogeneities existed in the protoplanetary disk's initial $^{26}Al/^{27}Al$, then comparative $^{26}Al/^{26}Mg$ dating of CAIs and chondrules might be invalid (Larsen et al. 2011; Krot et al. 2012; Luu et al. 2016). Indeed, a few chondrules from unequilibrated ordinary chondrites display ^{206}Pb-^{207}Pb ages that are equal to, if not slightly older than, 4567.3 Ma (Connelly and Bizzarro 2018; see Krot 2019 for a review). If this reinterpretation is correct, then some chondrules formed contemporaneously with CAIs (Kita et al. 2015; Schrader et al. 2017; Nagashima et al. 2018), with the majority of chondrules forming during the first 1 million years of the protoplanetary disk (Connelly and Bizzarro 2018). Resolution of these discrepancies remains an important challenge in chondrite chronology. However, whatever their ages relative to refractory inclusions, all primary chondrule minerals appear to have formed within the first 6 million years of solar system history, and they are thus among the oldest known solid phases. In the following sections we consider the primary mineralogy of chondrules.

Primary mineralogy of chondrules

The evolutionary system of mineralogy focuses on mineral "natural kinds," which we define as types of minerals that possess distinctive suites of chemical and physical attributes that arise from a well-defined formation process during a well-characterized interval of planetary evolution (Hazen 2019). The defining attributes of a mineral natural kind, in addition to its major element composition and atomic structure as employed by the IMA, can include any diagnostic combination of physical, chemical, and/or (in the case of terrestrial minerals younger than ~3.8 billion years) biological features of the mineral grain or its petrologic and environmental context. Because minerals display numerous relevant attributes, including trace and minor elements, stable and radioactive isotopes, crystal size and morphology, exsolution, twinning, zoning, solid and fluid inclusions, age, petrologic context, and more, this approach to classification relies on large and robust databases of mineral properties. Thus, we embrace the development of findable, accessible, interoperable, and reusable (i.e., "FAIR") mineral data resources, which provide the essential foundation for data-driven discovery in mineralogy (Ghiorso and Sack 1995; Holland and Powell 1998; Lehnert et al. 2000, 2007; Ghiorso et al. 2002; Downs and Hall-Wallace 2003; Downs 2006; Hazen et al. 2011, 2019a, 2019b; Golden et al. 2013; Hazen 2014; Morrison et al. 2020; see also mindat.org and rruff.info/ima, accessed 7 April 2020).

Primary chondrule minerals fit the definition of distinct natural kinds, because: (1) all of these minerals formed in a protoplanetary disk context of high local dust-to-gas relative to

solar average; (2) all of these minerals emerged within individual objects <5 cm diameter as a consequence of discrete rapid heating, partial to complete melting, and rapid cooling events; and (3) all chondrules appear to have formed within a narrow time interval between ~4567 and ~4561 million years ago. These minerals differ, therefore, from earlier stellar and nebular condensates (i.e., presolar grains and refractory inclusions) that apparently formed in regions of relatively low dust-to-gas ratio under sustained high temperatures. They also differ from contemporaneous and subsequent minerals that formed in the contexts of accreting and differentiating protoplanetary bodies.

In this context, we recognize 43 primary chondrule minerals, including clinoenstatite, plagioclase, kamacite, and many other phases (Table 2), as distinct natural kinds (e.g., primary chondrule clinoenstatite, or "*PC clinoenstatite*"). Note that we have decided not to further subdivide minerals according to types of chondrules, types of their host chondrite meteorites, distinct mineral morphotypes, or other criteria.

It is true that the majority of chondrules in any one chondrite group typically have similar properties—average size, textural type, and oxygen isotope ratios, for example—which suggest a local, common origin for most of the chondrules in any given meteorite group (Jones 2012; Kita and Ushikubo 2012). Nevertheless, there are also diverse chondritic components, including CAIs, AOAs, URIs, and atypical chondrules, which reveal a diversity of spatial and temporal sources. Furthermore, the uniformity in chondrule size distribution in any one chondrite group, coupled with the characteristic differences in average chondrule size from one chondrite group to the next, do not necessarily reflect a common origin for chondrules in a given group. Rather, these size characteristics may be at least in part the result of aerodynamic sorting, for example within nebular winds, during turbulent accretion at the surfaces of chondrule parent bodies, or in an asteroid's loosely consolidated regolith during outgassing (Akridge and Sears 1999; Kuebler et al. 1999; Cuzzi et al. 2001; Teitler et al. 2010). In that case, size sorting of some chondrules could have occurred long after chondrule formation and subsequent mixing. However, aerodynamic sorting cannot account for all differences among chondrules in a given meteorite (Rubin 2010). Even if most chondrules formed in proximity to each other, and if they accreted with a matrix that was formed more or less contemporaneously (e.g., see Hezel et al. 2018, and references therein), the emergence of chondrite bulk characteristics always postdates the origin of the primary chondrule minerals. Therefore, in this review, we lump all primary chondrule mineral occurrences for each mineral species.

We suggest that any attempt to subdivide primary chondrule minerals by combinations of attributes at this time would be speculative and premature. An important advantage of the evolutionary system of mineralogy, but one that also adds an admitted degree of arbitrariness to its protocols, is that individual mineral experts can subdivide IMA species into natural kinds according to their specific needs. Experts in chondrule textures, stable isotopes, or cathodoluminescence may thus wish to add mineral subtypes based on unambiguous differences in mineral attributes. However, lacking sufficiently robust chondrule mineral data resources, we choose not to subdivide primary chondrule minerals at this time beyond IMA recognized species or well-defined types of amorphous phases.

Systematic evolutionary mineralogy—Part III: Primary chondrule mineralogy

In the following section we enumerate 43 primary chondrule minerals, which are defined as solid condensed phases that formed during rapid heating and cooling of chondrule precursors to temperatures close to the liquidus (at $<10^{-2}$ atm ambient pressure; i.e., not shock-induced phases), as well as phases formed during subsequent chondrule cooling. Primary chondrule minerals must have formed prior to sedimentation onto larger bodies and incorporation into chondrites. Most primary chondrule minerals formed by melt crystallization in partially to fully molten droplets, but we also include: (1) minerals formed by reactions between condensed phases and hot nebular gas (Krot et al. 2004b; Libourel et al. 2006), and (2) varied solid-state reactions during initial cooling, including silicate glass devitrification, polymorphic transformations, exsolution, and cation ordering (e.g., Rubin and Ma 2021).

In Table 2 we tabulate 43 primary chondrule minerals, encompassing 40 IMA-approved species, the unapproved species ferropseudobrookite, and two amorphous phases. These primary chondrule minerals incorporate 15 structurally essential chemical elements, as well as three significant minor elements (Fig. 1).

Each mineral natural kind is given a binomial designation: the first name, in this case "*PC*" for all examples, indicates primary chondrule minerals, whereas the second name for the most part conforms to the name of an approved IMA mineral species. However, in several instances we deviate from IMA nomenclature:

- **Schreibersite [$(Fe,Ni)_3P$] and nickelphosphide [$(Ni,Fe)_3P$]:** We lump these two IMA-approved phosphide species into *PC schreibersite* because they represent a continuous solid-solution series, almost always with Fe > Ni, and they form by the same primary mechanisms.
- **Armalcolite and ferropseudobrookite:** Fujimaki et al. (1981a, 1981b) used "ferropseudobrookite" ($Fe^{2+}Ti_2O_5$) as the name for the Mg-absent end-member related to armalcolite [$(Mg,Fe^{2+})Ti_2O_5$]. Though not an approved IMA mineral species, we refer to this occurrence as *PC ferropseudobrookite*.
- **Chromite:** Chromite ($Fe^{2+}Cr_2O_4$) and other Cr-bearing oxide spinel group minerals are common primary phases in chondrules. Many occurrences conform to the IMA definition of chromite, but a few Cr-rich grains are closer to hercynite ($Fe^{2+}Al_2O_4$) or magnesiochromite ($MgCr_2O_4$) end-members, at times with significant spinel ($MgAl_2O_4$) and ülvospinel ($Fe^{2+}Ti_2O_4$) content. We lump all of these Cr-bearing oxide spinel minerals together into *PC chromite*.
- **Roedderite and merrihueite:** Roedderite and merrihueite, $[(Na,K)_2Mg_5Si_{12}O_{30}]$ and $[(K,Na)_2(Fe,Mg)_5Si_{12}O_{30}]$, respectively, form a continuous solid-solution of phases formed by the same primary process, and thus represent a single natural kind in our evolutionary system. Because most examples fall within the roedderite field, we lump occurrences together and assign the name *PC roedderite.*

- **Orthoenstatite:** Unlike in most terrestrial igneous rocks, the monoclinic (space group $P2_1/c$) form of $MgSiO_3$, clinoenstatite, is the most common polymorph. Therefore, for clarity we employ the common name "orthoenstatite" for orthorhombic $MgSiO_3$ (space group *Pbca*) instead of the IMA-approved name, "enstatite."
- **Silica glass and silicate glass:** Glassy phases are important components of rapidly quenched chondrules, with some chondrules approaching 100 vol% solid amorphous silicate. These condensed phases are not approved by the IMA, but we recognize *PC silica glass* (i.e., close to end-member SiO_2) and *PC silicate glass*.

Native elements and alloys

Several alloys of iron and nickel, as well as the carbon allotrope graphite, occur as primary chondrule minerals. Iron-nickel alloys are among the most common of these phases, comprising several vol% of most chondrules and more than 90 vol% of some metal-rich examples (Brearley and Jones 1998; Scott and Krot 2014; Rubin and Ma 2021). Fe-Ni alloys, which typically incorporate Co, Cr, Cu, and other siderophile elements, condensed from the solar nebula at temperatures estimated between 1350 and 1450 K (Ebel and Grossman 2000; Campbell et al. 2005b). They occur as the IMA-approved minerals iron (though usually cited as "kamacite" in the meteoritics literature), taenite, tetrataenite, and awaruite, as well as the distinctive exsolved mixture of kamacite and taenite known as "plessite." Fe-Ni alloys commonly hold significant amounts of other elements; high C, P, or Si contents, for example, may lead to exsolution of new minerals, such as graphite, carbides, schreibersite, perryite, or silica glass (see below). Note that alloys dominant in copper and in cobalt have been reported from chondrites, but they appear to be secondary phases and will be considered in Parts IV and V (Rubin 1990, 1994a; Brearley and Jones 1998; Rubin and Ma 2021).

Iron (α-Fe).—Body-centered cubic ($Im3m$) iron, commonly referred to as kamacite in the meteoritics literature, is the most stable low-Ni iron alloy and is among the most common primary chondrule minerals. We designate this phase "*PC iron*" (see Table 2). PC iron is found with up to ~8 wt% Ni, though typical Ni contents are 3 to 7 wt%. Kamacite occurs in a range of textures (e.g., Brearley and Jones 1998; Rubin and Ma 2021), for example, as blebs to 50 μm diameter in mesostasis of type I chondrules, often in association with sulfides; in ordinary chondrites as polycrystalline intergrowths with taenite and troilite; as spheroidal grains, often concentrated near the chondrule edge; as globules up to 1 mm diameter in enstatite chondrites; in irregular masses, often in association with sulfides and/or carbides; and as irregular grains that are likely fragments from previous generations of chondrules. PC iron grains are sometimes zoned, with cores typically more Ni-rich than rims (Nagahara 1982).

While most PC iron crystallized as an igneous phase from the metal-rich fraction of immiscible metal-silicate chondrule melts, kamacite in CB group chondrules may have formed by condensation directly from a vapor plume generated by an impact on a differentiated body (Rubin et al. 2003; Oulton et al. 2016; Rubin and Ma 2021). Kamacite in

these CB metal-rich chondrules occurs in a distinctive morphology, as globules up to a centimeter in diameter.

Taenite [γ-(Fe,Ni)].—The primitive cubic (*Pm*3*m*) alloy of iron and nickel, referred to as "austenite" in the metallurgical literature, typically has ~25 to 35 wt% Ni. *PC taenite* commonly occurs with PC iron, sulfides, and other opaque phases in rounded grains; as crystals that are isolated or associated with kamacite; or as polycrystalline aggregates (Afiattalab and Wasson 1980; Bevan and Axon 1980; Scott and Rajan 1981; Nagahara 1982; Brearley and Jones 1998). Taenite crystals, which are most abundant in Ni-rich LL ordinary chondrites, are commonly zoned from cores with 25 to 35 wt% Ni to rims that may exceed 50 wt% Ni (Wood 1967).

Taenite can incorporate significant amounts of P or C, which may exsolve as phosphides or carbides on cooling (e.g., Brearley and Jones 1998). In addition, under conditions of relatively slow cooling, taenite may exsolve thin (<2 μm thick) lamellae of kamacite to produce the distinctive mixed phase known as "plessite" (Massalski et al. 1966; Buchwald 1975; Brearley and Jones 1998; Goldstein and Michael 2006).

Tetrataenite (FeNi).—Tetrataenite, a low-temperature ordered Fe-Ni alloy (tetragonal, *P*4/*mmm*; Clarke and Scott 1980), is a widely distributed, though volumetrically minor, phase in type 3 (unequilibrated) ordinary chondrites (Bevan and Axon 1980; Scott and Rajan 1981; Nagahara 1982; Rubin 1994b; Rubin and Ma 2021). *PC tetrataenite* occurs as 10 to 60 μm diameter grains or as rims up to 5 μm thick on taenite (Taylor and Heymann 1971; Scott and Clarke 1979), forming through cooling and/or annealing of taenite below 350 °C (Clarke and Scott 1980). As such, tetrataenite is one of several chondrule minerals that spans a continuous paragenetic range from primary to secondary. Though ideally a 50:50 mixture of Fe and Ni, the observed range of Ni in chondritic tetrataenite grains is 48 to 57 wt%, with minor Co and Cu. Metal grains in carbonaceous chondrites may significantly exceed 50 wt% Ni, resulting in fine-grained mixtures of tetrataenite and awaruite (Kimura and Ikeda 1992).

Awaruite (Ni_2Fe to Ni_3Fe).—The Ni-dominant alloy awaruite, with face-centered cubic structure (*Fm*3*m*), is rare as a primary phase in chondrules (Taylor et al. 1981; Smith et al. 1993), and it is possible that all such occurrences are of secondary origin through aqueous alteration (Rubin, personal communication, 4 June 2020). *PC awaruite* typically occurs with 65 to 75 wt% Ni and forms as small anhedral grains in association with sulfides and carbides. Rubin (1991) described euhedral zoned crystals of presumably PC awaruite from a low-Fe olivine chondrule in the Allende CV chondrite. PC awaruite is thought to form in oxidizing nebular environments, in which oxidation of kamacite results in a Ni-enriched metal, crystallization of Ni-rich taenite, and subsequent transformation of taenite into tetrataenite and awaruite at temperatures below ~500 °C. Awaruite also forms via secondary processes in chondrules and chondrite matrices (Pederson 1999; Rubin and Ma 2021).

Graphite (C).—*PC graphite* is a common, if minor, primary chondrule mineral in enstatite chondrites, where it occurs as irregular to euhedral crystal inclusions up to 50 μm diameter in kamacite (Leitch and Smith 1980). Graphite probably formed by exsolution from a C-rich Fe-Ni alloy on cooling (Keil 1968). Keil (1968) noted that the amount of exsolved graphite

increases with metamorphism; therefore, graphite is likely one of several chondrule minerals (e.g., troilite, olivine, and plagioclase) that occurs in a continuum as both a primary and secondary phase. Furthermore, other occurrences of less well-ordered graphite in chondrules have been ascribed to impact processes and are considered in Part IV of this series (Rubin 1997a; Rubin and Scott 1997).

Carbides

The iron carbides, cohenite and haxonite, are common primary chondrule phases (Brearley and Jones 1998; Rubin and Ma 2021). The rare iron carbide edscottite (Fe_5C_2) has been reported as a matrix phase in the Semarkona LL3.0 ordinary chondrite, but it has not yet been observed as a primary chondrule phase (Ma and Rubin 2019).

Cohenite [$(Fe,Ni)_3C$].—*PC cohenite* occurs in association with other opaque phases in some type 3 ordinary chondrites (Taylor et al. 1981; Scott et al. 1982; Scott and Jones 1990; Krot et al. 1997b), as well as in enstatite chondrites (Mason 1966; Herndon and Rudee 1978; Rubin 1983; Shibata 1996). In unequilibrated ordinary chondrites, it is found as polycrystalline masses with magnetite and sulfides in carbide-magnetite assemblages, which may have formed by reactions of kamacite and troilite with nebular gas (Taylor et al. 1981), though Krot et al. (1997b) and Rubin (personal communication; 27 March 2020) suggest a later origin by reaction with C-H-O fluids. In the CO3 chondrite Allan Hills 77307, cohenite occurs as grains <30 μm in kamacite (Shibata 1996). PC cohenite contains up to ~4 wt% Ni (Scott and Jones 1990).

Haxonite [$(Fe,Ni)_{23}C_6$].—*PC haxonite* containing up to ~5 wt% Ni occurs with PC cohenite in the carbide-magnetite assemblages of unequilibrated (type 3) ordinary chondrites, as well as in CO3 and EH3 chondrites (Scott and Jones 1990; Rubin 1983; Shibata 1996; Rubin and Ma 2021). An alternative view posits that carbide-magnetite assemblages are of secondary origin through parent-body aqueous alteration (Rubin, personal communication, 4 June 2020). If so, then all haxonite occurrences in chondrules may be secondary, as well.

Nitrides and oxynitrides

Osbornite (TiN) and nierite (Si_3N_4) have been reported from chondrites, but their presence has been ascribed to parent body metamorphism, shock alteration, or (in the case of some isotopically anomalous nierite grains) presolar origins (Buseck and Holdsworth 1972; Grossman et al. 1988; Scott 1988; Weisberg et al. 1988; Alexander et al. 1994; Russell et al. 1995; Rubin 1997b; Hazen and Morrison 2020; Rubin and Ma 2021).

Sinoite (Si_2N_2O).—Sinoite (Si_2N_2O) is known as both a primary chondrule mineral and as an impact product in enstatite chondrites (El Goresy et al. 2011; Lin et al. 2011; see also Part IV). Micrometer-scale *PC sinoite* needles, possibly condensed from nebular gas, occur in metal nodules from an EL3 clast from the Alhamata Sitta breccia (El Goresy et al. 2011; Lin et al. 2011). Associated minerals include graphite, oldhamite, enstatite, and Ca-rich clinopyroxene.

Phosphides

With the exception of primary chondrule schreibersite, phosphide minerals are not known from the most unequilibrated chondrites. Occurrences of andreyivanovite (FeCrP) and florenskyite (FeTiP) are also reported from chondrite meteorites, but their origins have been ascribed to impact processes (Ivanov et al. 2000; Zolensky et al. 2008).

Schreibersite [$(Fe,Ni)_3P$].—*PC schreibersite* exsolves on cooling from P-rich Fe-Ni alloys in type 3 ordinary chondrites and enstatite chondrites, where it is closely associated with kamacite (Brearley and Jones 1998; Rubin and Ma 2021). It typically occurs as rims on, or inclusions in, kamacite, with individual grains as large as 300 μm in diameter. Schreibersite can contain up to ~50 wt% Ni, and often incorporates more than 1 wt% Co and Cr, as well (Wasson and Wai 1970; Rambaldi and Wasson 1984; Zanda et al. 1994; see Brearley and Jones 1998, Table A3.32). Lehner et al. (2010) investigated trace and minor elements in schreibersite associated with kamacite and perryite and concluded that some schreibersite first formed by condensation from a reduced gas.

Ni-dominant grains of schreibersite have been recognized by the IMA as the mineral "nickelphosphide"—ideally Ni_3P, but originally described as $(Ni,Fe)_3P$ (Britvin et al. 1999). However, because this phase is evidently part of a continuous solid-solution series, and a single paragenetic mode by exsolution from an Fe-Ni alloy on cooling is invoked, we lump nickelphosphide with the much more common schreibersite.

Silicides

Meteorites hold at least eight different Fe-, Ni-, and Mnbearing silicides (Rubin and Ma 2021), but perryite is the only example thought to be a primary chondrule mineral.

Perryite [$(Ni,Fe)_8(Si,P)_3$].—*PC perryite* is found as a widespread, if volumetrically minor, phase in type 3 unequilibrated enstatite chondrites (Keil 1968; Reed 1968; Lehner et al. 2010). It occurs in association with kamacite, schreibersite, sulfides, and other rare phases in the reduced enstatite chondrule mineral suite (Rubin and Ma 2021). The composition of PC perryite generally has >60 mol% Si in the Si-P site and >90 mol% Ni in the Ni-Fe site (Wasson and Wai 1970; El Goresy et al. 1988; see Brearley and Jones 1998, Table A3.33). Lehner et al. (2010) suggest that perryite formed initially by condensation from a reduced gas and was then incorporated as inclusions in kamacite, while additional perryite precipitated from Si- and P-saturated Fe-Ni alloy on cooling.

Sulfides

More than 50 sulfide minerals have been identified in meteorites (Rubin and Ma 2021), at least nine of which are thought to occur as primary chondrule minerals. However, the enumeration of primary vs. secondary sulfide phases in chondrules (as well as in the matrix, refractory inclusions, and metal-rich portions of chondrites) is challenging (e.g., Weisberg and Kimura 2012; Singerling and Brearley 2018). Sulfide minerals arise from a continuum of processes involving direct condensation from a hot gas phase, reactions between S-rich gas and condensed phases, crystallization from a melt, exsolution from metal, and a variety

of alteration processes associated with impacts, metamorphism, and aqueous/hydrothermal interactions.

Troilite is by far the most common primary chondrule sulfide; it is the only sulfide to occur widely in CC, OC, and EC chondrules. The sulfides of chondrules in enstatite chondrites are of special interest, as these low-silica rocks contain unusual sulfides of elements such as Na, K, Mg, Ca, Mn, Cr, and Ti that more typically form oxides and silicates (Brearley and Jones 1998; Avril et al. 2013; Weyrauch et al. 2018; Rubin and Ma 2021). Thus, alabandite, caswellsilverite, daubréelite, niningerite, oldhamite, and wassonite are confirmed primary phases. However, other sulfides from enstatite chondrites, including bornite, chalcopyrite, covellite, djerfisherite, idaite, pyrite, and pyrrhotite, are almost certainly secondary minerals that formed by impact and/or parent body processing (e.g., El Goresy et al. 1988; Weisberg and Kimura 2012; Ebel and Sack 2013). For representative analyses of chondrule sulfides see Brearley and Jones (1998), Tables A3.24 to A3.31.

Troilite (FeS).—*PC troilite* is one of the most abundant primary phases in chondrules (Brearley and Jones 1998, and references therein, Table A3.24). In unequilibrated ordinary chondrites it occurs as rounded grains with Fe-Ni alloys (Jones and Scott 1989; Jones 1990, 1996; Rubin et al. 1999), as a constituent of carbide-magnetite assemblages (Krot et al. 1997b), as an accessory phase in silica-rich chondrules (Brigham et al. 1986), and in metal-troilite rims surrounding chondrules (Lauretta et al. 1996). In carbonaceous chondrites, PC troilite occurs, for example, in the chondrules of CO and CK chondrites as spherical or irregular metal-sulfide assemblages (Rubin et al. 1985, 1988; Shibata 1996; Singerling and Brearley 2018). And troilite comprises up to 10 vol% of chondrules in some enstatite chondrites (El Goresy et al. 1988; Ikeda 1989a). Ikeda (1989a) recognized several different types of troilite-bearing EC nodules, including kamacite-troilite, niningerite-troilite, and djerfisherite-troilite nodules, as well as clasts in association with daubréelite (El Goresy et al. 1988).

Pentlandite [$(Fe,Ni)_9S_8$].—*PC pentlandite* likely occurs as a primary chondrule mineral in unequilibrated ordinary chondrites (Jones and Scott 1989; Jones 1990, 1996), often intergrown with troilite in metal-sulfide or carbide-magnetite aggregates (Krot et al. 1997b). Barth et al. (2018) report pentlandite in association with magnetite and troilite in a high-temperature association from the Acfer 094 unequilibrated carbonaceous chondrite—an occurrence that suggests formation by reaction of Fe-Ni metal with hot S-rich nebular gas prior to parent body accretion. Chondrules in carbonaceous chondrites also contain accessory pentlandite in association with Fe-Ni metal, troilite, and/or magnetite (Scott and Jones 1990). Note, however, that Rubin (personal communications, 27 March 2020) suggests that pentlandite occurrences in chondrules, as well as the carbide-magnetite assemblages in which they are found, are almost always secondary.

Alabandite (MnS).—*PC alabandite* is one of several unusual sulfides found in the highly reduced assemblages within chondrules of enstatite chondrites (Mason 1966; Buseck and Holdsworth 1972; Fogel 1997; Avril et al. 2013; Weyrauch et al. 2018). *PC alabandite* [(Mn,Fe)S] is found exclusively in EL chondrites, in which it typically incorporates 10 to 30 mol% FeS, and is sometimes given the name “ferroan alabandite” (e.g., Brearley and Jones

1998; Weisberg and Kimura 2012). Alabandite also forms a solid solution with niningerite (MgS), with compositions up to ~10 mol% MgS (Rubin 1984b; Weyrauch et al. 2018; see Brearley and Jones 1998, Table A3.25 and A3.26).

Caswellsilverite ($NaCrS_2$).—*PC caswellsilverite* is a rare accessory phase in chondrules of enstatite chondrites, found in association with alabandite, daubréelite, oldhamite, and other unusual sulfides (Mason 1966; El Goresy et al. 1988; Ikeda 1989a; Rubin and Ma 2021).

Daubréelite ($FeCr_2S_4$).—*PC daubréelite* occurs as one of several unusual sulfides in reduced chondrule assemblages in enstatite chondrites (Mason 1966; Buseck and Holdsworth 1972; Ikeda 1989a; Izawa et al. 2010; Avril et al. 2013). It often occurs in association with troilite, from which it may have exsolved on cooling (El Goresy et al. 1988).

Niningerite (MgS).—Keil and Snetsinger (1967) described the rare magnesium sulfide niningerite from reduced mineral assemblages in EH enstatite chondrites, in which it may constitute the most abundant chondrule sulfide mineral. *PC niningerite* has been described from several EH3 enstatite chondrites in association with other rare sulfides, notably oldhamite, and in nodules with Fe-Ni metal, troilite, and silicate (El Goresy et al. 1988; Ikeda 1989a; Izawa et al. 2010; Avril et al. 2013; Weyrauch et al. 2018). Niningerite invariably incorporates iron (up to ~30 mol% FeS in EH3, with greater FeS contents in equilibrated chondrules) and manganese (<20 mol% MnS); it typically displays Mg-Fe-Mn zoning (Ehlers and El Goresy 1988; see Brearley and Jones 1998, Table A3.25). The Fe-dominant phase, named keilite, is only known from enstatite chondrites that have been shock melted (Shimizu et al. 2002).

Oldhamite (CaS).—*PC oldhamite* is a common accessory primary chondrule phase in enstatite chondrites, where it occurs as small grains in metal-sulfide nodules with other reduced phases, including alabandite, caswellsilverite, daubréelite, and niningerite (Mason 1966; Crozaz and Lundberg 1995; Fogel 1997; Nakamura-Messenger et al. 2012; Weyrauch et al. 2018). Calcium sulfide has also been reported as crystals up to 200 μm diameter within a metal matrix in the ungrouped, highly reduced meteorite Acfer 370 (Pratesi et al. 2019). Oldhamite in EH3 chondrites is close to end-member composition, with minor Mg, Cr, and Fe (El Goresy et al. 1988; Ikeda 1989a).

Sphalerite (ZnS).—*PC sphalerite* occurs as large unzoned primary crystals in EH3 enstatite chondrite Y-691, though it is more commonly encountered in chondrites as a secondary phase that occurs as “porous grains” associated with the breakdown of djerfisherite (El Goresy and Ehlers 1989).

Wassonite (TiS).—Nakamura-Messenger et al. (2012) described *PC wassonite* as a primary chondrule phase from the Yamato 691 EH3 enstatite chondrite, where it was found as 12 sub-μm grains in a barred olivine chondrule crystallized from a melt.

Oxides

Nine oxide phases, incorporating Mg, Ca, Fe^{2+}, Al, Cr, Fe^{3+}, Ti, and Zr as essential elements, have been described as primary chondrule minerals (Brearley and Jones 1998; Rubin and Ma 2017, 2021). Of these phases, only three (spinel, chromite, and magnetite) are widespread as primary minerals in chondrules, while four (armalcolite, perovskite, rutile, and zirconolite) are known only as minor phases in plagioclase-olivine inclusions from carbonaceous chondrites (Sheng et al. 1991a). A single occurrence of micrometer-scale corundum grains with high dislocation density from a chondrule in the Allende CV chondrite appears to be a shock phase (Müller et al. 1995) and is considered in Part IV.

Spinel Group Oxides [$(Mg, Fe^{2+})(Al,Cr,Fe^{3+})_2O_4$]

Three members of the spinel group of oxides—spinel (ideally $MgAl_2O_4$), chromite ($Fe^{2+}Cr_2O_4$), and magnetite $\left(Fe^{2+}Fe_2^{3+}O_4\right)$—are the most common primary oxide phases in chondrules. Significant solid solution among other end-members, including hercynite ($Fe^{2+}Al_2O_4$), magnesiochromite ($MgCr_2O_4$), and ülvospinel $\left(Fe^{2+}Fe_2^{3+}O_4\right)$, is observed (e.g., Brearley and Jones 1998, see Table A3.6). However, almost all primary chondrule spinel group minerals appear to fall well within the compositional fields of three end-members—*PC spinel*, *PC chromite*, and *PC magnetite*. Note that spinel crystals in the chromite-hercynite-magnesiochromite compositional field have been described from chondrules in CV carbonaceous chondrites (Weinbruch et al. 1990; Müller et al. 1995), but we lump these examples together as *PC chromite* because they form a continuous solid solution with other Cr-rich oxide spinels and they arise by the same paragenetic processes. Note that we employ the names "*PC spinel*," "*PC chromite*," and "*PC magnetite*" to designate three distinct complex *phase regions*—not the end-member compositions.

Spinel ($MgAl_2O_4$).—Spinel, ranging in composition from near end-member $MgAl_2O_4$ to examples with significant Fe^{2+}, Cr^{3+}, and/or Ti^{4+}, is one of the most common primary oxide phases in chondrules. We use the name *PC spinel* to designate this complex phase space, which is found in unequilibrated ordinary chondrites (Ikeda 1980), notably in their Ca-Al-rich chondrules in association with fassaite and plagioclase (Bischoff and Keil 1983, 1984; McCoy et al. 1991a; Wang et al. 2016). PC spinel is an occasional minor phase in CO3 carbonaceous chondrites, typically in association with olivine in type I and II chondrules (McSween 1977b; Ikeda 1982). In CM chondrites, PC spinel occurs in association with fassaite (Simon et al. 1994), and as inclusions in forsterite (Fuchs et al. 1973) with variable Fe^{2+} and Cr contents to several wt%. Near end-member spinel grains are associated with fassaite, forsterite, and plagioclase in plagioclase-olivine inclusions in CV chondrites (Sheng et al. 1991a). Finally, PC spinel has been identified from barred olivine-pyroxene chondrules in the Yamato-691 enstatite chondrite, where it occurs in association with fassaite and/or plagioclase (Ikeda 1988a, 1989b).

Chromite ($Fe^{2+}Cr_2O_4$).—Oxide spinel phases with significant Cr content are common primary and secondary accessory phases in various chondrules and their associated opaque assemblages. Most of these occurrences conform to the IMA definition of chromite, as they are closer in composition to $Fe^{2+}Cr_2O_4$ than to other spinel end-members. Other examples,

either on average or in zoned regions, may lie closer to the spinel ($MgAl_2O_4$), hercynite ($Fe^{2+}Al_2O_4$), or magnesiochromite ($MgCr_2O_4$) end-members, at times with significant ülvospinel ($Fe^{2+}Ti_2O_4$) content, as well (for representative analyses see Brearley and Jones 1998, Table A3.6). For the purposes of primary chondrule mineralogy, we lump these compositionally varied Cr-bearing phases together as *PC chromite*.

PC chromite is known from relatively unequilibrated ordinary chondrites as euhedral crystals in mesostasis (Jones 1990; Johnson and Prinz 1991), as inclusions in olivine (Ruzicka 1990), and in Na-Al- and Na-Cr-rich chondrules associated with Na-rich glass and olivine (McCoy et al. 1991a). Chromite crystals commonly incorporate inclusions of primary silicates, notably forsterite, Ca-poor pyroxene, and calcic pyroxene (Alwmark et al. 2011). Rare chromium-rich chondrules <300 μm in diameter feature chromite grains in mesostasis with plagioclase (Ramdohr 1967; Krot et al. 1993). OC chromite is variable in composition, at times extending into the spinel compositional field, and grains are often zoned (Bunch et al. 1967; Ikeda 1980; Krot et al. 1993).

In type 3 carbonaceous chondrites, chromite occurs as a primary chondrule phase in type IIA chondrules (relatively oxidized and olivine-dominant) in the Allende CV3, Renazzo CR, in CO chondrites within olivine phenocrysts, and Adelaide (ungrouped) meteorites (Davy et al. 1978; Johnson and Prinz 1991; Weinbruch et al. 1994; Murakami and Ikeda 1994; Ikeda and Kimura 1995; Wasson and Rubin 2003), though it is more commonly observed in assemblages that have been thermally altered (Tomeoka and Buseck 1990; Weinbruch et al. 1990; Müller et al. 1995).

Magnetite $\left(Fe^{2+}Fe_2^{3+}O_4\right)$**.—***PC magnetite* is found in a variety of contexts in chondrules, some of which may be primary in origin (though Rubin, personal communication, 4 June 2020, suggests that all chondrule magnetite occurrences are secondary). Barth et al. (2018) reported magnetite in association with pentlandite and troilite in a high-temperature association from the Acfer 094 unequilibrated carbonaceous chondrite; they suggested that magnetite formed by reaction of Fe-Ni metal with hot O-rich nebular gas. In CO, CV, and other relatively unequilibrated carbonaceous chondrites, magnetite is often found in aggregates in association with kamacite and troilite (Haggerty and McMahon 1979; Nagahara and Kushiro 1982; Ikeda 1983; Scott and Jones 1990). Note that magnetite is also often found as a secondary phase in ordinary and carbonaceous chondrites (Brearley and Jones 1998), for example, by the oxidation of troilite (Herndon et al. 1975).

Rutile (TiO_2).—Rutile is known as a primary chondrule phase only as a minor accessory mineral from plagioclase-olivine inclusions (Sheng et al. 1991a). *PC rutile* occurs in grains up to 50 μm in diameter associated with armalcolite, ilmenite, perovskite, and fassaite.

Ilmenite ($FeTiO_3$).—*PC ilmenite* is a minor primary accessory phase in Na-Al-rich chondrules in type 3 ordinary chondrites (Bischoff and Keil 1984). *PC ilmenite* also occurs as a minor accessory phase in plagioclase-olivine inclusions, where it is found as grains up to 50 μm in diameter with armalcolite, perovskite, and rutile (Sheng et al. 1991a).

Armalcolite [$(Mg,Fe^{2+})Ti_2O_5$].—Sheng et al. (1991a) report *PC armalcolite* as a rare accessory primary phase in plagioclaseolivine inclusions from carbonaceous chondrites, in which armalcolite is accompanied by several Ti-bearing oxides, including ilmenite, perovskite, rutile, and zirconolite. *PC armalcolite's* Mg/Fe ratio ranges from 1.2 to 4.3.

Ferropseudobrookite ($Fe^{2+}Ti_2O_5$).—Fujimaki et al. (1981a, 1981b) described two euhedral crystals of "ferropseudobrookite" from an EL3 chondrite, Allan Hills 77015, in a unique Mg-poor chondrule with albite, a silica mineral, and glass. Note that ferropseudobrookite (ideally $Fe^{2+}Ti_2O_5$, though here it contains significant Ca, Ti, and Cr in the Fe^{2+} site) is not an approved IMA species. Nevertheless, we recognize *PC ferropseudobrookite*, as this Fe^{2+}-dominant, Mg-absent mineral differs from both armalcolite and pseudobrookite $\left(Fe_2^{3+}TiO_5\right)$.

Perovskite ($CaTiO_3$).—*PC perovskite* is one of several minor accessory phases found as primary chondrule minerals only in plagioclase-olivine inclusions (Sheng et al. 1991a). It occurs as 10 to 50 μm diameter grains in association with armalcolite, ilmenite, and rutile.

Zirconolite ($CaZrTi_2O_7$).—*PC zirconolite* occurs as micrometer-scale irregular blebs surrounding perovskite in plagioclaseolivine inclusions (POIs) from unequilibrated carbonaceous chondrites (Sheng et al. 1991a). Zirconolite grains from POIs feature significant Fe^{2+} substitution for Ca, while they hold as much as 10 wt% Y_2O_3 plus REE oxides.

Phosphates

Most chondritic phosphate minerals appear to be secondary phases, formed through aqueous and thermal alteration of prior P-bearing phases, notably as fine-grained constituents of matrices (e.g., Rubin and Grossman 1985; Jones et al. 2014; Lewis and Jones 2016; Rubin and Ma 2017). However, merrillite has been found in unusual glass-rich, Si-rich, or Cr-rich chondrules from unequilibrated ordinary chondrites—occurrences that probably represent primary chondrule mineralization.

Merrillite [$Ca_9NaMg(PO_4)_7$].—Krot and Rubin (1994) report two occurrences of merrillite from glass-rich chondrules in ordinary chondrites, which we provisionally classify as *PC merrillite*. Two anhedral merrillite crystals (~150 μm maximum dimension) are associated with olivine in a glass chondrule in the Hedjaz (L3.7) ordinary chondrite, while a spinel grain in a glass chondrule from Allan Hills 77043 (L3.5) holds a 10 μm diameter euhedral merrillite inclusion. Brigham et al. (1986) describe merrillite from a silica-pyroxene chondrule in the Bremervorde (H3) ordinary chondrite, while Krot et al. (1993) record merrillite as a relatively common accessory mineral in unusual Cr-rich chondrules, for example, in Raguli (H3.8). As with merrillite occurrences in glass-rich chondrules, it is not certain whether these grains formed during initial cooling of a P-rich precursor, most likely a P-rich Fe-Ni alloy (i.e., primary origin), or during a subsequent alteration process (Jones et al. 2014; Lewis and Jones 2016).

Silicates

Silicate minerals, most notably Mg-Fe olivine, Ca-rich and Ca-poor pyroxenes, and plagioclase, are the dominant phases in most chondrules. Relatively few other silicates have been reported as primary phases in chondrules—a reflection of their igneous origins from nebular precursors.

Silica group minerals (SiO_2)

Silica-rich chondrules constitute an important, if volumetrically minor, compositional extreme in unequilibrated chondrite meteorites (Brearley and Jones 1998; Krot et al. 2004b; Scott and Krot 2014; Rubin and Ma 2021). In addition, silica forms rims around Mg-rich chondrules from CR chondrites (Krot et al. 2004b). Three phases—cristobalite, tridymite, and silica glass—have been reported as primary chondrule minerals (Brearley and Jones 1998; Kimura et al. 2005; Hezel et al. 2006). Additionally, quartz occurs as a secondary phase in metamorphosed enstatite chondrites that were re-equilibrated at $T < 867$ °C (Kimura et al. 2005), while coesite, seifertite, and stishovite have been identified as silica polymorphs formed during shock events to $P > 0.6$ GPa (Rubin and Ma 2021).

Cristobalite (SiO_2).—*PC cristobalite* has been reported from silica-rich chondrules in many type 3 and type 4 ordinary and enstatite chondrites, where it occurs in association with low-Ca pyroxene and may approach 30 vol% of some chondrules (Rubin 1983; Bridges et al. 1995; Brigham et al. 1986; Brearley and Jones 1998; Kimura et al. 2005; Hezel et al. 2006; Rubin and Ma 2021). Textures and associations suggest that cristobalite is the liquidus phase in some SiO_2-dominant chondrules, so it crystallized from the original chondrule melt (Kimura et al. 2005).

Tridymite (SiO_2).—*PC tridymite* occurs in many silica-rich chondrules in type 3 and type 4 ordinary and enstatite chondrites (Ikeda 1989b; Schulze et al. 1994; Bridges et al. 1995; Newton et al. 1995; Brearley and Jones 1998; Kimura et al. 2005; Hezel et al. 2006; Rubin and Ma 2021). At low-Mg, high-Si compositions, tridymite is the liquidus phase rather than cristobalite; therefore, tridymite is assumed to be a primary chondrule mineral that crystallized from melt (Kimura et al. 2005).

Silica Glass (SiO_2).—*PC silica glass* (SiO_2 > 90 mol%), in association with primary low-Ca pyroxene and secondary fayalitic olivine, is an important constituent of silica-rich chondrules, which represent <2 vol% of ordinary chondrites (Brigham et al. 1986; Wasson and Krot 1994; Brearley and Jones 1998). Silica-glass-rich chondrules have also been described from carbonaceous chondrites (Olsen 1983; Kimura et al. 2005) and from an enstatite chondrite as isolated <5 μm diameter inclusions in Fe-Ni alloys, presumably exsolved from the Si-rich metal on cooling (Ivanov et al. 1996). Kimura et al. (2005) suggest that some occurrences of silica glass represent the final product from rapid cooling of a Si-rich chondrule melt.

Olivine [$(Mg,Fe)_2SiO_4$].—Ferromagnesian olivine group minerals are found in all chondrite groups and are among the most abundant chondrule primary phases. Hundreds of references in work spanning the past half century document occurrences of olivine, which

occurs in numerous different textures and contexts within chondrules (as well as in CAIs, AOAs, and other primary meteoritic constituents). This diversity reflects a variety of primary mineralization processes, including crystallization from a chondrule melt, condensation from nebular gas, and condensation within an impact plume, as well as subsequent modification via reaction with hot nebular gases (Brearley and Jones 1998; Scott and Krot 2014; Rubin and Ma 2021).

An important question in the context of the evolutionary system of mineralogy is whether there are multiple natural kinds of primary chondrule olivine (as well as other major silicate phases, including primary chondrule pyroxene and plagioclase, for example). Numerous attributes of an olivine occurrence provide insight on its paragenesis and subsequent history, including major, minor, and trace element composition; stable isotope composition; grain morphology and zoning; chondrule texture; dislocation density; solid inclusions; and petrographic context. If sufficiently comprehensive data resources become available, then cluster analysis might reveal several different kinds of primary chondrule olivine with idiosyncratic combinations of attributes. However, until such time as those data resources are developed, we recognize *PC olivine* as the only primary chondrule olivine. Note that in a few instances, the most FeO-rich zoned regions of some primary olivine grains may extend into the fayalite field, with Fe > Mg. Therefore, we lump all of these examples into *PC olivine*, which represents a wide range of $[(Mg,Fe)_2SiO_4]$ compositions.

A few instances of the Fe-dominant olivine, fayalite, occur: (1) in rare silica-bearing chondrules with cristobalite and Ca-free pyroxene (Brigham et al. 1986; Wasson and Krot 1994); (2) as rims around forsterite in type I chondrules (Hua et al. 1988;Murakami and Ikeda 1994; Krot et al. 1995); and (3) as $Fa_{88–99}$ grains to 100 μm diameter in association with magnetite, troilite, and pentlandite (Hua and Buseck 1995). These occurrences have all been ascribed to secondary processes in chondrites (Krot et al. 1997b; Brearley and Jones 1998; Brearley 2014), though a few earlier researchers suggested that fayalite rims could be primary as a consequence of condensation from an oxidized nebular gas (e.g., Hua et al. 1988; Weinbruch et al. 1990, 1994; Krot and Rubin 1996; Krot et al. 1997b).

In the most unequilibrated ordinary chondrites, olivine phenocrysts, often nucleated on prior generations of relict olivine (Rubin 2006; Rubin and Ma 2021), are invariably Mg-rich ($Fo_{65–99}$) with minor Mg-Fe zoning—attributes that reflect crystallization from the melt (Rubin and Wasson 1987; Jones 1990; Weinbruch et al. 1990, 1994; Brearley and Jones 1998, see Table A3.1). Olivine of similar composition occurs as inclusions in clinoenstatite (Jones 1994), while more Fe-rich ($Fo_{60–70}$) micrometerscale crystallites may occur in the mesostasis (Töpel-Schadt and Müller 1985). Within a given unequilibrated meteorite, olivine compositions in adjacent chondrules may differ significantly; however, olivine chemistry re-equilibrates by inter-chondrule diffusion as a consequence of parent-body alteration. Therefore, for meteorites of grade 3.6 and higher, the olivine phenocrysts in adjacent chondrules typically attain uniform compositions in major and minor elements (McCoy et al. 1991b; Sears et al. 1992).

Carbonaceous chondrites display a wider range of both averaged and zoned olivine compositions, with phenocrysts in CO3, CM2, and CV3 chondrites covering the range from

near end-member forsterite in type I chondrules to $Fo_{37–50}$ in the rims of zoned olivine in type II chondrules (McSween 1977a; Desnoyers 1980; Cohen et al. 1983; Scott and Taylor 1983; Sheng et al. 1991b; Murakami and Ikeda 1994; Simon et al. 1995; Brearley and Jones 1998, and references therein).

Primary olivine in the ferromagnesian chondrules of type 3 enstatite chondrites is uniformly forsteritic, with most samples $Fo_{92–99}$ (Grossman et al. 1985; Ikeda 1988b), though rare zoned examples display more fayalitic rims to Fo_{75} (Lusby et al. 1987).

Low-calcium pyroxenes [$(Mg,Fe,Ca)SiO_3$]

Low-Ca pyroxene group minerals, ideally $(Mg, Fe^{2+},Ca)_2Si_2O_6$, but often with significant Al and/or Ti and most commonly with <40 mol% of the Fe end-member, are extremely common primary constituents of chondrules (Ikeda 1982; Noguchi 1989; Brearley and Jones 1998, Table A3–2; Rubin and Ma 2021). Almost all primary chondrule pyroxenes are either low-Ca varieties (orthoenstatite, clinoenstatite, and pigeonite) or high-Ca varieties (diopside, augite, and “fassaite”). Note that iron-rich pyroxenes, including those with >50 mol% hedenbergite [$(Ca,Fe)SiO_3$; Sheng et al. 1991] and ferrosilite ($FeSiO_3$; Rubin and Ma 2021) components, are invariably of secondary origin. Indeed, many primary chondrule pyroxenes lie relatively close to the $MgSiO_3$–$CaMgSi_2O_6$ join.

Orthopyroxene is the most common low-Ca pyroxene in terrestrial igneous rocks; however, orthoenstatite (officially named “enstatite” by the IMA) is relatively uncommon as a primary chondrule phase compared to clinoenstatite and pigeonite, which are both monoclinic ($P2_1/c$) pyroxenes with similar unit-cell dimensions. Clinoenstatite is defined by IMA protocols as end-member $MgSiO_3$, whereas pigeonite is ostensibly a more Ca- and Fe-rich variant, with up to 15 mol% $CaSiO_3$. A continuous solid solution exists among clinoenstatite, clinoferrosilite ($FeSiO_3$), and pigeonite. However, Ca-poor chondrule clinoenstatite is often found as phenocrysts surrounded by a significantly more Ca-rich pigeonite layer. We therefore recognize *PC clinoenstatite* and *PC pigeonite*, along with *PC orthoenstatite*, as distinct natural kinds in the Mg-Fe-(Ca) pyroxene solid solution, each spanning a significant range of Mg-Fe-Ca phase space. Note, however, that in the absence of coexisting phases with contrasting Ca contents, the distinction between “clinoenstatite” and “pigeonite” may be arbitrary.

Orthoenstatite [$(Mg,Fe)SiO_3$].—Orthorhombic enstatite (space group *Pbca*) is the stable low-temperature form of $(Mg,Fe)SiO_3$, and is thus the low-Ca pyroxene phase most commonly found in gradually cooled terrestrial igneous rocks (e.g., Deer et al. 1966). Nevertheless, it is significantly less common than clinoenstatite as a primary phase in rapidly cooled chondrules and may, in some instances, point to a secondary process from thermal metamorphism and consequent inversion of clinoenstatite.

In ordinary and carbonaceous chondrites orthoenstatite occurs as rare phenocrysts in association with clinoenstatite and forsterite (Ikeda 1982; Watanabe et al. 1986; Noguchi 1989; Jones 1996). Orthoenstatite is also found as layers surrounding clinoenstatite in some chondrules in the Allende CV3 carbonaceous chondrite (Noguchi 1989), while in EH3

enstatite chondrites orthoenstatite has been reported as the dominant pyroxene in barred olivine-pyroxene chondrules (Zhang et al. 1996).

Clinoenstatite [(Mg,Fe)SiO_3].—*PC clinoenstatite* is the most common pyroxene in ferromagnesian chondrules, occurring prominently as phenocrysts in unequilibrated ordinary chondrites. The widespread occurrence of this high-temperature polymorph of $MgSiO_3$, rather than orthoenstatite, points to its formation from a melt at >985 °C (Boyd and Schairer 1964), with subsequent rapid cooling of chondrules. Examples from numerous meteorites show $FeSiO_3$ contents ranging from <1 to ~35 mol% (Brearley and Jones 1998, see Figs. 10, 14, 23, 24, 29, 33, 38, 41, 47, 49, 53, 55, 56, 58, 59, 62, 65, and 66; Table A3.2). Clinoenstatite is often polysynthetically twinned (e.g., Müller et al. 1995) and is commonly encased in more calcic pyroxenes, either augite or by a layer of pigeonite surrounded by augite (Noguchi 1989).

Pigeonite [(Mg,Fe,Ca)SiO_3].—Pigeonite with 5 to 15 mol% $CaSiO_3$ component occurs in the chondrules of type 3 ordinary chondrites, both as individual crystals and as a thin layer between clinoenstatite cores and augitic mantles (Noguchi 1989). Pigeonite often displays exsolution lamellae of calcic clinopyroxene (space group $C2/c$) or anti-phase domains (a consequence of high-temperature inversion)—both of which may point to multiple heating and cooling events (Ashworth and Barber 1977). In carbonaceous chondrites, low-Fe pigeonite ($Fs_{<02}$) also occurs in close association with augite, for example, as intergrowths in the Cochabamba CM2 chondrite (Müller et al. 1979), or as an intermediate layer between a clinoenstatite core and augite overgrowth in the Allende CV3 chondrite (Noguchi 1989). In addition, the plagioclase-olivine inclusions of CV chondrites sometimes hold Fe-poor ($Fs_{<01}$), Al-rich (to several mol%) pigeonite (Sheng et al. 1991a). Finally, EH3 enstatite chondrites hold various pyroxenes, including pigeonite (Kitamura et al. 1987; Ikeda 1989b), some of which hold >10 mol% $CaSiO_3$ components (Ikeda 1988b; Kitamura et al. 1988).

High-calcium clinopyroxenes [(Ca,Mg,Fe)(Mg,Fe,Al,Ti^{3+}) (Al,Ti^{4+},Si)SiO_6]

Clinopyroxenes with Ca ≈ (Mg + Fe) are common primary phases in chondrules. The nomenclature of these monoclinic pyroxenes (space group $C2_1/c$) is complicated by the frequent use of two approved IMA names, diopside ($CaMgSi_2O_6$) and augite [$(Ca,Mg,Fe)_2Si_2O_6$], in concert with unapproved or discredited terminology, including “fassaite,” “Al-Ti-diopside,” and “aluminous diopside” (Morimoto et al. 1988; Sack and Ghiorso 2017; Rubin and Ma 2017, 2021; see rruff.info/ima, accessed 7 April 2020). In extreme instances, clinopyroxene compositions may approach such end-members as kushiroite ($CaAl_2SiO_6$; Kimura et al. 2009), grossmanite ($CaTi^{3+}AlSiO_6$; Ma and Rossman 2009), or the as yet unnamed end-member ($CaMgTi^{4+}SiO_6$), all of which extend the continuous clinopyroxene compositional range to [(Ca,Mg,Fe)(Mg,Fe,Al,Ti^{3+}) (Al,Ti^{4+},Si)SiO_6]. Specific instances of compositional extremes, for example Al- and Ti-rich clinopyroxenes, reflect the idiosyncratic average compositions of their host chondrules. However, inasmuch as these calcic clinopyroxenes all form in similar ways within a molten droplet, we recognize only one kind of primary chondrule calcic clinopyroxene, *PC augite*.

Augite [(Ca,Mg,Fe)(Mg,Fe,±Al,±Ti^{3+})(±Al,±Ti^{4+},Si)SiO_6].—*PC augite* occurs commonly in chondrules in type 3 ordinary chondrites, carbonaceous chondrites, and enstatite chondrites, both as phenocrysts and as overgrowths (<20 μm thick) on clinoenstatite, at times with a thin intermediate pigeonite layer. Augite also is found as exsolution lamellae in low-Ca pyroxene. While compositions vary significantly, most *PC augite* have $CaSiO_3$ from 30 to 45 mol% and $FeSiO_3$ from ~0 to 15 mol% (Brearley and Jones 1998; see Figs. 10, 17, 23, 25, 29, 34, 38, 42, 47, 49, 60, 65, and 67; Table A3.3). Examples of PC augite that are close to diopside in composition (i.e., with $MgSiO_3$ > 35 mol %, $CaSiO_3$ > 45 mol%, and correspondingly low Fe, Al, and Ti) have been reported by Noguchi (1989) as crystals ($Wo_{48–50}$) in glass in a single chondrule from the ALH-77003 CO chondrite. Additional reports of chondrule “fassaite” crystals in glassy mesostasis with a wide range of compositions rich in Al and Ti have been reported from Al-rich and Ca-Al-rich chondrules in type 3 ordinary chondrites (Bischoff and Keil 1984; Wang et al. 2016). Al-Ti-rich clinopyroxenes are also recorded from low-Fe chondrules and plagioclase-olivine inclusions in Allende and other CV3 meteorites (Noguchi 1989; Sheng et al. 1991a), as well as in CR chondrites (Noguchi 1995).

Plagioclase feldspar group ($CaAl_2Si_2O_8$ to $NaAlSi_3O_8$)

Plagioclase feldspar is a common phase in typical ferromagnesian chondrules of ordinary chondrites, especially in devitrified mesostasis, where it may represent both a primary phase formed on initial chondrule cooling and a secondary phase crystallized during subsequent metamorphism in the parent body (Brearley and Jones 1998; Lewis and Jones 2016, 2019). This continuum from primary to secondary feldspar is reflected as increases in the average size of plagioclase crystallites, the volume ratio of mesostasis crystals to glass, and the degree of plagioclase Al-Si disorder. The range of chondrule plagioclase compositions in ordinary chondrites, though usually well within the anorthite field ($An_{60–90}$; Ikeda 1982; Miúra and Tomisaka 1984), occasionally extends to An_{02} within the albite field in unequilibrated ordinary chondrites (Brearley and Jones 1998, see Table A3.5; Lewis and Jones 2019, and references therein). In addition, a near end-member albite occurrence is associated with silica in a single chondrule (Fujimaki et al. 1981a, 1981b).

Plagioclase-rich chondrules are found in some type 3 CO chondrites, in which primary calcic plagioclase laths ($An_{70–90}$) occur in association with augite and orthopyroxene (Greshake 1997; Jones 1997; Brearley and Jones 1998). Plagioclase also plays a significant role in varied, less common Al-(Ca)-rich chondrules in ordinary chondrites, in which calcic plagioclase occurs as a fine-grained mineral in both the groundmass and mesostasis (Wang et al. 2016). Note, however, that albitic plagioclase is not a primary phase in Na-Al-rich chondrules, in which Na-rich glass is the dominant sodium phase.

Plagioclase occurs occasionally as a primary phase in the chondrules of carbonaceous chondrites. $An_{>80}$ is found as a primary phase in a small fraction of Allende (CV3) ferromagnesian chondrules, at times in association with low-calcium pyroxenes (Simon and Haggerty 1980; Noguchi 1989; Brearley and Jones 1998, see Table A3.5). CV chondrites also hold plagioclase-olivine inclusions, in which calcic plagioclase (commonly $An_{\sim 95}$) and forsteritic olivine phenocrysts are the dominant phases (Sheng et al. 1991a). Plagioclase

(~An_{90}) was also reported in association with augite in a single silica-bearing chondrule from the Murchison CM chondrite (Olsen 1983). In addition, plagioclase is not uncommon as a phase in the mesostasis of carbonaceous chondrites (Murakami and Ikeda 1994; Ikeda and Kimura 1995). Plagioclase ($An_{48–88}$) has also been reported as a primary phase in enstatite chondrites, occurring as laths in mesostasis (Ikeda 1988b, 1989b), as well as in Al-rich chondrules (Bischoff et al. 1985; Wang et al. 2016).

Most reports of primary plagioclase feldspar, especially in type I chondrules, lie in the calcium-dominant field, if not close to anorthite ($An_{>80}$). By contrast, most albitic plagioclase (and all K-bearing feldspars) are described as secondary in origin (e.g., Ikeda 1989b; Rubin and Kallemeyn 1989, 1994; Schulze et al. 1994; Lewis and Jones 2016, 2019). We recognize two primary chondrite feldspar group minerals. Most occurrences of primary chondrule plagioclase lie well within the anorthite range, though a few outliers may display sodium content greater than calcium as part of a continuous solid solution. We name all such phases as *PC anorthite*. In addition, the common occurrences of Na-rich plagioclase (An_{02} to An_{32}) in FeO-rich chondrules in the unequilibrated Semarkona (LL3.00) chondrite (Lewis and Jones 2019), as well as the rare occurrence of albite with silica reported by Fujimaki et al. (1981a), are designated *PC albite*.

Anorthite [$(Ca,Na)(Al,Si)_2Si_2O_8$).—*PC anorthite* is a common phase as phenocrysts or as crystallites in mesostasis in both ordinary and carbonaceous chondrites.

Albite ($NaAlSi_3O_8$).—Fujimaki et al. (1981a, 1981b) report a rare occurrence of *PC albite* ($Ab_{>98}$) associated with silica and ferropseudobrookite in a single chondrule from the L3 ordinary chondrite ALH77015.

Nepheline [$Na_3K(Al_4Si_4O_{16})$].—Most chondrules are too silicarich to form feldspathoids as stable primary phases. However, nepheline has been reported as both a primary and (more commonly) secondary phase (Ikeda 1988b; Sheng et al. 1991a). *PC nepheline* is found as epitaxially oriented intergrowths with anorthite in unequilibrated ordinary chondrites (Ikeda 1982), including in some plagioclase-rich chondrules (Jones 1997). It also occurs in association with Na-bearing plagioclase in Al-Ca-Na-rich chondrules in ordinary chondrites (Brearley and Jones 1998; Rubin and Ma 2021). Note, however, that some experts suggest that all nepheline occurrences in chondrules are of secondary origin (R. Jones, personal communication, 4 June 2020).

Sapphirine [$Mg_4(Mg_3Al_9)O_4(Si_3Al_9O_{36})$].—*PC sapphirine* is one of several minor accessory phases found as primary chondrule minerals only in plagioclase-olivine inclusions (POIs) from the Allende CV carbonaceous chondrite (Sheng et al. 1991a). Sapphirine occurs as widely distributed 5 × 25 μm crystal prisms in a Na- and Cl-rich mesostasis. Sapphirine from POIs incorporates excess Mg+Si at the expense of Al, as well as significant Cr and Ti, in accord with experimental studies of sapphirine crystallization from a melt (Sheng et al. 1991b).

Merrihueite[$(K,Na)_2(Fe,Mg)_5Si_{12}O_{30}$] and roedderite[$(Na,K)_2Mg_5Si_{12}O_{30}$].— Silica-rich chondrules in several unequilibrated ordinary and enstatite chondrites have been

reported to hold minerals of the merrihueite-roedderite solid-solution series (Dodd et al. 1965; Rambaldi et al. 1986; Krot and Wasson 1994). Wood and Holmberg (1994) proposed that these unusual silicates formed by the reaction of silica-rich phases with alkali-rich nebular gas. The compositions of these occurrences span the range from $0.1 < Na/(Na+K) < 0.8$, and with $0 < Fe/(Fe+Mg) < 0.8$ (Wood and Holmberg 1994). IMA protocols could thus assign as many as four different mineral names to the Na-Mg (roedderite), K-Fe (merrihueite), Na-Fe, and K-Mg compositional variants, all of which are observed in these meteorites. However, these minerals form a continuous solid-solution of phases formed by the same primary process and thus represent a single natural kind in our evolutionary system. Because most examples fall within the roedderite field, we assign the name *PC roedderite* to these examples. Note, however, that some experts ascribe all such occurrences to secondary process (R. Jones, personal communications, June 4, 2020).

Silicate Glass (Ca,Mg,Al,Si,O).—*PC silicate glass* is an important constituent of many chondrules. In extreme cases, chondrules can be >99 vol% silicate glass, with a significant population having 55 to 85 vol% glass (Krot and Rubin 1994). Silicate glass as a primary phase in chondrules spans a wide range of compositions (Brearley and Jones 1998, and references therein). As with other common silicate phases in chondrules, cluster analysis of large databases of silicate glass might reveal distinctive natural kinds that could warrant a splitting of *PC silicate glass*.

Network graph of stellar and primary nebular minerals

The evolutionary system of mineralogy can be illustrated using bipartite mineral network graphs, which display relationships among mineral phases and their attributes, in this instance their paragenetic modes and chemical groups (Morrison et al. 2017, 2020; Hazen et al. 2019b; Hazen and Morrison 2020; Morrison and Hazen 2020). Figure 2 displays a bipartite force-directed network graph of primary stellar, interstellar, and nebular minerals formed prior to ~4561 Ma, in which 96 different phases, including 10 amorphous condensed phases, are represented by diamond-shaped nodes. Each of these mineral nodes is linked to one or more nodes representing a paragenetic mode of formation. Three different star-shaped nodes (AGB, SN-II, and CNova) represent stellar environments that impart distinctive isotopic signatures to minerals. A cloud-shaped node indicates interstellar dense molecular clouds (DMC), whereas five flattened disk icons represent different primary mineral-forming nebular environments (Circumstellar, CAI, AOA, URI, and PC).

Information about mineral compositions is indicated by the color of diamond-shaped mineral nodes: black (C-bearing), green (lacking C or O), blue (contains O, but not C or Si), and red (contains Si and O). The sizes of the star-, cloud-, and disk-shaped symbols indicate the numbers of different minerals to which they are associated.

Note that while most mineral nodes are members of a well-connected network, eight low-temperature interstellar and nebular condensed molecular phases that all formed at $T < 100$ K delineate a separate network from 88 high-temperature stellar and nebular condensates ($T >> 300$ K). In future contributions to this series, which will consider phases formed at

intermediate temperatures in planetary surface environments, new links will occur between these two mineral-forming environments.

This bipartite network of mineral evolution is a visual representation of all confirmed stellar, interstellar, and primary nebular minerals described in Parts I, II, and III of the evolutionary system of mineralogy. Of the 96 species in Figure 2, spinel is the most ubiquitous, occurring in 7 of the 9 different paragenetic modes considered thus far; consequently, spinel assumes a highly centralized position in this network graph. Iron, corundum, and forsterite, each linked to 5 modes of formation, were the next most widespread minerals prior to the formation of planetesimals. On the other hand, more than two-thirds of these minerals—68 of 96 species—are thus far only recorded from a single paragenetic mode.

Of the 43 primary chondrule mineral species considered in Part III, 27 occur here for the first time. This significant increase in mineral diversity associated with chondrule formation in part reflects chemical fractionation within the solar nebula and the consequent increasing importance of such key elements as Na, K, Cr, Mn, and S, all of which are moderately volatile and thus were incorporated into solid phases as the nebular disk cooled.

The topology of this network graph reflects important aspects of mineral evolution. Nodes for a few of the commonest minerals (fewer than 20 species) are centrally located; those diamond-shaped icons are surrounded by several nodes for paragenetic modes. But the majority of minerals are represented by starbursts of nodes that decorate the periphery of the graph, each diamond representing a species that at this stage of mineral evolution is only linked to a single paragenetic mode. In future contributions, as we add new paragenetic modes, many new mineral species formed by different processes at new combinations of temperature, pressure, and composition will enhance this pattern. New starbursts will appear, while a greater number of minerals will have multiple links to paragenetic modes and thus shift to the network's crowded interior. In this way, as new modes of mineral paragenesis are considered, this informationrich graphical approach will provide a dynamic, interactive view of the entire sweep of mineral evolution.

Implications

Part III of the evolutionary system of mineralogy represents a vital transition between the genesis of dust and gas in stars and the solid condensed phases that would become planets and moons. Dynamic electromagnetic, shock front, and impact processes provided the principal high-temperature sources required to form igneous droplets—the chondrules that accreted to become the first macroscopic rocks of our solar system. However, soon thereafter gravity took control as planetesimals began to form and collide, and new suites of minerals emerged.

The catalog of 43 phases is misleading in at least two ways regarding the diversity and distribution of primary chondrule minerals. First, the primary origins of eight of these phases (awaruite, graphite, haxonite, pentlandite, magnetite, merrillite, nepheline, and roedderite) have been questioned. For each of these minerals, some experts assert that all chondrule occurrences formed by secondary processes. Of the remaining 35 minerals, an additional 15

(sinoite, perryite, alabandite, caswellsilverite, daubréelite, niningerite, oldhamite, sphalerite, wassonite, rutile, armacolite, ferropseudobrookite, perovskite, zirconolite, and sapphirine) are extremely rare and of restricted occurrence, while seven more (tetrataenite, cohenite, schreibersite, magnetite, ilmenite, cristobalite, and silica glass) are more widespread but volumetrically minor. Thus, only a dozen phases probably account for more than 99 vol% of primary chondrule mineralogy. This distribution reflects the mineralogical parsimony of high-temperature assemblages of the nebula's major rock-forming elements—in essence, a nebular manifestation of J. Willard Gibbs' "phase rule" (Gibbs 1876–1878). We will discover a similar restricted mineral diversity among the primary phases that arise from planetesimal differentiation into mantle and core (the subject of Part IVA). However, a dramatic rise in mineral diversity occurred as a consequence of pervasive alteration of these equilibrium phases—reworking by impact processes (Part IVB), as well as aqueous, hydrothermal, and metamorphic alteration that resulted in hundreds of new minerals before the assembly of today's planets and moons (Part V).

This study of primary meteorite phases reveals an intriguing sociological aspect to the science of meteorite mineralogy. The bold outlines of primary chondrule mineralogy, on which our contribution is grounded, were made in the 1960s and 1970s. Thousands of publications expanded and refined that knowledge base in the 1980s and 1990s. By 1998, Adrian Brearley and Rhian Jones could summarize chondrite mineralogy and petrology in a 398-page treatise with more than 1000 references by almost as many coauthors. Our review of chondrule mineralogy would not have been possible without that immense body of research and the summary of Brearley and Jones (1998).

Mineralogical fashion, and funding, has changed. While many dedicated workers continue to probe these most ancient rocks and make important discoveries, the study of meteorite mineralogy and petrology appears to be less of a priority than in decades past. New discoveries, particularly related to scarce isotopes and to submicrometer-scale phases discovered by microbeam techniques, are breathtaking. Nevertheless, one comes away from this vast literature feeling that much more remains to be discovered about chondrites and their ancient mineralogy. Thousands of meteorites have been collected but remain to be investigated. Numerous trace elements and stable isotope systems are yet to be explored. Undiscovered nanoscale minerals and poorly characterized non-crystalline solid phases beckon. We suspect that another golden age of meteorite mineralogy, perhaps including the promise of data-driven discovery using large and growing planetary materials data resources, lies before us.

Acknowledgments

We are deeply grateful to reviewers Rhian Jones and Alan Rubin, as well as Steven Simon, for their meticulous, thoughtful, and constructive reviews of this manuscript, which was substantially improved as a consequence. We are also grateful to Denton Ebel and Alan Rubin, who contributed invaluable detailed reviews of an earlier version of this contribution. Rubin and Chi Ma provided access to important work in press, including a draft of their forthcoming book, *Meteorite Mineralogy*. We are grateful to Conel M.O'D. Alexander, Asmaa Boujibar, Carol Cleland, Robert T. Downs, Olivier Gagné, Sergey Krivovichev, Glenn MacPherson, Larry Nittler, Michael Walter, and Shuang Zhang for thoughtful discussions and comments.

Funding

This publication is a contribution to the Deep Carbon Observatory, the 4D Initiative, and the Deep-time Digital Earth (DDE) program. Studies of mineral evolution and mineral ecology have been supported by the Deep Carbon Observatory, the Alfred P. Sloan Foundation, the W.M. Keck Foundation, the John Templeton Foundation, the NASA Astrobiology Institute ENIGMA team, a private foundation, and the Carnegie Institution for Science. Any opinions, findings, or recommendations expressed herein are those of the authors and do not necessarily reflect the views of the National Aeronautics and Space Administration.

References cited

Abel T, Bryan GL, and Norman ML (2002) The formation of the first stars in the Universe. Science, 295, 93–98. [PubMed: 11711636]

Abreu NM, and Brearley AJ (2011) Deciphering the nebular and asteroidal record of silicates and organic material in matrix of the reduced CV3 chondrite Vigarano. Meteoritics & Planetary Science, 46, 252–274.

Afiattalab F, and Wasson JT (1980) Composition of the metal phases in ordinary chondrites: Implications regarding classification and metamorphism. Geochimica et Cosmochimica Acta, 44, 431–446.

Akridge DG, and Sears DWG (1999) The gravitational and aerodynamic sorting of meteoritic chondrules and metal: Experimental results with implications for chondritic meteorites. Journal of Geophysical Research, 104, 11,853–11,864.

Alexander CMO'D, and Ebel DS (2012) Questions, questions: Can the contradictions between the petrologic, isotopic, thermodynamic, and astrophysical constraints on chondrule formation be resolved? Meteoritics & Planetary Science, 47, 1157–1175.

Alexander CMO'D, Swan P, and Prombo CA (1994) Occurrence and implications of silicon nitride in enstatite chondrites. Meteoritics, 29, 79–85.

Alexander CMO'D, Grossman JN, Ebel DS, and Ciesla FJ (2008) The formation conditions of chondrules and chondrites. Science, 320, 1617–1619. [PubMed: 18566282]

Alwmark C, Schmitz B, Holm S, Marone F, and Stampanoni M (2011) A 3-D study of mineral inclusions in chromite from ordinary chondrites using synchrotron radiation X-ray tomographic microscopy—Method and application. Meteoritics & Planetary Science, 46, 1071–1081.

Amelin Y, and Krot AN (2007) Pb isotopic ages of the Allende chondrules. Meteoritics & Planetary Science, 42, 1321–1335.

Amelin Y, Krot AN, Hutcheon ID, and Ulyanov AA (2002) Lead isotopic ages of chondrules and calcium–aluminum-rich inclusions. Science, 297, 1678–1683. [PubMed: 12215641]

Amelin Y, Kaltenbach A, Iizuka T, Stirling CH, Ireland TR, Petaev M, and Jacobsen SB (2010) U-Pb chronology of the Solar System's oldest solids with variable $^{238}U/^{235}U$. Earth and Planetary Science Letters, 300, 343–350.

Ashworth JR, and Barber DJ (1977) Electron microscopy of some stony meteorites. Philosophical Transactions of the Royal Society of London, A, 286, 493–506.

Asphaug E, Jutzi M, and Movshovitz N (2011) Chondrule formation during planetesimal accretion. Earth and Planetary Science Letters, 308, 369–379.

Avril C, Malavergne V, Caracas R, Zanda B, Reynard B, Charon E, Bobocioiu E, Brunet F, Borensztajn S, Pont S, and others. (2013) Raman spectroscopic properties and Raman identification of CaS-MgS-MnS-FeS-Cr_2FeS_4 sulfides in meteorites and reduced sulfur-rich systems. Meteoritics & Planetary Science, 48, 1415–1426.

Baecker B, Rubin AE, and Wasson JT (2017) Secondary melting events in Semarkona chondrules revealed by compositional zoning in low-Ca pyroxene. Geochimica et Cosmochimica Acta, 211, 256–279.

Barth MIF, Harries D, Langenhorst F, and Hoppe P (2018) Sulfide-oxide assemblages in Acfer 094—Clues to nebular metal-gas interactions. Meteoritics & Planetary Science, 53, 187–203.

Bell KR, Cassen PM, Wasson JT, and Woolum DS (2000) The FU Orionis phenomenon and solar nebula material. In Mannings V, Boss AP, and Russell SS, Eds., Protostars and Planets IV, pp. 897–926. University of Arizona Press.

Berg T, Maul J, Schönhense G, Marosits E, Hoppe P, Ott U, and Palme H (2009) Direct evidence for condensation in the early Solar System and implications for nebular cooling rates. The Astrophysical Journal, 702, L172–L176.

Bertout C (1989) T Tauri stars—Wild as dust. Annual Reviews of Astronomy & Astrophysics, 27, 351–395.

Bertulani CA (2013) Nuclei in the Cosmos. World Scientific.

Bevan AWR, and Axon HJ (1980) Metallography and thermal history of the Tieschitz unequilibrated meteorite—Metallic chondrules and the origin of polycrystalline taenite. Earth and Planetary Science Letters, 47, 353–360.

Bigolski JN, Weisberg MK, Connolly HC Jr., and Ebel DS (2016) Microchondrules in three unequilibrated ordinary chondrites. Meteoritics & Planetary Science, 51, 235–260.

Bischoff A, and Keil K (1983) Ca-Al-rich chondrules in ordinary chondrites. Nature, 303, 588–592.

Bischoff A (1984) Al-rich objects in ordinary chondrites: Related origin of carbonaceous and ordinary chondrites and their constituents. Geochimica et Cosmochimica Acta, 48, 693–709.

Bischoff A, Keil K, and Stöffler D (1985) Perovskite-hibonite-spinel-bearing inclusions and Al-rich chondrules and fragments in enstatite chondrites. Chemie der Erde, 44, 97–106.

Bischoff A, Wurm G, Chaussidon M, Horstmann M, Metzler K, Weyrauch M, and Weinauer J (2017) The Allende multicompound chiondrule (ACC)—Chondrule formation in a local super-dense region of the early Solar System. Meteoritics & Planetary Science, 52, 906–924.

Bizzarro M, Connelly JN, and Krot AN (2017) Chondrules—Ubiquitous chondritic solids tracking the evolution of the solar protoplanetary disk. In Pessah M and Gressel O, Eds., Formation, Evolution, and Dynamics of Young Solar Systems. Astrophysics and Space Science Library, Cham, Switzerland, Springer, pp. 161–195.

Bollard J, Connelly JN, and Bizzarro M (2015) Pb-Pb dating of individual chondrules from the CBa chondrite Gujba: Assessment of the impact plume formation model. Meteoritics & Planetary Science, 50, 1197–1216. [PubMed: 27429545]

Bollard J, Connelly JN, Whitehouse MJ, Pringle EA, Bonal L, Jørgensen JK, Nordlund A, Moynier F, and Bizzarro M (2017) Early formation of planetary building blocks inferred from Pb isotopic ages of chondrules. Science Advances, 3, e1700407. [PubMed: 28808680]

Bond HE, Nelan EP, VandenBerg DA, Schaefer GH, and Harmer D (2013) HD 140283: A star in the solar neighborhood that formed shortly after the Big Bang. The Astrophysical Journal, 765, L12 (5 pp).

Boss AP (1996) A concise guide to chondrule formation models. In Hewins RH, Jones RH and Scott ERD, Eds., Chondrules and the Protoplanetary Disk, pp. 257–264. Cambridge University Press.

Boss AP, and Durisen RH (2005) Sources of shock waves in the protoplanetary disk. Astronomical Society of the Pacific Conference Series, 341, 821–838.

Bouvier A, and Wadhwa M (2010) The age of the Solar System redefined by the oldest Pb-Pb age of a meteoritic inclusion. Nature Geoscience, 3, 637–641.

Bowman JD, Rogers AEE, Monsalve RA, Mozdzen TJ, and Mahesh N (2018) An absorption profile centred at 78 megahertz in the sky-averaged spectrum. Nature, 555, 67–70. [PubMed: 29493587]

Boyd FR, and Schairer JF (1964) The system $MgSiO_3$-$CaMgSi_2O_6$. Journal of Petrology, 5, 275–309.

Bradley JP (1994a) Nanometer-scale mineralogy and petrography of fine-grained aggregates in anhydrous interplanetary dust particles. Geochimica et Cosmochimica Acta, 58, 2123–2134.

Bradley JP (1994b) Chemically anomalous, pre-accretionally irradiated grains in interplanetary dust from comets. Science, 265, 925–929. [PubMed: 17782142]

Brearley AJ (2014) Nebular versus parent body processing. Treatise on Geochemistry, 2nd ed., 1, 247–268.nd

Brearley AJ, and Jones RH (1998) Chondritic meteorites. Reviews in Mineralogy, 36, 3.01–3.398.

Bridges JC, Franchi LA, Hutchison R, Morse AD, Long JVP, and Pillinger CT (1995) Cristobalite- and tridymite-bearing clasts in Parnallee (LL3) and Farmington (L5). Meteoritics, 30, 715–727.

Brigham CA, Yabuki H, Ouyang Z, Murrell MT, El Goresy A, and Burnett DS (1986) Silica-bearing chondrules and clasts in ordinary chondrites. Geochimica et Cosmochimica Acta, 50, 1655–1666.

Britvin SN, Kolomensky VD, Boldyreva MM, Bogdanova AN, Kretser YL, Boldyreva ON, and Rudashesky NS (1999) Nickelphosphide (Ni,Fe)3P, the nickel analog of schreibersite. Zapiski Vserossijskogo Mineralogicheskogo Obshchestva, 128, 64–72.

Buchwald VF (1975) Handbook of Iron Meteorites. University of California Press.

Budde G, Kleine T, Kruijer TS, Burkhardt C, and Metzler K (2015) Tungsten isotopic constraints on the age and origin of chondrules. Proceedings of the National Academy of Sciences, 113, 2886–2891.

Budde G, Burkhardt C, Brennecka GA, Fischer-Gödde M, Kruijer TS, and Kleine T (2016) Molybdenum isotopic complementarity of chondrules and matrix and the dichotomy of carbonaceous and noncarbonaceous meteorites. Earth and Planetary Science Letters, 454, 293–303.

Bullock EM, MacPherson GJ, Nagashima K, Krot AN, Petaev MI, Jacobsen SB, and Ulyanov AA (2012) Forsterite-bearing Type B refractory inclusions from CV3 chondrites: From aggregates to volatilized melt droplets. Meteoritics & Planetary Science, 47, 2128–2147.

Bunch TE, Keil K, and Snetsinger KG (1967) Chromite compositions in relation to chemistry and texture of ordinary chondrites. Geochimica et Cosmochimica Acta, 31, 1568–1582.

Burbidge EM, Burbidge GR, Fowler WA, and Hoyle F (1957) Synthesis of the elements in stars. Review of Modern Physics, 29, 547–650.

Burke EAJ (2006) The end of CNMMN and CCM—Long live the CNMNC! Elements, 2, 388.

Burkhardt C, Kleine T, Oberli F, Pack A, Bourdon B, and Wieler R (2011) Molybdenum isotopic anomalies in meteorites: Constraints on solar nebula evolution and the origin of the Earth. Earth and Planetary Science Letters, 312, 390–400.

Burkhardt C, Dauphas N, Hans U, Bourdon B, and Kleine T (2019) Elemental and isotopic variability in Solar System materials by mixing and processing of primordial disk reservoirs. Geochimica et Cosmochimica Acta, 261, 145–170.

Buseck PR, and Holdsworth EF (1972) Mineralogy and petrology of the Yilmia enstatite chondrite. Meteoritics, 7, 429–447.

Cameron AGW (1957) Nuclear reactions in stars and nucleogenesis. Publications of the Astronomical Society of the Pacific, 69, 201–222.

Campbell AJ, and Humayun M (2004) Formation of metal in the CH chondrites ALH 85085 and PCA 91467. Geochimica et Cosmochimica Acta, 68, 3409–3422.

Campbell AJ, Humayun M, and Weisberg MK (2002) Siderophile element constraints on the formation of metal in the metal-rich chondrites Bencubbin, Weatherford, and Gujba. Geochimica et Cosmochimica Acta, 66, 647–660.

Campbell AJ (2005a) Compositions of unzoned and zoned metal in the CBb chondrites HH 237 and QUE 94627. Meteoritics & Planetary Science, 40, 1131–1148.

Campbell AJ, Zanda B, Perron C, Meibom A, and Petaev MI (2005b) Origin and thermal history of Fe-Ni metal in primitive chondrites. Astronomical Society of the Pacific Conference Series, 341, 407–431.

Chambers JE (2004) Planetary accretion in the early Solar System. Earth and Planetary Science Letters, 223, 241–252.

Charles CRJ, Robin P-YF, Davis DW, and McCausland PJA (2018) Shapes of chondrules determined from the petrofabric of the CR2 chondrite NWA 801. Meteoritics & Planetary Science, 53, 935–951.

Chaumard N, Humayun M, Zanda B, and Hewins RH (2018) Cooling rates of type I chondrules from Renazzo: Implications for chondrule formation. Meteoritics & Planetary Science, 53, 984–1005.

Chiang E, and Youdin AN (2010) Forming planetesimals in solar and extrasolar nebulae. Annual Review of Earth and Planetary Sciences, 38, 493–522.

Clarke RS Jr., and Scott ERD (1980) Tetrataenite—Ordered FeNi, a new mineral in meteorites. American Mineralogist, 65, 624–630.

Cody GD, Heying E, Alexander CMO'D, Nittler RR, Kilcoyne ALD, Sandford SA, and Stroud RM (2011) Establishing a molecular relationship between chondritic and cometary organic solids. Proceedings of the National Academy of Sciences, 108, 19171–19176.

Cohen RE, Kornacki AS, and Wood JA (1983) Mineralogy and petrology of chondrules and inclusions in the Mokoia CV3 chondrites. Geochimica et Cosmochimica Acta, 47, 1739–1757.

Connelly JN, and Bizzarro M (2009) Pb-Pb dating of chondrules from CV chondrules by progressive dissolution. Chemical Geology, 259, 143–151.

Connelly JN (2018) The absolute Pb-Pb isotope ages of chondrules: Insights into the dynamics of the solar protoplanetary disk. In Russell SA, Connolly HC Jr. and Krot AN, Eds., Chondrules: Records of protoplanetary disk processes, pp. 300–323. Cambridge University Press.

Connelly JN, Amelin Y, Krot AN, and Bizzarro M (2008) Chronology of the Solar System's oldest solids. The Astrophysical Journal, 67, L121–L124.

Connelly JN, Bizzarro M, Krot AN, Nordlund Å, Wielandt D, and Ivanova MA (2012) The absolute chronology and thermal processing of solids in the solar protoplanetary disk. Science, 338, 651–655. [PubMed: 23118187]

Connolly HC Jr., Jones BD, and Hewins RH (1998) The flash melting of chondrules: An experimental investigation into melting history and physical nature of chondrule precursors. Geochimica et Cosmochimica Acta, 62, 2725–2735.

Crozaz G, and Lundberg L (1995) The origin of oldhamite in unequilibrated enstatite chondrites. Geochimica et Cosmochimica Acta, 59, 3817–3831.

Cuvillier P, Chaumard N, Leroux H, Zanda B, Hewins RH, Jacob D, and Devouard B (2018) A TEM study of exsolution in Ca-rich pyroxenes from the Paris and Renazzo chondrites: Determination of type I chondrule cooling rates. Meteoritics & Planetary Science, 53, 482–492.

Cuzzi JN, and Alexander CMO'D. (2006) Chondrule formation in particle-rich nebular regions at least hundreds of kilometers across. Nature, 441, 483–485. [PubMed: 16724060]

Cuzzi JN, Hogan RC, Paque JM, and Dobrovolskis AR (2001) Size-selective concentration of chondrules and other small particles in protoplanetary nebula turbulence. The Astrophysical Journal, 546, 496–508.

D'Alessio P, Calvet N, and Woolum DS (2005) Thermal structure of protoplanetary disks. Astronomical Society of the Pacific Conference Series, 341, 353–372.

Davis AM (2011) Stardust in meteorites. Proceedings of the National Academy of Sciences, 108, 19142–19146.

Davis AM, and Richter FM (2014) Condensation and evaporation of Solar System materials. In Davis AM, Holland HD, and Turekian KK, Eds., Treatise on Geochemistry, vol. 1: Meteorites, comets, and planets, 2nd ed., pp. 335–360. Elsevier-Pergamon.

Davis AM, Hashimoto A, Clayton RN, and Mayeda TK (1990) Isotope mass fractionation during evaporation of forsterite (Mg2SiO4). Nature, 347, 655–658.

Davy R, Whitehead SG, and Pitt G (1978) The Adelaide meteorite. Meteoritics, 13, 121–140.

Deer WA, Howie RA, and Zussman J (1966) An Introduction to the Rock-Forming Minerals. Wiley.

Desch SJ, and Connolly HC Jr. (2002) A model for the thermal processing of particles in solar nebula shocks: Application to the cooling rates of chondrules. Meteoritics & Planetary Science, 37, 183–207.

Desch SJ, and Cuzzi JN (2000) The generation of lightning in the solar nebula. Icarus, 143, 87–105.

Desch SJ, Morris MA, and Connolly HC Jr. (2010) A critical examination of the x-wind model chondrule and calcium-rich, aluminum-rich inclusion formation and radionuclide production. The Astrophysical Journal, 725, 692–711.

Desch SJ, Morris MA, Connolly HC Jr., and Boss AP (2012) The importance of experiments: Constraints on chondrule formation models. Meteoritics & Planetary Science, 47, 1139–1156.

Desch SJ, Kalyaan A, and Alexander CMO'D. (2018) The effect of Jupiter's formation on the distribution of refractory elements and inclusions in meteorites. The Astrophysical Journal Supplement Series, 238, 11 (31 pp).

Desnoyers C (1980) The Niger (I) carbonaceous chondrite and implications for the origin of aggregates and isolated olivine grains in C2 chondrite. Earth and Planetary Science Letters, 47, 223–234.

Dobriça E, and Brearley AJ (2016) Microchondrules in two unequilibrated ordinary chondrites: Evidence for formation by splattering from chondrules during stochastic collisions in the Solar System. Meteoritics & Planetary Science, 51, 884–905.

Dodd RT, Schmus WR, and Marvin UB (1965) Merrihueite, a new alkaliferromagnesian silicate from the Mezö-Madaras chondrite. Science, 149, 972–974. [PubMed: 17832577]

Downs RT (2006) The RRUFF Project: An integrated study of the chemistry, crystallography, Raman and infrared spectroscopy of minerals. Program and Abstracts of the 19th General Meeting of the International Mineralogical Association in Kobe, Japan, O03–13.

Downs RT, and Hall-Wallace M (2003) The American Mineralogist Crystal Structure Database. American Mineralogist, 88, 247–250.

Ebel DS (2006) Condensation of rocky materials in astrophysical environments. In Lauretta DS and McSween HY Jr., Eds., Meteorites and the Early Solar System II, pp. 253–277. University of Arizona Press.

Ebel DS, and Grossman L (2000) Condensation in dust-rich systems. Geochimica et Cosmochimica Acta, 65, 469–477.

Ebel DS, and Sack RO (2013) Djerfisherite: Nebular source of refractory potassium. Contributions to Mineralogy and Petrology, 166, 923–934.

Ebel DS, Weisberg MK, and Beckett JR (2012) Thermochemical stability of low-iron, manganese-enriched olivine in astrophysical environments. Meteoritics & Planetary Science, 47, 585–593.

Ebel DS, Alexander CMO'D, and Libourel G. (2018) Vapor-melt exchange: Constraints on chondrite formation conditions and processes. In Russell SA, Connelly HC, and Krot AN, Eds., Chondrules: Records of protoplanetary disk processes, pp.151–174. Cambridge University Press.

Ebert S, and Bischoff A (2016) genetic relationship between Na-rich chondrules and Ca, Al-rich inclusions?—Formation of Na-rich chondrules by melting of refractory and volatile precursors in the solar nebula. Geochimica et Cosmochimica Acta, 177, 182–204.

Ehlers K, and El Goresy A (1988) Normal and reverse zoning in niningerite: A novel key parameter to the thermal histories of EH-chondrites. Geochimica et Cosmochimica Acta, 52, 877–887.

El Goresy A, and Ehlers K (1989) Sphalerite in EH chondrites: 1. Textural relations, compositions, diffusion profiles, and pressure temperature histories. Geochimica et Cosmochimica Acta, 53, 1657–1668.

El Goresy A, Yabuki H, Ehlers K, Woolum D, and Pernicka E (1988) Qingzhen an Yamato-691: A tentative alphabet for EH chondrites. Proceedings of the NIPR Symposium on Antarctic Meteorites, 1, 65–101.

El Goresy A, Zinner E, Matsunami S, Palme H, Spettel B, Lin Y, and Nazarov M (2002) Efremovka 101.1: A CAI with ultrarefractory REE patterns and enormous enrichments of Sc, Zr, and Y in fassaite and perovskite. Geochimica et Cosmochimica Acta, 66, 1459–1491.

El Goresy A, Boyer M, and Miyahara M (2011) Almahata Sita MS-17 EL-3 chondrite fragment: contrasting oldhamite assemblages in chondrules and matrix and significant oldhamite REE-patterns. Meteoritics & Planetary Science, 46, Abstract 5079.

Fedkin AV, and Grossman L (2013) Vapor saturation of sodium: Key to unlocking the origin of chondrules. Geochimica et Cosmochimica Acta, 112, 225–250.

Fedkin AV, Grossman L, Humayun M, Simon SB, and Campbell AJ (2015) Condensates from vapor made by impacts between metal-, silicate-rich bodies: Comparison with metal and chondrules in CB chondrites. Geochimica et Cosmochimica Acta, 164, 236–261.

Fogel RA (1997) On the significance of diopside and oldhamite in enstatite chondrites and aubrites. Meteoritics, 32, 577–591.

Friedrich JM, Weisberg MK, Ebel DS, Biltz AE, Corbett BM, Iotzov IV, Khan WS, and Wolman MD (2015) Chondrule size and related physical properties: A compilation and evaluation of current data across all meteorite groups. Chemie der Erde, 75, 419–443. DOI: 10.1016/j.chemer.2014.08.003.

Friend P, Hezel DC, and Mucerschi D (2016) The conditions of chondrule formation, Part II: Open system. Geochimica et Cosmochimica Acta, 173, 198–209.

Fuchs LH, Olsen E, and Jensen KJ (1973) Mineralogy, mineral chemistry, and composition of the Murchison (C2) meteorite. Smithsonian Contributions to Earth Science, 10, 1–39.

Fujimaki H, Matsu-Ura M, Sunagawa I, and Aoki K (1981a) Chemical compositions of chondrules and matrices in the ALHA-77015 chondrite (L3). Memoirs of the NIPR Special Issue, 20, 161–174.

Fujimaki H, Matsu-Ura M, Aoki K, and Sunagawa I (1981b) Ferropseudobrookitesilica mineral-albite-chondrule in the ALH-7701 5 chondrite (L3). Memoirs of the NIPR Special Issue, 20, 119–123.

Galy A, Young E, Ash RD, and O'Nions RK (2000) The formation of chondrules at high gas pressures in the solar nebula. Science, 290, 1751–1754. [PubMed: 11099410]

Ghiorso MS, and Sack RO (1995) Chemical mass transfer in magmatic processes IV. A revised and internally consistent thermodynamic model for the interpolation and extrapolation of liquid-solid equilibria in magmatic systems at elevated temperatures and pressures. Contributions to Mineralogy and Petrology, 119, 197–212.

Ghiorso MS, Hirschmann MM, Reiners PW, and Kress VC III (2002) The pMELTS: A revision of MELTS for improved calculation of phase relations and major element partitioning related to partial melting of the mantle to 3 GPa. Geochemistry, Geophysics, Geosystems, 3, 10.1029/2001GC000217.

Gibbs JW (1876–1878) On the equilibrium of heterogeneous substances. Transactions of the Connecticut Academy of Arts and Sciences, 3, 108–248, 343–524.

Gilmour JD, Crowther SA, Busfield A, Holland G, and Whitby JA, (2009) An early I-Xe age for CB chondrite chondrule formation, and a re-evaluation of the closure age of Shallowater enstatite. Meteoritics & Planetary Science, 44, 573–579.

Golden J, McMillan M, Downs RT, Hystad G, Stein HJ, Zimmerman A, Sverjensky DA, Armstrong J, and Hazen RM (2013) Rhenium variations in molybdenite (MoS2): Evidence for progressive subsurface oxidation. Earth and Planetary Science Letters, 366, 1–5.

Goldstein JI, and Michael JR (2006) The formation of plessite in meteoritic metal. Meteoritics & Planetary Science, 41, 553–570.

Gooding JL, and Keil K (1981) Relative abundance of chondrule primary textural types in ordinary chondrites and their bearing on conditions of chondrule formation. Meteoritics, 16, 17–43.

Gounelle M, Young ED, Shahar A, Tonui E, and Kearsley A (2007) Magnesium isotopic constraints on the origin of CB_b chondrites. Earth and Planetary Science Letters, 256, 521–533.

Greshake A (1997) The primitive matrix components of the unique carbonaceous chondrite Acfer 094: A TEM study. Geochimica et Cosmochimica Acta, 61, 437–452. [PubMed: 11539920]

Grossman JN, and Brearley AJ (2005) The onset of metamorphism in ordinary and carbonaceous chondrites. Meteoritics & Planetary Science, 40, 87–122.

Grossman L, and Steele IM (1976) Amoeboid olivine aggregates in the Allende meteorite. Geochimica et Cosmochimica Acta, 40, 149–155.

Grossman JN, Rubin AE, Rambaldi ER, Rajan RS, and Wasson JT (1985) Chondrules in the Qingzhen type-3 enstatite chondrite: Possible precursor components and components and comparison to ordinary chondrite chondrules. Geochimica et Cosmochimica Acta, 49, 1781–1795.

Grossman JN, Rubin AE, and MacPherson GJ (1988) ALH 85085: A unique volatile-poor carbonaceous chondrite with implications for nebular fractionation processes. Earth and Planetary Science Letters, 91, 33–54.

Haggerty SE, and McMahon BM (1979) Magnetite-sulfide-metal complexes in the Allende meteorite. Proceedings of the Lunar and Planetary Science Conference, 10, 851–870.

Hashimoto A (1983) Evaporation metamorphism in the early solar nebula–evaporation experiments on the melt $FeO\text{-}MgO\text{-}SiO_2\text{-}CaO\text{-}Al_2O_3$ and chemical fractionations of primitive materials. Geochemical Journal, 17, 111–145.

Hazen RM (2014) Data-driven abductive discovery in mineralogy. American Mineralogist, 99, 2165–2170.

Hazen RM (2019) An evolutionary system of mineralogy: Proposal for a classification based on natural kind clustering. American Mineralogist, 104, 810–816.

Hazen RM, and Ferry JM (2010) Mineral evolution: Mineralogy in the fourth dimension. Elements, 6, 9–12.

Hazen RM, and Morrison SM (2020) An evolutionary system of mineralogy, part I: stellar mineralogy (>13 to 4.6 Ga). American Mineralogist, 105, 627–651.

Hazen RM, Papineau D, Bleeker W, Downs RT, Ferry JM, McCoy TL, Sverjensky DA, and Yang H (2008) Mineral evolution. American Mineralogist, 93, 1693–1720.

Hazen RM, Bekker A, Bish DL, Bleeker W, Downs RT, Farquhar J, Ferry JM, Grew ES, Knoll AH, Papineau D, and others. (2011) Needs and opportunities in mineral evolution research. American Mineralogist, 96, 953–963.

Hazen RM, Sverjensky DA, Azzolini D, Bish DL, Elmore SC, Hinnov L, and Milliken RE (2013) Clay mineral evolution. American Mineralogist, 98, 2007–2029.

Hazen RM, Bromberg Y, Downs RT, Eleish A, Falkowski PG, Fox P, Giovannelli D, Hummer DR, Hystad G, Golden JJ, and others. (2019a) Deep carbon through deep time: Data-driven insights. In Orcutt B, Danielle I, Dasgupta R, Eds., Deep Carbon: Past to Present, pp. 320–352. Cambridge University Press.

Hazen RM, Downs RT, Elesish A, Fox P, Gagné O, Golden JJ, Grew ES, Hummer DR, Hystad G, Krivovichev SV, and others. (2019b) Data-driven discovery in mineralogy: Recent advances in data resources, analysis, and visualization. China Engineering, 5, 397–405.

Heck PR, Greer J, Kööp L, Trappitsch R, Gyngard F, Busemann H, Maden C, Ávila JN, Davis AM, and Wieler R (2020) Lifetimes of interstellar dust from cosmic ray exposure ages of presolar grains. Proceedings of the National Academy of Sciences, DOI: 10.1073/pnas.1904573117.

Herndon JM, and Rudee ML (1978) Thermal history of the Abee enstatite chondrite. Earth and Planetary Science Letters, 41, 101–106.

Herndon JM, Rowe MW, Larson EE, and Watson DE (1975) Origin of magnetite and pyrrhotite in carbonaceous chondrites. Nature, 253, 516–518.

Hewins RH, and Zanda B (2012) Chondrules: Precursors and interactions with the nebular gas. Meteoritics & Planetary Science, 47, 1120–1138.

Hewins RH, Jones RH, and Scott ERD, Eds. (1996) Chondrules and the Protoplanetary Disk. Cambridge University Press.

Hewins RH, Connolly HC Jr., Lofgren GE, and Libourel G (2005) Experimental constraints on chondrule formation. Astronomical Society of the Pacific Conference Series, 341. 286–316.

Hezel DC, Palme H, Nasdala L, and Brenker FE (2006) Origin of SiO_2-rich components in ordinary chondrites. Geochimica et Cosmochimica Acta, 70, 1548–1564.

Hezel DC, Bland PA, Palme H, Jacquet E, and Bigolski J (2018) Composition of chondrules and matrix and their complementary relationship in chondrites. In Russell SA, Connolly HC Jr., and Krot AN, Eds., Chondrules: Records of protoplanetary disk processes, pp. 91–121. Cambridge University Press.

Hobart KK, Crapster-Pregont EJ, and Ebel DS (2015) Decoding the history of a layered chondrule through olivine grain orientation measurements using EBSD. Proceedings of the Lunar and Planetary Science Conference, 46, Abstract 1978.

Holland TJB, and Powell R (1998) An internally consistent thermodynamic data set for phases of petrological interest. Journal of Metamorphic Petrology, 16, 309–343.

Holst JC, Olsen MB, Paton C, Nagashima K, Schiller M, Wielandt D, Larsen KK, Connelly JN, Jørgensen JK, Krot AN, and others. (2013) ^{182}Hf-^{182}W age dating of a ^{26}Al-poor inclusion and implications for the origin of short-lived radioisotopes in the early Solar System. Proceedings of the National Academy of Sciences, 110, 8819–8823.

Hood LL, and Weidenschilling SJ (2012) The planetesimal bow shock model of chondrule formation: A more quantitative assessment of the standard (fixed Jupiter) case. Meteoritics & Planetary Science, 47, 1715–1727.

Howes LM, Casey AR, Asplund M, Keller SC, Yong D, Nataf DM, Poleski R, Lind K, Kobayashi C, Owen CI, and others. (2015) Extremely metal-poor stars from the cosmic dawn in the bulge of the Milky Way. Nature, 527, 484–487. [PubMed: 26560034]

Hua X, and Buseck PR (1995) Fayalite in Kaba and Mokoia carbonaceous chondrites. Geochimica et Cosmochimica Acta, 59, 563–578.

Hua X, Adam J, Palme H, and El Goresy A (1988) Fayalite-rich rims, veins, and halos around and in forsteritic olivines in CAIs and chondrules in carbonaceous chondrites: Types, compositional profiles and constraints on their formation. Geochimica et Cosmochimica Acta, 52, 1389–1408.

Hubbard A, and Ebel DS (2014) Protoplanetary dust porosity and FU Orionis outbursts: Solving the mystery of Earth's missing volatiles. Icarus, 237, 84–96.

Hubbard A (2015) Semarkona: Lessons for chondrule and chondrite formation. Icarus, 245, 32–37.

Hubbard A (2018) Evaluating non-shock, non-collisional models for chondrule formation. In Russell SA, Connolly HC Jr., and Krot AN, Eds., Chondrules: Records of protoplanetary disk processes, pp. 400–427. Cambridge University Press.

Hutchison R (2004) Meteorites: A petrologic, chemical and isotopic synthesis. Cambridge University Press.

Iida A, Nakamoto T, Susa H, and Nakagawa Y (2001) A shock model for chondrule formation in a protoplanetary disk. Icarus, 153, 430–450.

Ikeda Y (1980) Petrology of the Allan Hills-764 chondrite (LL3). Memoirs of the NIPR Special Issue, 17, 50–82.

Ikeda Y (1982) Petrology of the ALH-77003 chondrite (C3). Memoirs of the NIPR Special Issue, 25, 34–65.

Ikeda Y (1983) Alteration of chondrules and matrices in the four Antarctic carbonaceous chondrites ALH 77307 (C3), Y-790123 (C2), Y-75293 (C2), and Y-74662 (C2). Memoirs of the NIPR Special Issue, 30, 93–108.

Ikeda Y (1988a) Petrochemical study of the Yamato-691 enstatite chondrite (E3) I: Major element chemical compositions of chondrules and inclusions. Proceedings of the NIPR Symposium on Antarctic Meteorites, 1, 3–13.

Ikeda Y (1988b) Petrochemical study of the Yamato-691 enstatite chondrite (E3) II: Descriptions and mineral compositions of unusual silicate-inclusions. Proceedings of the NIPR Symposium on Antarctic Meteorites, 1, 14–37.

Ikeda Y (1989a) Petrochemical study of the Yamato-691 enstatite chondrite (E3) IV: Description and mineral chemistry of opaque nodules. Proceedings of the NIPR Symposium on Antarctic Meteorites, 2, 109–146.

Ikeda Y (1989b) Petrochemical study of the Yamato-691 enstatite chondrite (E3) III: Description and mineral compositions of chondrules. Proceedings of the NIPR Symposium on Antarctic Meteorites, 2, 75–108.

Ikeda Y, and Kimura M (1995) Anhydrous alteration of Allende chondrules in the solar nebula I. Description and alteration of chondrules with known oxygen-isotope compositions. Proceedings of the NIPR Symposium on Antarctic Meteorites, 8, 97–122.

Ivanov I, MacPherson GJ, Zolensky ME, Kononkova NN, and Migdisova LF (1996) The Kaidun meteorite: Composition and origin of inclusions in the metal of an enstatite chondrite clast. Meteoritics & Planetary Science, 31, 621–626.

Ivanov AV, Zolensky ME, Saito A, Ohsumi K, Yang V, Kononkova NN, and Mikouchi T (2000) Florenskyite, FeTiP, a new phosphide from the Kaidun meteorite. American Mineralogist, 85, 1082–1086.

Ivanova MA, Kononkova NN, Krot AN, Greenwood RC, Franchi IA, Verchovsky AB, Trieloff M, Korochantseva EV, and Brandstätter F (2008) The Isheyevo meteorite: Mineralogy, petrology, bulk chemistry, oxygen, nitrogen, carbon isotopic compositions, and ^{40}Ar-^{39}Ar ages. Meteoritics & Planetary Science, 43, 915–940.

Izawa MRM, King PL, Flemming RL, Peterson RC, and McCausland PJA (2010) Mineralogical and spectroscopic investigation of enstatite chondrites by X-ray diffraction and infrared reflectance spectroscopy. Journal of Geophysical Research Planets, 115, E7, E07008 (18 pp.).

Jacquet E, Piani L, and Weisberg MK (2018) Chondrules in enstatite chondrites. In Russell SA, Connolly HC Jr., and Krot AN, Eds., Chondrules: Records of protoplanetary disk processes, pp. 175–195. Cambridge University Press.

Johansen A, Blum J, Tanaka H, Ormel C, Bizzarro M, and Rickman H (2014) The multifaceted planetesimal formation process. In Beuther H, Klesson RS, Dullemond CP, and Henning T, Eds., Protostars and Planets VI, pp. 547–570. University of Arizona Press.

Johnson CA, and Prinz M (1991) Chromite and olivine in type II chondrules in carbonaceous and ordinary chondrites: Implications for aqueous alteration. Geochimica et Cosmochimica Acta, 55, 893–904.

Johnson BC, Minton DA, Melosh HJ, and Zuber MT (2012) Impact jetting as the origin of chondrules. Nature, 517, 339–341.

Johnson BC, Bowling TJ, and Melosh HJ (2014) Jetting during vertical impacts of spherical projectiles. Icarus, 238, 13–22.

Johnson BC, Ciesla FJ, Dullemond CP, and Melosh HJ (2018) Formation of chondrules by planetesimal collisions. In Russell SA, Connolly HC Jr., and Krot AN, Eds., Chondrules: Records of Protoplanetary Disk Processes, pp. 343–360. Cambridge University Press.

Jones RH (1990) Petrology and mineralogy of type II, FeO-rich, chondrules in Semarkona (LL3.0): Origin by closed-system fractional crystallization, with evidence for supercooling. Geochimica et Cosmochimica Acta, 54, 1785–1802.

Jones RH (1994) Petrology of FeO-poor, porphyritic pyroxene chondrules in the Semarkona chondrite. Geochimica et Cosmochimica Acta, 58, 5325–5340.

Jones RH (1996) FeO-rich, porphyritic olivine chondrules in unequilibrated ordinary chondrites. Geochimica et Cosmochimica Acta, 60, 3115–3138.

Jones RH (1997) Alteration of plagioclase-rich chondrules in CO3 chondrites: Evidence for late-stage sodium and iron metasomatism in a nebular environment. In Zolensky ME, Krot AN, and Scott ERD, Eds., Workshop on parent-body and nebular modification of chondritic materials, pp. 30–31. Lunar and Planetary Institute.

Jones RH (2012) Petrographic constraints on the diversity of chondrule reservoirs in the protoplanetary disk. Meteoritics & Planetary Science, 47, 1176–1190.

Jones RH, and Scott ERD (1989) Petrology and thermal history of type IA chondrules in the Semarkona (LL3.0) chondrite. Proceedings of the Lunar and Planetary Science Conference, 19, 523–536.

Jones RH, McCubbin FM, Dreeland L, Guan Y, Burger PV, and Shearer CK (2014) Phosphate minerals in LL chondrites: A record of the action of fluids during metamorphism on ordinary chondrite parent bodies. Geochimica et Cosmochimica Acta, 132, 120–140.

Jones RH, Villeneuve J, and Libourel G (2018) Thermal histories of chondrules: Petrologic observations and experimental constraints. In Russell SA, Connolly HC Jr., and Krot AN, Eds., Chondrules: Records of protoplanetary disk processes, pp. 57–90. Cambridge University Press.

Kawasaki N, Kato C, Itoh S, Wakaki S, Ito M, and Yurimoto H (2015) ^{26}Al-^{26}Mg chronology and oxygen isotope distributions of multiple melting for a Type C CAI from Allende. Geochimica et Cosmochimica Acta, 169, 99–114.

Keil K (1968) Mineralogical and chemical relationships among enstatite chondrites. Journal of Geophysical Research, 73, 6945–6976.

Keil K, and Snetsinger KG (1967) Niningerite: A new meteoritic sulfide. Science, 155, 451–453. [PubMed: 17737561]

Kerridge JF, and Matthews MS (1988) Meteorites and the Early Solar System. University of Arizona Press.

Kimura M, and Ikeda Y (1992) Mineralogy and petrology of an unusual Belgica-7904 carbonaceous chondrite. Proceedings of the NIPR Symposium on Antarctic Meteorites, 5, 74–119.

Kimura M, Weisberg MK, Lin Y, Suzuki A, Ohtani E, and Okazaki R (2005) Thermal history of the enstatite chondrites from silica polymorphs. Meteoritics & Planetary Science, 40, 855–868.

Kimura M, Mikouchi T, Suzuki A, Miyahara M, Ohtani E, and El Goresy A (2009) Kushiroite, $CaAlAlSiO_6$: A new mineral of the pyroxene group from the ALH 85085 CH chondrite, and its genetic significance in refractory inclusions. American Mineralogist, 94, 1479–1482.

Kimura M, Barrat JA, Weisberg MK, Imae N, Yamaguchi A, and Kojima H (2014) Petrology and bulk chemistry of Yamato-82094, a new type of carbonaceous chondrite. Meteoritics & Planetary Science, 49, 346–357.

King EA, Ed. (1983) Chondrules and their Origins. Lunar and Planetary Institute.

King AR, and Pringle JE (2010) The accretion disc dynamo in the solar nebula. Monthly Notices of the Royal Astronomical Society, 404, 1903–1909.

Kita NT, and Ushikubo T (2012) Evolution of protoplanetary disk inferred from ^{26}Al chronology of individual chondrules. Meteoritics & Planetary Science, 47, 1108–1119.

Kita NT, Yin Q-Z, MacPherson GJ, Ushikubo T, Jacobsen B, Nagashima K, Kurahashi E, Krot AN, and Jacobsen SB (2013) ^{26}Al-^{26}Mg isotope systematics of the first solids in the early Solar System. Meteoritics & Planetary Science, 48, 1383–1400.

Kita NT, Tenner TJ, Ushikubo T, Bouvier A, Wadhwa M, Bullock ES, and MacPherson GJ (2015) Why do U-Pb ages of chondrules and CAIs have more spread than their 26Al ages? 78th Annual Meteoritic Society Meeting, 5360.

Kitamura M, Watanabe S, Isobe H, and Morimoto N (1987) Diopside in chondrules of Yamato-691 (EH3). Memoirs of the NIPR Special Issue, 46, 2113–122.

Kitamura M, Isobe H, and Watanabe S (1988) Relict minerals and their assemblages in Yamato-691 (EH3). Proceedings of the NIPR Symposium on Antarctic Meteorites, 1, 38–50.

Kleine T, Budde G, Hellman JL, Kruijer TS, and Burkhardt C (2018) Tungsten isotopes and the origin of chondrules and chondrites. In Russell SA, Connolly HC Jr., and Krot AN, Eds., Chondrules: Records of Protoplanetary Disk Processes, pp. 276–299. Cambridge University Press.

Kööp L, Nakashima D, Heck PR, Kita NT, Tenner TJ, Krot AN, Nagashima K, Park C, and Davis AM (2016a) New constraints on the relationship between ^{26}Al and oxygen, calcium, and titanium isotopic variation in the early Solar System from a multielement isotopic study of spinel-hibonite inclusions. Geochimica et Cosmochimica Acta, 184, 151–172.

Kööp L, Davis AM, Nakashima D, Park C, Krot AN, Nagashima K, Temmer TJ, Heck PR, and Kita NT (2016b) A link between oxygen, calcium and titanium isotopes in ^{26}Al-poor hibonite-rich CAIs from Murchison and implications for the heterogeneity of dust reservoirs in the solar nebula. Geochimica et Cosmochimica Acta, 189, 70–95.

Kööp L, Heck PR, Busemann H, Davis AM, Greer J, Maden C, Meier MMM, and Wieler R (2018) High early solar activity inferred from helium and neon excess in the oldest meteorite inclusions. Nature Astronomy, 2, 709–713.

Krivovichev SV (2012) Topological complexity of crystal structures: quantitative approach. Acta Crystallographica, A68, 393–398.

Krivovichev SV (2013) Structural complexity of minerals: information storage and processing in the mineral world. Mineralogical Magazine, 77, 275–326.

Krot AN (2019) Refractory inclusions in carbonaceous chondrites: Records of early Solar Systems processes. Meteoritics & Planetary Science, 54, 1647–1691. [PubMed: 31379423]

Krot AN, and Rubin AE (1994) Glass-rich chondrules in ordinary chondrites. Meteoritics, 29, 697–707.

Krot AN (1996) Microchondrule-bearing chondrule rims: Constraints on chondrule formation. In Hewins RH, Jones RH, and Scott ERD, Eds., Chondrules and the Protoplanetary Disk, pp. 181–184. Cambridge University Press.

Krot AE, and Wasson JT (1994) Silica-merrihueite/roedderite-bearing chondrules and clasts in ordinary chondrites: New occurrences and possible origin. Meteoritics, 29, 707–718.

Krot AN, Ivanova MA, and Wasson JT (1993) The origin of chromitic chondrules and the volatility of Cr under a range of nebular conditions. Earth and Planetary Science Letters, 119, 569–584.

Krot AN, Scott ERD, and Zolensky ME (1995) Mineralogical and chemical modification of components in CV3 chondrites: Nebular or asteroidal processing? Meteoritics, 30, 748–775.

Krot AN, Rubin AE, Keil K, and Wasson JT (1997a) Microchondrules in ordinary chondrites: Implications for chondrule formation. Geochimica et Cosmochimica Acta, 61, 463–473.

Krot AN, Zolensky ME, Wasson JT, Scott ERD, Keil K, and Ohsumi K (1997b) Carbide magnetite assemblages in type 3 ordinary chondrites. Geochimica et Cosmochimica Acta, 61, 219–237.

Krot AN, Ulyanov AA, Meibom A, and Keil K (2001a) Forsterite-rich accretionary rims around Ca, Al-rich inclusions from the reduced CV3 chondrite Efremovka. Meteoritics & Planetary Science, 36, 611–628.

Krot AN, Meibom A, Russell SS, Alexander CMO'D, Jeffries TE, and Keil K (2001b) A new astrophysical setting for chondrule formation. Science, 291, 1776–1779. [PubMed: 11230691]

Krot AN, Petaev MI, Russell SS, Itoh S, Fagan TJ, Yurimoto H, Chizmadia L, Weisberg MK, Komatsu M, Ulyanov AA, and Keil K (2004a) Amoeboid olivine aggregates and related objects in carbonaceous chondrites: records of nebular and asteroid processes. Chemie der Erde Geochemistry, 64, 185–239.

Krot AN, Libourel G, Goodrich CA, and Petaev MI (2004b) Silica-rich igneous rims around magnesian chondrules in CR carbonaceous chondrites: Evidence for fractional condensation during chondrule formation. Meteoritics & Planetary Science, 39, 1931–1955.

Krot AN, Amelin Y, Cassen P, and Meibom A (2005) Young chondrules in CB chondrites from a giant impact in the early Solar System. Nature, 436, 989–992. [PubMed: 16107841]

Krot AN, Nagashima K, Bizzarro M, Huss GR, Davis AM, McKeegan KD, Meyer BS, and Ulyanov AA (2008) Multiple generations of refractory inclusions in the metal-rich carbonaceous chondrites Acfer 182/214 and Isheyevo. The Astrophysical Journal, 672, 713–721.

Krot AN, Makide K, Nagashima K, Huss GR, Ogliore RC, Ciesla FJ, Yang L, Hellebrand E, and Gaidos E (2012) Heterogeneous distribution of ^{26}Al at the birth of the Solar System: Evidence from refractory grains and inclusions. Meteoritics & Planetary Science, 47, 1948–1979.

Krot AN, Keil K, Scott ERD, Goodrich CA, and Weisberg MK (2014) Classification of meteorites and their genetic relationships. Treatise on Geochemistry, 2nd ed., 1, 2–63.

Krot AN, Nagashima K, van Kooten EMM, and Bizzarro M (2017) Calciumaluminum-rich inclusions recycled during formation of porphyritic chondrules from CH carbonaceous chondrites. Geochimica et Cosmochimica Acta, 201, 185–223.

Krot AN, Nagashima K, Libourel G, and Miller KE (2018) Multiple mechanisms of transient heating events in the protoplanetary disk. In Russell SA, Connolly HC Jr., and Krot AN, Eds., Chondrules: Records of protoplanetary disk processes, pp. 11–56. Cambridge University Press.

Krot AN, Ma C, Nagashima K, Davis AM, Beckett JR, Simon SB, Komatsu M, Fagan TJ, Brenker F, Ivanova MA, and Bischoff A (2019) Mineralogy, petrology, and oxygen isotopic compositions of ultra-refractory inclusions from carbonaceous chondrites. Geochemistry, 79, 125519 (29 pp.).

Kruijer TS, Touboul M, Fischer-Godde M, Bermingham KR, and Kleine T (2014) Protracted core formation and rapid accretion of protoplanets. Science, 344, 1150–1154. [PubMed: 24904163]

Kruijer TS, Burkhardt C, Budde G, and Kleine T (2017) Age of Jupiter from the distinct genetics and formation times of meteorites. Proceedings of the National Academy of Sciences, doi: 10.1073/pnas.1704461114.

Kuebler KE, McSween HY Jr., Carlson WD, and Hirsch D (1999) Sizes and masses of chondrules and metal-troilite grains in ordinary chondrites: Possible implications for nebular sorting. Icarus, 141, 96–106.

Kurahashi E, Kita NT, Nagahara H, and Morishita Y (2008) ^{26}Al-^{26}Mg systematics of chondrules in a primitive CO chondrite. Geochimica et Cosmochimica Acta, 72, 3865–3882.

Lambrechts M, Johansen A, and Morbidelli A (2014) Separating gas-giant and icegiant planets by halting pebble accretion. Astronomy & Astrophysics, 572, A35.

Larsen K, Trinquier A, Paton C, Schiller M, Wielandt D, Ivanova M, Connelly JN, Nordlund A, Krot AN, and Bizzarro M (2011) Evidence for magnesiumisotope heterogeneity in the solar protoplanetary disk. The Astrophysical Journal, 735, L37–L40.

Lauretta DS, Kremser DT, and Fegley BJ (1996) A comparative study of experimental and meteoritic metal-sulfide assemblages. Proceedings of the NIPR Symposium on Antarctic Meteorites, 9, 97–110.

Lehner SW, Buseck PR, and McDonough WF (2010) Origin of kamacite, schreibersite, and perryite in metal-sulfide nodules of the enstatite chondrite Sahara 97072 (EH3). Meteoritics & Planetary Science, 45, 289–303.

Lehnert KA, Su Y, Langmuir CH, Sarbas B, and Nohl U (2000) A global geochemical database structure for rocks. Geochemistry, Geophysics, Geosystems, 1.

Lehnert KA, Walker D, and Sarbas B (2007) EarthChem: A geochemistry data network. Geochimica et Cosmochimica Acta, 71, A559.

Leitch CA, and Smith JV (1980) Petrography, mineral chemistry and origin of Type I enstatite chondrites. Geochimica et Cosmochimica Acta, 46, 2083–2097.

Lewis JA, and Jones RH (2016) Phosphate and feldspar mineralogy of equilibrated L chondrites: The record of metasomatism during metamorphism in ordinary chondrite parent bodies. Meteoritics & Planetary Science, 51, 1886–1913.

Lewis JA (2019) Primary feldspar in the Semarkona LL3.00 chondrite: Constraints on chondrule formation and secondary alteration. Meteoritics & Planetary Science, 54, 72–89.

Libourel G, Krot AN, and Tissandier L (2006) Role of gas-melt interaction during chondrule formation. Earth and Planetary Science Letters, 251, 232–240.

Lin Y, El Goresy A, Boyer M, Feng L, Zhang J, and Hao J (2011) Earliest solid condensates consisting of the assemblage oldhamite, sinoite, graphite and excess 36S in lawrencite from Almahata Sitta MS-17 EL3 chondrite. Workshop on Formation of the First Solids in the Solar System, Abstract 9040.

Luck J-M, Ben Othman D, and Albarède F (2005) Zn and Cu isotopic variations in chondrites and iron meteorites: Early solar nebula reservoirs and parent-body processes. Geochimica et Cosmochimica Acta, 69, 5351–5363.

Lusby D, Scott ERD, and Keil K (1987) Ubiquitous high-Fe silicates in enstatite chondrites. Proceedings of the Lunar and Planetary Science Conference (Journal of Geophysical Research), 17, E679–E695.

Luu T-H, Hin RC, Coath CD, and Elliott T (2016) High precision Mg-isotope measurements of bulk chondrites and the homogeneity of ^{26}Al in the solar nebula. 79th Annual Meteoritical Society Meeting, no. 6485.

Ma C, and Rossman GR (2009) Grossmanite, $CaTi^{3+}AlSiO_6$, a new pyroxene from the Allende meteorite. American Mineralogist, 94, 1491–1494.

Ma C, and Rubin AE (2019) Edscottite, Fe_5C_2, a new iron carbide mineral from the Ni-rich Wedderburn IAB iron meteorite. American Mineralogist, 104, 1351–1355.

MacPherson GJ (2014) Calcium-aluminum-rich inclusions in chondritic meteorites. In Davis AM, Holland HD, and Turekian KK, Eds., Treatise on Geochemistry, vol. 1: Meteorites, comets, and planets, 2nd ed., p.139–179. Elsevier-Pergamon.

MacPherson GJ, Bullock ES, Janney PE, Kita N, Ushikubo T, Davis AM, Wadhwa M, and Krot AN (2010) Early solar nebula condensates do not have supracanonical initial ^{26}Al/^{27}Al. The Astrophysical Journal, 711, L117–L121.

MacPherson GJ, Kita NT, Ushikubo T, Bullock ES, and Davis AM (2012) Well-resolved variations in the formation ages for Ca-Al-rich inclusions in the early Solar System. Earth and Planetary Science Letters, 331, 43–54.

Mai C, Desch SJ, and Boley AC, and Weiss BP (2018) Magnetic fields recorded by chondrules formed in nebular shocks. The Astrophysical Journal, 857, 96 (13 pp.).

Mann CR, Boley AC, and Morris MA (2016) Planetary embryo bow shocks as a mechanism for chondrule formation. The Astrophysical Journal, 818, 103–123.

Marrocchi Y, Euverte R, Villeneuve J, Batanova V, Welsch B, Ferrière L, and Jacquet E (2019) Formation of CV chondrules by recycling of amoeboid olivine aggregate-like precursors. Geochimica et Cosmochimica Acta, 247, 121–141.

Mason B (1966) The enstatite chondrites. Geochimica et Cosmochimica Acta, 30, 23–39.

Massalski TB, Park FR, and Vassalmillet LF (1966) Speculations about plessite. Geochimica et Cosmochimica Acta, 30, 649–662.

McCoy TJ, Pun A, and Keil K (1991a) Spinel-bearing, Al-rich chondrules in two chondrite finds from Roosevelt County, New Mexico: Indicators of nebular and parent-body processes. Meteoritics, 26, 301–309.

McCoy TJ, Scott ERD, Jones RH, Keil K, and Taylor GJ (1991b) Composition of chondrule silicates in LL3–5 chondrites and implications for their nebular history and parent body metamorphism. Geochimica et Cosmochimica Acta, 55, 601–619.

McNally CP, Hubbard A, Yang C-C, and Mac Low M-M (2014) Temperature fluctuations driven by magnetorotational instability in protoplanetary disks. The Astrophysical Journal, 791, 62 (15pp).

McSween HY Jr. (1977a) Carbonaceous chondrites of the Ormans type: A metamorphic sequence. Geochimica et Cosmochimica Acta, 44, 477–491.

McSween HY Jr. (1977b) On the nature and origin of isolated olivine grains in carbonaceous chondrites. Geochimica et Cosmochimica Acta, 411–418.

Mendybaev RA, Beckett JR, Grossman L, Cooper RF, and Bradley JP (2002) Volatilization kinetics of silicon carbide in reducing gases: An experimental study with application to the survival of presolar grains in the solar nebula. Geochimica et Cosmochimica Acta, 66, 661–682.

Mills SJ, Hatert F, Nickel EH, and Ferrais G (2009) The standardization of mineral group hierarchies: Application to recent nomenclature proposals. European Journal of Mineralogy, 21, 1073–1080.

Miúra Y, and Tomisaka T (1984) Composition and structural substitution of meteoritic plagioclases (I). Memoirs of the NIPR Special Issue, 9, 210–225.

Miyamoto M, Mikouchi T, and Jones RH (2009) Cooling rates of porphyritic olivine chondrules in the Semarkona (LL3.00) ordinary chondrite: A model for diffusional equilibration of olivine during fractional crystallization. Meteoritics & Planetary Science, 44, 521–530.

Morbidelli A, Bitsch B, Crida A, Gounelle M, Guillot T, Jacobson SA, Johansen A, Lambrechts M, and Lega E (2016) Fossilized condensation lines in the Solar System protoplanetary disk. Icarus, 267, 368–376.

Morimoto N, Fabries J, Ferguson AK, Ginzburg IV, Ross M, Seifert FA, Zussman J, Aoki K, and Gottardi G (1988) Nomenclature of pyroxenes. American Mineralogist, 73, 1123–1133.

Morlok A, Sutton YC, Braithwaite N.St.J., and Grady MM (2012) Chondrules born in plasma? Simulation of gas-grain interaction using plasma arcs with applications to chondrule and cosmic spherule formation. Meteoritics & Planetary Science, 47, 2269–2280.

Morris MA, and Boley AC (2018) Formation of chondrules by shock waves. In Russell SA, Connolly HC Jr., and Krot AN, Eds., Chondrules: Records of protoplanetary disk processes. Cambridge University Press, pp. 375–399.

Morrison SM, and Hazen RM (2020) An evolutionary system of mineralogy, part II: interstellar and solar nebula primary condensation mineralogy (>4.565 Ga). American Mineralogist, 105, 1508–1535.

Morrison SM, Liu C, Eleish A, Prabhu A, Li C, Ralph J, Downs RT, Golden JJ, Fox P, Hummer DR, and others. (2017) Network analysis of mineralogical systems. American Mineralogist, 102, 1588–1596.

Morrison SM, Downs RT, Eleish A, Fox P, Hummer DR, Hystad G, Golden JJ, Liu C, Prabhu A, Zahirovic S, and Hazen RM (2020) Exploring carbon minerals: Recent advances in C mineral evolution, mineral ecology, and network analysis. Frontiers in Earth Sciences, 8, Article 208, doi: 10.3389/feart.2020.00208.

Moynier F, Dauphas N, and Podosek FA (2009) Search for ^{70}Zn anomalies in meteorites. The Astrophysical Journal Letters, 700, L92–L95.

Mueller G (1962) Interpretation of micro-structures in carbonaceous meteorites. Nature, 196, 929–932.

Müller WF, Kurat G, and Kracher A (1979) Chemical and crystallographic study of cronstedtite in the matrix of the Cochabamba (CM2) carbonaceous chondrite. Tschermaks Mineralogie und Petrographische Mitteilungen, 26, 293–304.

Müller WF, Weinbruch S, Walter R, and Müller-Beneke G (1995) Transmission electron microscopy of chondrule minerals in the Allende meteorite: Constraints on the thermal and deformational history of granular olivine-pyroxene chondrules. Planetary and Space Science, 43, 469–483.

Murakami T, and Ikeda Y (1994) Petrology and mineralogy of the Yamato-86751 CV3 chondrite. Meteoritics, 29, 397–409.

Nagahara H (1982) Ni-Fe metals in Type 3 ordinary chondrites. Memoirs of the NIPR Special Issue, 25, 86–96.

Nagahara H, and Kushiro I (1982) Petrology of chondrules, inclusions and isolated olivine grains in ALH-77307 (CO3) chondrite. Memoirs of the NIPR Special Issue, 25, 66–77.

Nagashima K, Kita NT, and Luu T-H (2018) 26Al-26Mg systematics of chondrules. In Russell SA, Connlly HC Jr., and Krot AN, Eds., Chondrules: Records of protoplanetary disk processes, pp. 247–275. Cambridge University Press.

Nakamura-Messenger K, Clemett SJ, Rubin AE, Choi B-G, Zhang S, Rahman Z, Oikawa K, and Keller LP (2012) Wassonite: A new titanium monosulfide mineral in the Yamato 691 enstatite chondrite. American Mineralogist, 97, 807–815.

Newton J, Bischoff A, Arden JW, Franchi IA, Geiger T, Greshake A, and Pillinger CT (1995) Acfer 094, a uniquely primitive carbonaceous chondrite from the Sahara. Meteoritics, 30, 47–56.

Noguchi T (1989) Texture and chemical composition of pyroxenes in chondrules in carbonaceous and unequilibrated ordinary chondrites. Proceedings of the NIPR Symposium on Antarctic Meteorites, 2, 169–199.

Noguchi T (1995) Petrology and mineralogy of the PCA 91082 chondrite and its comparison with the Yamato-793495 (CR) chondrite. Proceedings of the NIPR Symposium on Antarctic Meteorites, 8, 33–62.

Olsen EJ (1983) SiO2-bearing chondrules in the Murchison (C2) meteorite. In King EA, Ed., Chondrules and their origins, pp. 223–234. Lunar and Planetary Institute.

Oulton J, Humayun M, Fedkin A, and Grossman L (2016) Chemical evidence for differentiation, evaporation and recondensation from silicate clasts in Gujba. Geochimica et Cosmochimica Acta, 177, 254–274.

Pederson TP (1999) Schwertmannite and awaruite as alteration products in iron meteorites. Meteoritics, 62, 5117.

Pollack JB, Hubickyj O, Bodenheimer P, Lisauer JJ, Podolak M, and Greenzweig Y (1996) Formation of the giant planets by concurrent accretion of solids and gas. Icarus, 124, 62–85.

Pratesi G, Caporali S, Greenwood RC, Moggi Cecchi V, and Franchi IA (2019) A detailed mineralogical, petrographic, and geochemical study of the highly reduced chondrite, Acfer 370. Meteoritics & Planetary Science, 54, 2996–3017.

Prinz M, Weisberg MK, and Nehru CE (1988) Gunlock, a new type 3 ordinary chondrite with a golfball-sized chondrule. Meteoritics, 23, 297.

Rambaldi ER, and Wasson JT (1984) Metal and associated phases in Krymka and Chainpur: Nebular formational processes. Geochimica et Cosmochimica Acta, 48, 1885–1897.

Rambaldi ER, Rajan RS, and Housley RM (1986) Roedderite in the Qingzhen (EH3) chondrite. Meteoritics, 21, 141–149.

Ramdohr P (1967) Chromite and chromite chondrules in meteorites. Geochimica et Cosmochimica Acta, 31, 1961–1967.

Reed SJB (1968) Perryite in the Kota-Kota and South Oman enstatite chondrites. Mineralogical Magazine, 36, 850–854.

Richter FM, Mendybaev RA, Christensen JN, Ebel D, and Gaffney A (2011) Laboratory experiments bearing on the origin and evolution of olivine-rich chondrules. Meteoritics & Planetary Science, 46, 1152–1178.

Robertson BE, Ellis RS, Furlanetto SR, and Dunlop JS (2015) Cosmic reionization and early star-forming galaxies: A joint analysis of new constraints from Planck and the Hubble Space Telescope. The Astrophysical Journal, 802, L19–L23.

Rubin AE (1983) The Adhi Kot breccia and implications for the origins of chondrites and silica-rich clasts in enstatite chondrites. Earth and Planetary Science Letters, 64, 201–212.

Rubin AE (1984a) Coarse-grained chondrule rims in type 3 chondrites. Geochimica et Cosmochimica Acta, 48, 1779–1789.

Rubin AE (1984b) The Blithfield meteorite and the origin of sulfide-rich, metal-poor clasts and inclusions in brecciated enstatite chondrites. Earth and Planetary Science Letters, 67, 273–283.

Rubin AE (1989) An olivine-microchondrule-bearing clast in the Krymka meteorite. Meteoritics, 24, 191–192.

Rubin AE (1990) Kamacite and olivine in ordinary chondrites: Intergroup and intragroup relationships. Geochimica et Cosmochimica Acta, 54, 1217–1232.

Rubin AE (1991) Euhedral awaruite in the Allende meteorite: Implications for the origin of awaruite- and magnetite-bearing nodules in CV3 chondrites. American Mineralogist, 76, 1356–1362.

Rubin AE (1994a) Metallic copper in ordinary chondrites. Meteoritics, 29, 93–98.

Rubin AE (1994b) Euhedral tetrataenite in the Jelica meteorite. Mineralogical Magazine, 58, 215–221.

Rubin AE (1997a) Igneous graphite in enstatite chondrites. Mineralogical Magazine, 61, 699–703.

Rubin AE (1997b) Sinoite (Si2N2O): Crystallization from EL chondrite impact melts. American Mineralogist, 82, 1001–1006.

Rubin AE (2000) Petrologic, geochemical and experimental constraints on models of chondrule formation. Earth-Science Reviews, 50, 3–27.

Rubin AE (2006) A relict-grain-bearing porphyritic olivine compound chondrule from LL3.0 Semarkona that experienced limited remelting. Meteoritics & Planetary Science, 41, 1027–1038.

Rubin AE (2010) Physical properties of chondrules in different chondrite groups: Implications for multiple melting events in dusty environments. Geochimica et Cosmochimica Acta, 74, 4807–4828.

Rubin AE (2011) Origin of the differences in refractory-lithophile-element abundances among chondrite groups. Icarus, 213, 547–558.

Rubin AE (2018) Evaluation of petrologic evidence for high partial pressures of SiO(g) in the solar nebula. Meteoritics & Planetary Science, 53, 2596–2607.

Rubin AE, and Grossman JN (1985) Phosphate-sulfide assemblages and Al/Ca ratios in type 3 chondrites. Meteoritics, 20, 479–489.

Rubin AE, and Kallemeyn GW (1989) Carlisle Lakes and Allan Hills 85151: Members of a new chondrite grouplet. Geochimica et Cosmochimica Acta, 53, 3035–3044.

Rubin AE (1994) Pecora Escarpment 91002: A member of the new Rumuruti (R) chondrite group. Meteoritics, 29, 255–264.

Rubin AE, and Ma C (2017) Meteoritic minerals and their origins. Chemie der Erde, 77, 325–385.

Rubin AE (2021) Meteorite Mineralogy. Cambridge University Press.

Rubin AE, and Scott ERD (1997) Abee and related EH chondrite impact-melt breccias. Geochimica et Cosmochimica Acta, 61, 425–435.

Rubin AE, and Wasson JT (1987) Chondrules, matrix and coarse-grained chondrule rims in the Allende meteorite. Geochimica et Cosmochimica Acta, 52, 425–432.

Rubin AE (1988) Chondrules and matrix in the Ornans CO3 meteorite: Possible precursor components. Geochimica et Cosmochimica Acta, 52, 425–432.

Rubin AE, Scott ERD, and Keil K (1982) Microchondrule-bearing clast in the Piancaldoli LL3 meteorite: A new type 3 chondrite and its relevance to the history of chondrules. Geochimica et Cosmochimica Acta, 46, 1763–1776.

Rubin AE, James JA, Keck BD, Weeks KS, Sears DWG, and Jarosewich E (1985) The Colony meteorite and variations in CO3 chondrite properties. Meteoritics, 20, 175–196.

Rubin AE, Wang D, Kallemeyn GW, and Wasson JT (1988) The Ningqiang meteorite: Classification and petrology of an anomalous CV chondrite. Meteoritics, 23, 13–23.

Rubin AE, Sailer AL, and Wasson JT (1999) Troilite in the chondrules of type-3 ordinary chondrites: Implications for chondrule formation. Geochimica et Cosmochimica Acta, 63, 2281–2298.

Rubin AE, Kallemeyn GW, Wasson JT, Clayton RN, Mayeda TK, Grady M, Verchovsky AB, Eugster O, and Lorenzetti S (2003) Formation of metal and silicate nodules in Gujba: A new Bencubbin-like meteorite fall. Geochimica et Cosmochimica Acta, 67, 3283–3298.

Russell SA, Connolly HC Jr., and Krot AN, Eds. (2018) Chondrules: Records of Protoplanetary Disk Processes. Cambridge University Press.

Russell SS, Lee MR, Arden JW, and Pillinger CT (1995) The isotopic composition and origins of silicon nitride in the ordinary and enstatite chondrites. Meteoritics, 30, 399–404.

Ruzicka A (1990) Deformation and thermal histories of chondrules in the Chainpur (LL3.4) chondrite. Meteoritics, 25, 101–114.

Ruzicka A (2012) Chondrule formation by repeated evaporative melting and condensation in collisional debris clouds around planetesimals. Meteoritics & Planetary Science, 47, 2218–2236.

Sack RO, and Ghiorso MS (2017) Ti^{3+}- and Ti^{4+}-rich fassaites at the birth of the Solar System: Thermodynamics and applications. American Journal of Science, 317, 807–845.

Sanders IS, and Scott ERD (2012) The origin of chondrules and chondrites: Debris from low-velocity impacts between molten planetesimals? Meteoritics & Planetary Science, 47, 2170–2192.

Sanders IS (2018) Making chondrules by splashing molten planetesimals: The dirty impact plume model. In Russell SA, Connolly HC Jr., and Krot AN, Eds., Chondrules: Records of protoplanetary disk processes, pp. 361–374. Cambridge University Press.

Schatz H (2010) The evolution of elements and isotopes. Elements, 6, 13–17.

Schertl H-P, Mills SJ, and Maresch WV (2018) A Compendium of IMA-Approved Mineral Nomenclature. International Mineralogical Association.

Schrader DL, Nagashima K, Krot AN, Ogliore RC, Yin Q-Z, Amelin Y, Stirling CH, and Kaltenbach A (2017) Distribution of ^{26}Al in the CR chondrite chondrule-forming region of the protoplanetary disk. Geochimica et Cosmochimica Acta, 201, 275–302.

Schulze H, Bischoff A, Palme H, Spettel B, Dreibus G, and Otto J (1994) Mineralogy and chemistry of Rumuruti: The first meteorite fall of the new R chondrite group. Meteoritics, 29, 275–286.

Scott ERD (1988) A new kind of primitive chondrite, Allan Hills 85085. Earth and Planetary Science Letters, 91, 1–18.

Scott ERD, and Clarke RS Jr. (1979) Identification of clear taenite in meteorites as ordered FeNi. Nature, 281, 113–124.

Scott ERD, and Jones RH (1990) Disentangling nebular and asteroidal features of CO3 of carbonaceous chondrites. Geochimica et Cosmochimica Acta, 54, 2485–2502.

Scott ERD, and Krot AN (2014) Chondrites and their components. In Davis AM, Holland HD, and Turekian KK, Eds., Treatise on geochemistry, Vol. 1: Meteorites, comets, and planets, Second Edition, pp. 65–137. Elsevier-Pergamon.

Scott ERD, and Rajan S (1981) Metallic minerals, thermal histories, and parent bodies of some xenolithic ordinary chondrites. Geochimica et Cosmochimica Acta, 45, 53–67.

Scott ERD, and Taylor GJ (1983) Chondrules and other components in C, O, and E chondrites: Similarities in their properties and origins. Journal of Geophysical Research, 88, B275–B286.

Scott ERD, Taylor GJ, and Maggiore P (1982) A new LL3 chondrite, Allan Hills 79003, and observations on matrices in ordinary chondrites. Meteoritics, 17, 19–31.

Scott ERD, Jones RH, and Rubin AE (1994) Classification, metamorphic history, and pre-metamorphic composition of chondrules. Geochimica et Cosmochimica Acta, 58, 1203–1209.

Sears DWG, and Hasan FA (1987) The type three ordinary chondrites: A review. Surveys in Geophysics, 9, 43–97.

Sears DWG, Kallemeyn GW, and Wasson JT (1982) The compositional classification of chondrites. II. The enstatite chondrite groups. Geochimica et Cosmochimica Acta, 46, 597–608.

Sears DWG, Lu J, Benoit PH, DeHart JM, and Lofgren GE (1992) A compositional classification scheme for meteoritic chondrules. Nature, 357, 207–210.

Sears DWG, Morse AD, Hutchison R, Guimon RK, Lu J, Alexander CMO'D, Benoit PH, Wright I, Pillinger C, Xie T, and Lipschutz ME (1995) Metamorphism and aqueous alteration in low petrographic type ordinary chondrites. Meteoritics, 30, 169–181.

Sheng YJ, Hutcheon ID, and Wasserburg GJ (1991a) Origin of plagioclase-olivine inclusions in carbonaceous chondrites. Geochimica et Cosmochimica Acta, 55, 581–599.

Sheng YJ, Beckett JR, Hutcheon ID, and Wasserberg GJ (1991b) Experimental constraints on the origin of plagioclase-olivine inclusions and CA chondrules. Abstracts of the Lunar and Planetary Science Conference, 22, 1231.

Shibata Y (1996) Opaque minerals in Antarctic CO3 carbonaceous chondrites. Yamato-74135, −790992, −79717, −81020, −81025, −82050, and Allan Hills 77307. Proceedings of the NIPR Symposium on Antarctic Meteorites, 9, 79–96.

Shimizu M, Yoshida H, and Mandarino JA (2002) The new mineral species keilite, (Fe,Mg)S, the iron-dominant analogue of niningerite. Canadian Mineralogist, 40, 1687–1692.

Shu FH, Shang H, and Lee T (1996) Toward an astrophysical theory of chondrites. Science, 271, 1545–1552.

Simon SB, and Haggerty SE (1980) Bulk compositions of chondrules in the Allende meteorite. Proceedings of the Lunar and Planetary Science Conference, 11, 901–927.

Simon SB, Grossman L, Podosek FA, Zinner E, and Prombo CA (1994) Petrography, composition, and origin of large chromian spinels from the Murchison meteorite. Geochimica et Cosmochimica Acta, 58, 1313–1334.

Simon SB, Grossman L, Casanova I, Symes S, Benoit P, Sears DWG, and Wacker JF (1995) Axtell, a new CV3 chondrite from Texas. Meteoritics, 30, 42–46.

Singerling SA, and Brearley AJ (2018) Primary iron sulfides in CM and CR carbonaceous chondrites: Insights into nebular processes. Meteoritics & Planetary Science, 53, 2078–2106.

Smith DGW, Miura Y, and Launspach S (1993) Fe, Ni, and Co variations in the metals from some Antarctic chondrites. Earth and Planetary Science Letters, 120, 487–498.

Sorrell W (1995) Nebular lightning and the chondrule factory. Comments of Astrophysics, 18, 151–159.

Stöffler D, Keil K, and Scott ERD (1991) Shock metamorphism of ordinary chondrite meteorites. Geochimica et Cosmochimica Acta, 55, 3845–3867.

Tachibana S, and Huss GR (2005) Sulfur isotopic composition of putative primary troilite in chondrules from Bishunpur and Semarkona. Geochimica et Cosmochimica Acta, 69, 3075–3097.

Taylor GJ, and Heymann D (1971) Postshock thermal histories of reheated chondrites. Journal of Geophysical Research, 76, 1879–1893.

Taylor GJ, Okada A, Scott ERD, Rubin AE, Huss GR, and Keil K (1981) The occurrence and implications of carbide-magnetite assemblages in unequilibrated ordinary chondrites. Proceedings of the Lunar and Planetary Science Conference, 12, 1076–1078.

Teitler SA, Paque JM, Cuzzi JN, and Hogan RC (2010) Statistical tests of chondrule sorting. Meteoritics & Planetary Science, 45, 1124–1135.

Tomeoka K, and Buseck PR (1990) Phyllosilicates in the Mokoia CV carbonaceous chondrite: Evidence for aqueous alteration in an oxidizing condition. Geochimica et Cosmochimica Acta, 54, 1787–1796.

Töpel-Schadt J, and Müller WF (1985) The submicroscopic structure of the unequilibrated ordinary chondrites, Chainpur, Mezö-Madaras, and Tieschitz. Meteoritics, 27, 136–143.

Trieloff M, Storck J-C, Mostefaoui S, El Goresy A, Hopp J, Ludwig T, and Altherr R (2013) A precise ^{53}Mn-^{53}Cr age of sphalerites from the primitive EH3 chondrite Sahara 97158. Meteoritics & Planetary Science Supplement, 76, 5251.

Trinquier A, Birck J, and Allegre CJ (2007) Widespread ^{54}Cr heterogeneity in the inner Solar System. The Astrophysical Journal, 655, 1179–1185.

Trinquier A, Elliott T, Ulfbeck D, Coath C, Krot AN, and Bizzarro M (2009) Origin of nucleosynthetic isotope heterogeneity in the solar protoplanetary disk. Science, 324, 374–376. [PubMed: 19372428]

Van Schmus WR, and Wood JA (1967) A chemical-petrologic classification for the chondrite meteorites. Geochimica et Cosmochimica Acta, 31, 747–754.

Wang Y, and Hsu W (2009) Petrology and mineralogy of the Ningqiang carbonaceous chondrite. Meteoritics & Planetary Science, 44, 763–780.

Wang Y, Hsu W, Li X, Li Q, Liu Y, and Tang G (2016) Petrology, mineralogy, and oxygen isotope compositions of aluminum-rich chondrules from CV3 chondrites. Meteoritics & Planetary Science, 51, 116–137.

Warren P (2011) Stable-isotopic anomalies and the accretionary assemblage of the Earth and Mars: A subordinate role for carbonaceous chondrites. Earth and Planetary Science Letters, 311, 93–100.

Wasserburg GJ, Wimpenny J, and Yin Q-Z (2012) Mg isotopic heterogeneity, Al-Mg isochrons, and canonical ^{26}Al/^{27}Al in the early Solar System. Meteoritics & Planetary Science, 47, 1980–1997.

Wasson JT, and Krot AN (1994) Fayalite-silica association in unequilibrated ordinary chondrites: Evidence for aqueous alteration on a parent body. Earth and Planetary Science Letters, 122, 403–416.

Wasson JT, and Rubin AE (2003) Ubiquitous low-FeO relict grains in type-II chondrules and limited overgrowths on relicts and high-FeO phenocrysts following the final melting event. Geochimica et Cosmochimica Acta, 67, 2239–2250.

Wasson JT, and Wai CM (1970) Composition of the metal, schreibersite and perryite of enstatite achondrites and the origin of enstatite chondrites and achondrites. Geochimica et Cosmochimica Acta, 34, 169–184.

Wasson JT, Krot AN, Lee MS, and Rubin AE (1995) Compound chondrules. Geochimica et Cosmochimica Acta, 59, 1847–1869.

Watanabe S, Kitamura M, and Morimoto N (1986) Oscillatory zoning of pyroxenes in ALH-77214 (L3). Symposium on Antarctic Meteorites, 11, 74–75.

Weber D, and Bischoff A (1997) Refractory inclusions in the CR chondrite Acler 059-El Djouf 001: Petrology, chemical composition, and relationship to inclusion populations in other types of carbonaceous chondrites. Chemie der Erde, 57, 1–24.

Weinbruch S, Palme H, Müller WF, and El Goresy A (1990) FeO-rich rims and veins in Allende forsterite: Evidence for high-temperature condensation at oxidizing conditions. Meteoritics, 25, 115–125.

Weinbruch S, Armstrong JT, and Palme H (1994) Constraints on the thermal history of the Allende parent body as derived from olivine-spinel thermometry and Fe/Mg interdiffusion in olivine. Geochimica et Cosmochimica Acta, 58, 1019–1030.

Weinbruch S, Palme H, and Spettel B (2000) Refractory forsterite in primitive meteorites: Condensates from the solar nebula? Meteoritics & Planetary Science, 35, 161–171.

Weisberg MK, and Kimura M (2012) The unequilibrated enstatite chondrites. Chemie der Erde, 72, 101–115.

Weisberg MK, Prinz M, and Nehru CE (1988) Petrology of ALH85085: A chondrite with unique characteristics. Earth and Planetary Science Letters, 91, 19–32.

Weisberg MK, McCoy T, and Krot AN (2006) Systematics and evaluation of meteorite classification. In Lauretta D and McSween H, Eds., Meteorites and the early Solar System II, pp. 19–52. University of Arizona Press.

Weyrauch M, and Bischoff A (2012) Macrochondrules in chondrites—Formation by melting of mega-sized dust aggregates and/or by rapid collisions at high temperatures? Meteoritics & Planetary Science, 47, 2237–2250.

Weyrauch M, Horstmann M, and Bischoff A (2018) Chemical variations of sulfides and metal in enstatite chondrites—Introduction of a new classification scheme. Meteoritics & Planetary Science, 53, 394–415.

Whitby JA, Gilmour JD, Turner G, Prinz M, and Ash RD (2002) Iodine-xenon dating of chondrules from the Qingzhen and Kota Macro chondrules enstatite chondrites. Geochimica et Cosmochimica Acta, 66, 347–359.

Wlotzka F (1993) A weathering scale for the ordinary chondrites (abstract). Meteoritics, 28, 460.

Wombacher F, Rehkämper M, Mezger K, Bischoff A, and Münker C (2008) Cadmium stable isotope cosmochemistry. Geochimica et Cosmochimica Acta, 72, 646–667.

Wood JA (1967) Chondrules: Their metallic minerals, thermal histories, and parent planets. Icarus, 6, 1–49.

Wood JA (1996a) Processing of chondritic and planetary material in spiral density waves in the nebula. Meteoritics, 31, 641–645.

Wood JA (1996b) Unresolved issues in the formation of chondrules and chondrites. In Hewins R, Jones RH, and Scott ERD, Eds., Chondrules and the protoplanetary disk, pp. 55–70. Cambridge University Press.

Wood JA, and Hashimoto A (1993) Mineral equilibrium in fractionated nebular systems. Geochimica et Cosmochimica Acta, 57, 2377–2388.

Wood JA, and Holmberg BB (1994) Constraints placed on chondrule-forming process by merrihueite in the Mezo-Madaras chondrite. Icarus, 108, 309–324.

Zanda B, Bouret-Denise M, Peron C, and Hewins RH (1994) Origin and metamorphic redistribution of silicon, chromium, and phosphorus in the metal of chondrites. Science, 265, 1846–1849. [PubMed: 17797224]

Zhang A, and Hsu W (2009) Refractory inclusions and aluminum-rich chondrules in Sayh al Uhaymir 290 CH chondrite: Petrography and mineralogy. Meteoritics & Planetary Science, 44, 787–804.

Zhang Y, Huang S, Schneider D, Benoit PH, and Sears DWG (1996) Pyroxene structures, cathodoluminescence and thermal history of the enstatite chondrites. Meteoritics & Planetary Science, 31, 87–96.

Zhdankin V, Boldryev S, and Mason J (2017) Influence of a large-scale field on energy dissipation in magnetohydrodynamic turbulence. Monthly Notices of the Royal Astronomical Society, 468, 4025–4029.

Zolensky M, Gounelle MU, Mikouchi T, Ohsumi K, Le L, Hagiya K, and Tachikawa O (2008) Andreyivanovite: A second new phosphide from the Kaidun meteorite. American Mineralogist, 93, 1295–1299.

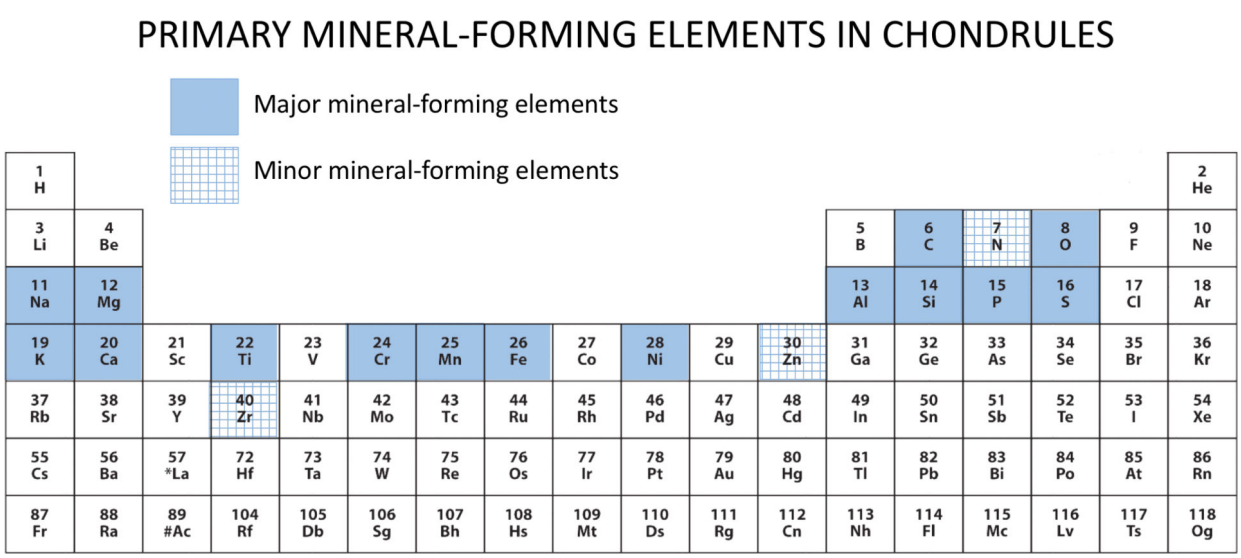

Figure 1.

Primary chondrule minerals form principally from 15 structurally essential elements, with important additional contributions from 3 additional minor elements.

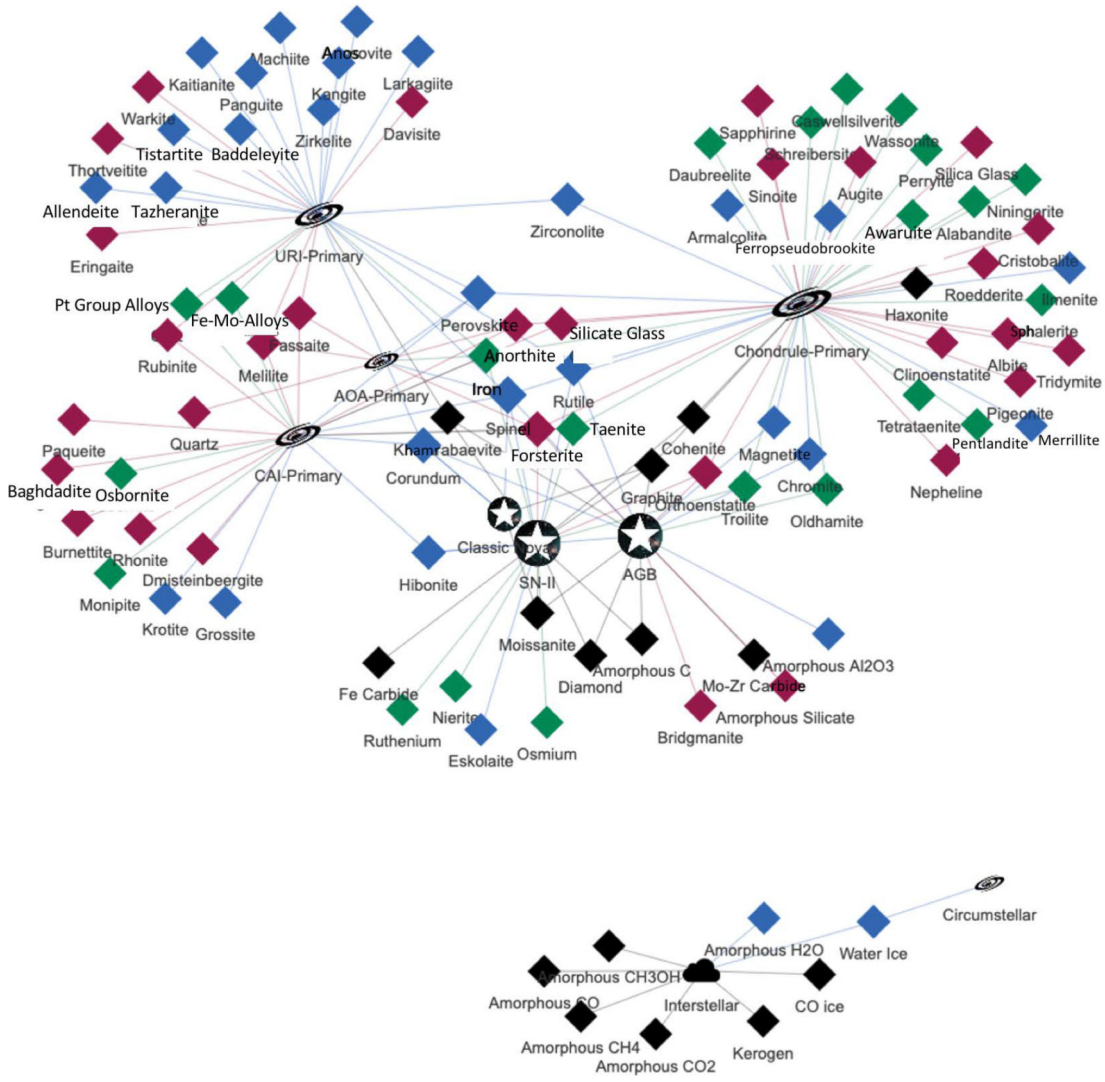

Figure 2.

Bipartite force-directed network graph (Morrison et al. 2017) of primary stellar, interstellar, and nebular minerals linked to their modes of paragenesis. Diamond-shaped nodes represent condensed crystalline and amorphous phases [black (C-bearing), green (not C or O), blue (contains O, but not C or Si), and red (contains Si + O)]. Star-shaped nodes represent three types of host stars: asymptotic giant branch stars (AGB), Type II supernovae (SN-II), and classical novae (CNova); the cloud-shaped node represents dense molecular clouds (DMC); and five disk-shaped nodes indicate circumstellar environments, CAI, AOA, URI, and PC minerals. The sizes of paragenetic mode nodes correspond to the numbers of links to mineral nodes. Note that 8 low-temperature phases of the interstellar medium are not linked to 88 high-temperature primary phases of stellar and nebular environments.

TABLE 1.

Chronology of nebular processes that affect mineral evolution

Object	Earliest age	Latest age	Description	Part	Reference[a]
Stardust	~13 Ga	4.58 Ga	Presolar grains are distinguished by their extreme isotopic anomalies.	I	*1–3*
URIs	4567.3 Ma	<4567.0 Ma	Though usually grouped with CAIs, ultra-refractory inclusions display extreme (×1000) enrichment in Sc, Zr, Ti, and other elements that lead to distinctive suites of minerals.	II	*4–7*
CAIs	4567.3 Ma	4567.0 Ma	CAIs formed in a high-temperature, high-gas/dust region near the proto-sun. Within 2 million years, most CAIs had migrated to beyond proto-Jupiter's orbit under the influence of strong solar winds.	II	*8–10*
AOAs	<4567.3 Ma	4567.0 Ma	Amoeboid olivine aggregates form at lower temperatures than CAIs and URIs, but still in a low-pressure region close to the proto-sun, with high gas/dust. Some AOAs incorporate CAIs and thus postdate the first CAIs.	II	*7, 11, 12*
Embryos	~4567 Ma		By the time the protoplanetary disk was ~1 million years old, embryonic Jupiter (mass >20 Earth mass) created a gravitational barrier between the inner and outer solar system. Isotopic studies of iron meteorites suggest that their parent bodies must have reached diameters of 1 to 100 km within the first 500 000 yrs.	III	*13–16*
Chondrules[b]	~4566 Ma	~4561 Ma	Chondrules vary widely in their physical and chemical characteristics, but most (if not all) chondrules significantly postdate CAIs. Chondrules represent igneous processing of nebular material at high temperatures in regions with high dust/gas.	III	*9, 17–19*
CO	4565.6	4564.7			*20*
CV	4565.1 ± 0.8				*21, 22*
	4565.6 ± 1.0				*23*
	4564.5 ± 0.5				*24*
	4564.3 ± 0.8				*25*
CR	4563.7 ± 0.6				*26*
	4563.6 ± 0.6				*27*
CB	4562.5 ± 0.2				*28*
	4562.7 ± 0.5				*29*
	4562.3 ± 0.4				*30*
EH	4564	4561			*31*
	4562.7 ± 0.5				

Notes: "Part" refers to the multi-part evolutionary system of mineralogy.

[a]1. Davis (2011); 2. Heck et al. (2020); 3. Hazen and Morrison (2020); 4. El Goresy et al. (2002); 5. Rubin and Ma (2017); 6. Krot et al. (2019); 7. Morrison and Hazen (2020); 8. Connelly et al. (2012); 9. Kita et al. (2013); 10. Krot (2019); 11. Grossman and Steele (1976); 12. Krot et al. (2004); 13. Kruijer et al. (2014); 14. Lambrechts et al. (2014); 15. Morbidelli et al. (2016); 16. Kruijer et al. (2017); 17. Bollard et al. 2017; 18. Nagashima et al. (2018); 19. Connelly and Bizzarro (2018); 20. Kurahashi et al. (2008); 21. Budde et al. (2015); 22. Kleine et al. (2018); 23. Amelin and Krot (2007); 24. Connelly et al. (2008); 25. Connelly and Bizzarro (2009); 26. Kleine et al. (2018); 27. Schrader et al. (2017); 28. Bollard et al. (2015); 29. Krot et al. (2005); 30. Gilmour et al. (2009); 31. Whitby et al. (2002); 32. Trieloff et al. (2013).

[b]Alternative Pb-Pb age measurements of unequilibrated chondrites suggest that the earliest chondrules formed contemporaneously with CAIs at 4567.30 ± 0.16 Ma, and extending to 4564.7 ± 0.3 Ma. According to this model, most chondrules were produced within the first 1 million years of the protoplanetary disk (Connelly et al. 2012; Bollard et al. 2017; Connelly and Bizzarro 2018; Krot 2019).

TABLE 2.

43 primary mineral phases in chondrules

Species (formula)	Natural kind	Characteristics	References
	Native elements		
Iron (Fe,Ni) [“kamacite”]	*PC iron*	Occurs as a primary phase with up to 10 wt% Ni	*1–3*
Taenite (Fe,Ni)	*PC taenite*	Typically 1 to 50 wt% Ni	*1, 4–7*
Tetrataenite (Fe,Ni)	*PC tetrataenite*	Typically ~50 wt% Ni	*1, 5, 6, 8, 9*
Awaruite (Ni_2Fe to Ni_3Fe)	*PC awaruite*	Typically 6 to 75 wt% Ni	*1, 10, 11*
Graphite (C)	*PC graphite*	A common minor phase in enstatite chondrites	*1, 12, 13*
	Carbides		
Cohenite [$(Fe,Ni)_3C$]	*PC cohenite*	Associated with haxonite and magnetite	*1, 3, 10, 14–18*
Haxonite [$(Fe,Ni)_{23}C_6$]	*PC haxonite*	Associated with cohenite and magnetite	*3, 15, 17, 18*
	Nitrides		
Sinoite (Si_2N_2O)	*PC sinoite*	Micron-scale needles in metal nodules from an EL3 clast	*19, 20*
	Phosphides		
Schreibersite [$(Fe,Ni)_3P$]	*PC schreibersite*	Occurs as exsolution from P-rich Fe-Ni alloys	*1, 21–23*
	Silicides		
Perryite [$(Ni,Fe)_8(Si,P)_3$]	*PC perryite*	A minor phase in enstatite chondrites	*12, 24, 25*
	Sulfides		
Troilite (FeS)	*PC troilite*	The most common primary chondrule sulfide	*1–3, 26–31*
Pentlandite [$(Fe,Ni)_9S_8$]	*PC pentlandite*	Occurs in unequilibrated OC and CC meteorites	*1, 27, 32–34*
Alabandite (MnS)	*PC alabandite*	Occurs with other reduced sulfides in EL chondrites	*1–3, 35–38*
Caswellsilverite ($NaCrS_2$)	*PC caswellsilverite*	Occurs with other reduced sulfides in enstatite chondrites	*1–3, 35–38*
Daubréelite ($FeCr_2S_4$)	*PC daubréelite*	Occurs with other reduced sulfides in enstatite chondrites	*1–3, 35–38*
Niningerite (MgS)	*PC niningerite*	Occurs with other reduced sulfides in EH chondrites	*1–3, 35–38*
Oldhamite (CaS)	*PC oldhamite*	Occurs with other reduced sulfides in enstatite chondrites	*1–3, 35–38*
Sphalerite (ZnS)	*PC sphalerite*	A rare primary phase in EH enstatite chondrite Y-691	*39*
Wassonite (TiS)	*PC wassonite*	A rare primary phase in EH enstatite chondrite Y-691	*40*
	Oxides		
Spinel ($MgAl_2O_4$)	*PC spinel*	Spinel is a common, if minor, primary OC chondrule phase	*1, 41–48*

Species (formula)	Natural kind	Characteristics	References
Chromite ($Fe^{2+}Cr_2O_4$)	*PC chromite*	A common oxide phase in NC and CC chondrules	*1, 49–52*
Magnetite ($Fe^{2+}Fe^{3+}{}_2O_4$)	*PC magnetite*	In carbide-magnetite assemblages; with Fe-Ni alloys	*1, 27, 34, 53–56*
Rutile (TiO_2)	*PC rutile*	A minor phase in plagioclase-olivine inclusions	*47*
Ilmenite ($FeTiO_3$)	*PC ilmenite*	In Na-Al-rich chondrules; plagioclase-olivine inclusions	*47, 57*
Armalcolite [$(Mg,Fe^{2+})Ti_2O_5$]	*PC armalcolite*	A minor phase in plagioclase-olivine inclusions	*47*
Ferropseudobrookite ($Fe^{2+}Ti_2O_5$)	*PC ferropseudobrookite*	Euhedral crystals in Allan Hills 77015 (EL3)	*58, 59*
Perovskite ($CaTiO_3$)	*PC perovskite*	A minor phase in plagioclase-olivine inclusions	*47*
Zirconolite ($CaZrTi_2O_7$)	*PC zirconolite*	A minor phase in plagioclase-olivine inclusions	*47*
	Phosphates		
Merrillite [$Ca_9NaMg(PO_4)_7$]	*PC merrillite*	Minor phase in glass-rich and silica-pyroxene chondrules	*48, 60, 61*
	Silicates		
Cristobalite (SiO_2)	*PC cristobalite*	Occurs in silica-rich chondrules in OC and EC chondrites	*18, 61–63*
Tridymite (SiO_2)	*PC tridymite*	Occurs in silica-rich chondrules in OC and EC chondrites	*61–64*
Silica Glass (SiO_2)	*PC silica glass*	In silica-rich chondrules from both NC and CC chondrites	*61, 63, 65, 66*
Olivine [$(Mg,Fe)_2SiO_4$]	*PC olivine*	A common primary chondrule phase in all chondrite types	*1–3, 67*
Orthoenstatite [$(Mg,Fe)SiO_3$]	*PC orthoenstatite*	Less common than clinoenstatite; in OC, EC, and CC	*1–3, 33, 68–71*
Clinoenstatite [$(Mg,Fe)SiO_3$]	*PC clinoenstatite*	A common primary chondrule phase in all chondrite types	*1–3, 70, 72*
Pigeonite [$(Mg,Fe,Ca)SiO_3$]	*PC pigeonite*	As crystals and as layers coating clinoenstatite	*1, 64, 70, 73–74*
Augite [$(Ca,Mg,Fe)(Mg,Fe,\pm Al,\pm Ti^{3+})(\pm Al,\pm Ti^{4+},Si)SiO_6$]	*PC augite*	A common primary chondrule phase	*1, 57, 70, 74–76*
Anorthite [$(Ca,Na)(Al,Si)_2Si_2O_8$]	*PC anorthite*	A common primary phase; notable in Al-rich chondrules	*1, 64, 77–82*
Albite ($NaAlSi_3O_8$)	*PC albite*	Occurs with ferropseudobrookite in Allan Hills 77015 (EL3)	*58, 59*
Nepheline [$Na_3K(Al_4Si_4O_{16})$]	*PC nepheline*	Epitaxial intergrowths with anorthite; Al-rich chondrules	*1, 68, 74, 77*
Sapphirine [$Mg_4(Mg_3Al_9)O_4(Si_3Al_9O_{36})$]	*PC sapphirine*	A minor phase in plagioclase-olivine inclusions	*47, 74*
Roedderite [$(Na,K)_2Mg_5Si_{12}O_{30}$]	*PC roedderite*	A minor phase in silica-rich chondrules	*83–86*
Silicate Glass (Ca,Mg,Al,Si,O)	*PC silicate glass*	Common in chondrule mesostasis	*60*

Notes:

1. Brearley and Jones (1998);

2. Rubin and Ma (2017);

[3] Rubin and Ma (2021);
[4] Afiattalab and Wasson (1980);
[5] Scott and Rajan (1981);
[6] Nagahara (1982);
[7] Wood (1967);
[8] Bevan and Axon (1980);
[9] Rubin (1994b);
[10] Taylor et al. (1981);
[11] Smith et al. (1993);
[12] Keil (1968);
[13] Leitch and Smith (1980);
[14] Scott et al. (1982);
[15] Scott and Jones (1990);
[16] Herndon and Rudee (1978);
[17] Shibata (1996);
[18] Rubin (1983);
[19] Lin et al. (2011);
[20] El Goresy et al. (2011);
[21] Wasson and Wai (1970);
[22] Rambaldi and Wasson (1984);
[23] Zanda et al. (1994);
[24] Reed (1968);
[25] Lehner et al. (2010);
[26] Rubin et al. (1999);
[27] Krot et al. (1997b);

[28] Lauretta et al. (1996);

[29] Singerling and Brearley (2018);

[30] El Goresy et al. (1988);

[31] Ikeda (1989a);

[32] Jones and Scott (1989);

[33] Jones (1996);

[34] Barth et al. (2018);

[35] Buseck and Holdsworth (1972);

[36] Fogel (1997);

[37] Avril et al. (2013);

[38] Weyrauch et al. (2018);

[39] El Goresy and Ehlers (1989);

[40] Nakamura-Messenger et al. (2012);

[41] Bischoff and Keil (1983);

[42] Ikeda (1980);

[43] McCoy et al. (1991a);

[44] Wang et al. (2016);

[45] McSween (1977b);

[46] Simon et al. (1994);

[47] Sheng et al. (1991b);

[48] Krot et al. (1993);

[49] Bunch et al. (1967);

[50] Davy et al. (1978);

[51] Johnson and Prinz (1991);

[52] Weinbruch et al. (1994);

53. Taylor et al. (1981);
54. Haggerty and McMahon (1979);
55. Ikeda (1983);
56. Scott and Jones (1990);
57. Bischoff and Keil (1984);
58. Fujimaki et al. (1981a);
59. Fujimaki et al. (1981b);
60. Krot and Rubin (1994);
61. Brigham et al. (1986);
62. Bridges et al. (1995);
63. Kimura et al. (2005);
64. Ikeda (1989b);
65. Wasson and Krot (1994);
66. Olsen (1983);
67. Scott and Krot (2014);
68. Ikeda (1982);
69. Watanabe et al. (1986);
70. Noguchi (1989);
71. Zhang et al. (1996);
72. Müller et al. (1995);
73. Kitamura et al. (1987);
74. Sheng et al. (1991a);
75. Wang et al. (2016);
76. Noguchi (1995);
77. Jones (1997);

78. Greshake (1997);
79. Bischoff et al. (1985);
80. Noguchi (1995);
81. Murakami and Ikeda (1994);
82. Ikeda and Kimura (1995);
83. Dodd et al. (1965);
84. Rambaldi et al. (1986);
85. Krot and Wasson (1994);
86. Wood and Holmberg (1994).